An adaptive model of information processing in the primate retina

Samir Shah

B ApSc , (University of British Columbia), 1987

Department of Electrical Engineering
McGill University
Montréal
September, 1993

A thesis submitted to the Faculty of Graduate Studies and Research
in partial fulfillment of the requirements for the degree of
Master of Engineering

LIST OF COPYRIGHT PERMISSIONS
FOR THESIS FIGURES

THESIS FIG NO	FIGURE CONTENT	FROM CITATION	PUBLISHER	SOURCE ARTICLE & FIG NO	PERMISSION GRANTED
2.1	Retina Schematic	{Uses 83}	MIT PRESS	THE NEUROSCIENCES, ed F Schmidt Fig 9, pg 178	YES
2.2	Photoreceptor Distrn	{Pirenne, 1967}	Associated Book Publishers	Pirenne, Vision and Eye, 1967 Fig 2.5, p 32 (picture distrn)	YES
2.3 5.2b	Horz Cell feedback in spikes resp	{dowling 87}	Belknap Press, Harvard Univ	Book "Retina An approach rate" p. 94, Fig 45	YES
2.4	Visual threshold	{dowling 87}		p 219, Fig 7.20	
3.2	light/dark adaptation	{dowling 87}		p 207, Fig 7.13	
2.7	Cell densities J. Rosenthaly	{kronauer, 33}	IEEE SMC	IEEE SMC-15, no , 1985 Fig 3, Pg 97	YES
3.6	amacrine on off ganglion cell response	{werblin 74a}	ROCKEFELLER UNIV PRESS	J Gen physiology, vol 63, 1974 p 95, Fig 8 Pg 46 fig4	YES
5.4b	on/horz/bipolar responses	{werblin 74b}		p 66 67 fig1-4	
5.5b		{werblin 74c}		~~J Gen Physiol, vol 66, 1975~~	
5.6b				~~p 627 fig1~~	
5.3b	I R curves			~~p 633 fig 2~~	
5.1(a)	monkey cone response	{schnapf 87}	SCIENTIFIC AMERICAN	J L Schnapf "How photoreceptors Sci Amer vol 156, April 1987 Fig 47 top right	YES
5.8b	P & M cell spatial freq resp	{derrington84}	The Physiological Society, UK	J physiol, 1984, v 357, p 219 240 Fig 3a, 10a	YES
5.9b	Temporal Freq resp in monkeys	{purpura 90}	CAMBRIDGE UNIV PRESS	Visual NeuroScience 1990, vol 4, Fig 4a, 2a	YES
5.10b	P cell M-cell Contrast gain in monkeys	{benardete 92}		Visual Neuroscience 1992, vol 5, p 483, Fig 1	YES
3.4a	Visual Acuity	{thomas 79}	Academic Press	Handbook of Perception, 1979 ch 7, Fig 3, p 237 visual acuity data	YES

Copyright permissions have been obtained for all previously copyrighted material (listed above). However, if required, the library has my permission to microfilm the thesis without any objectionable figure Attached are the letters, granting permission to use the above figures in the thesis. (from publishers, authors)

James Shd

Samir Shah,
Centre for Intelligent Machines,
McGill University,
3480 University St,
Montreal, Quebec, H3A 2A7
tel. (514) 398-8093
fax. (514) 398-7348

Sept 10,1993

Permissions and Copyright officer,
MIT Press,
55 Hayward St.,
Cambridge, MA 02142

Dear Sir/Madam,

As part of my Master's thesis requirements, my thesis titled "An adaptive model of information processing in the primate retina" will be microfilmed and made available in the National Library of Canada and at McGill University.

I would like your permission to reproduce the figures from the following sources in my thesis, and in any future journal articles based on the thesis:

Author: J.E. Dowling
Article: Information processing by local circuits: The
            vertebrate retina as a model system.
in Book: The Neurosciences: Fourth Study Program
eds.   :   F.O. Schmitt and F.G Worden
Publ. :   MIT Press, Cambridge, 1983
figure :   figure 9, pg. 178, (schematic of wiring in retina)

It is understood, of course, that full credit will be given to the author and publisher as a refrence within the figure text. A release form is given below for your convenience. The duplicate copy of this request is for your files.

Yours sincerely,

Samir Shah

Permission is granted for use of the material as stipulated.

Date:_____   Signature: _____

                                         Title: _____

The MIT Press
·55 Hayward St.
Cambridge, M. 02142

Invoice number	95205
Date	11/24/93
Permission fee for use specified below	US $ 25.00

Federal Identification
Number 04-21035

Sold to: Samir Shah
              Centre for Intelligent Machines
              McGill University
              3480 Unviersity St.
              Montreal, Quebec, H3A 2A7
              CANADA

Please make check payable
to The MIT Press and remit
to the Permissions Dept.

Thank you for your request for permission to reprint:

    Schmitt/THE NEUROSCIENCES 1 fig.

Subject to the conditions stated below, permission is granted to use the material described above. The material will appear in:

    Shah/AN ADAPTIVE MODEL OF INFORMATION PROCESSING...

Published by: National Library of Canada   Form of publication: microfilms

CONDITIONS OF THE PERMISSION:

1. All rights granted herein are nonexclusive and, unless otherwise stated, are valid through-
   out the world.

2. This permission does/does not allow translation of the quoted material into languages other
   than English.

3. Full credit and proper copyright notice must be given for material used. Full credit includes
   NAME OF AUTHOR (AND TRANSLATOR IF APPLICABLE), TITLE OF THE MIT PRESS PUBLICATION, and THE
   MIT PRESS AS PUBLISHER. Copyright notice identical to that appearing in the MIT Press pub-
   lication must be printed either on the copyright page of your work or on the first page of
   each quotation covered by this permission.

4. Payment of the required fee is due upon publication of your work or two years from the date
   of this invoice, whichever is earlier. Failure to remit within the required time period
   will automatically and without further notice void this permission. ONE COPY OF THIS INVOICE,
   OR CLEAR REFERENCE TO OUR INVOICE NUMBER, MUST ACCOMPANY PAYMENT.

5. This permission covers the present and all future English language editions of your work.

6. This permission does not cover any material in the MIT Press publication which is credited
   to another source. If an original source is credited anywhere in the material, this
   permission is contingent upon obtaining permission from that source.

The following condition applies to photocopy permission only:

7. Permission to photocopy is granted for not more than the number of copies specified above.
   The material may be copied for classroom and library use only. Payment of the fee is due
   within 30 days of the date of this invoice. Conditions 2,4,and 5 above do not apply to
   this permission to photocopy.

Other conditions:

8.

Approved, for the MIT Press
Abe Rybeck, Permissions

October 6, 1993

Copyright and Permissions Officer,
Associated Book Publishers
11 New Felter Lane
London EC4, U.K

Dear Sir/Madam,

As part of my Masters Thesis requirements, my thesis titled "An adaptive model of information processing in the primate retina" will be microfilmed and made available in the National Library of Canada and at McGill University

I would like your permission to reproduce in my thesis the figures from the following source(s):
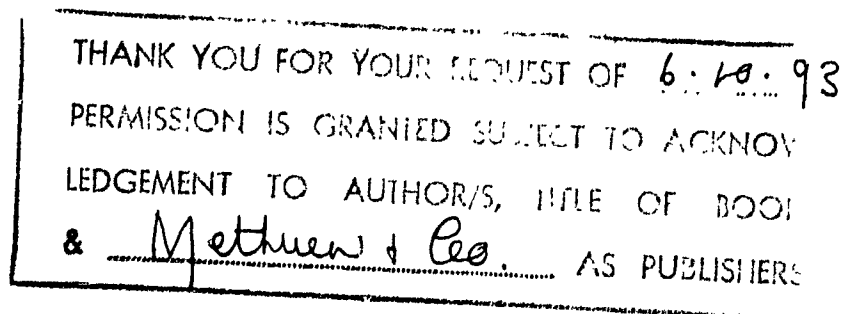
Authors: M.H. Pirenne
Book: Vision and the Eye, 2ed.
Publisher: Associated Book Publishers, 1967
Figures: Figure 2.5, pg. 32 (photoreceptor distribution)

It is understood, of course, that full credit will be given to the author and publisher as a refrence within the figure caption

Yours sincerely,

Samir Shah

THANK YOU FOR YOUR REQUEST OF *6 : 10 : 93*
PERMISSION IS GRANTED SUBJECT TO ACKNOWLEDGEMENT TO AUTHOR/S, TITLE OF BOOK
& *Methuen & Co* AS PUBLISHERS

934050

Samir Shah,
Centre for Intelligent Machines,
McGill University,
3480 University St,
Montreal, Quebec, H3A 2A7
tel. (514) 398-8093
fax. (514) 398-7348

Sept 10,1993

Permissions and Copyright officer,
Belknap Press,
79 Garden St.,
Cambridge, MA 02138

Dear Sir/Madam,

As part of my Master's thesis requirements, my thesis titled "An adaptive model of information processing in the primate retina" will be microfilmed and made available in the National Library of Canada and at McGill University.

I would like your permission to reproduce the figures from the following sources in my thesis, and in any future journal articles based on the thesis:

Author: J.E. Dowling
Book: The Retina: An approachable part of the brain
Publ: Belknap Press, Cambridge, 1987
Figures: fig. 4.5, page 92   (response of gecko rods)
           fig 7.20, page 219 (visual threshold vs. pigment bleached)
           fig 7.13 page 207 (light and dark adaptation)

It is understood, of course, that full credit will be given to the author and publisher as a refrence within the figure text. A release form is given below for your convenience. The duplicate copy of this request is for your files.

Yours sincerely,

Samir Shah

Permission is granted for use of the material as stipulated.

Date:_____   Signature: _____

                                         Title: _____

HARVARD

UNIVERSITY

PRESS

20 September 1993

Samir Shah
Centre for Intelligence Machines
McGill University
3480 University Street
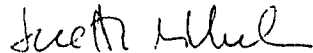Montreal, Quebec H3A 2A7
Canada

Dear Samir Shah,

Thank you for your letter of 10 September 1993 requesting permission to use Harvard University Press material in your forthcoming dissertation.

Permission is hereby granted for the material requested in your letter to be included in your dissertation. Permission is also granted for this material to be reproduced as part of your dissertation by University Microfilms when they fulfill single copy requests for your dissertation. Proper acknowledgment to the material's original source is requested.

Permission is not granted for publication in any other form. Permission for any other publication in any other form must be renegotiated.

Thank you for your consideration.

Sincerely,

Judith Michelman
Permissions Assistant

Samir Shah,
Centre for Intelligent Machines,
McGill University,
3480 University St,
Montreal, Quebec, H3A 2A7
tel. (514) 398-8093
fax. (514) 398-7348

Sept 10,1993

Permissions and Copyright officer,
IEEE Systems, Man, and Cybernetics Group,
Div. of IEEE Inc.,
Box 1331, Piscataway, NJ 08855

Dear Sir/Madam,

As part of my Master's thesis requirements, my thesis titled "An adaptive model of information processing in the primate retina" will be microfilmed and made available in the National Library of Canada and at McGill University.

I would like your permission to reproduce a figure from the following source in my thesis, and in any future journal articles based on the thesis:

Author: R.E. Kronauer and Y.Y. Zeevi
Article: Reorganization and Diversification of Signals in Vision
Journal: IEEE Transactions on systems, man, and cybernetics
Publ: vol. SMC-15, no.1, 1985, pp91-101
Figure: fig 8, pg. 97   (cone and ganglion cell densities)

It is understood, of course, that full credit will be given to the author and publisher as a refrence within the figure text. A release form is given below for your convenience. The duplicate copy of this request is for your files.

Yours sincerely,

Samir Shah

Permission is granted for use of the material as stipulated.

Date:_____   Signature: _____

                                     Title: _____

DIRECT NUMBER (908) 562   3966

September 21, 1993

Mr. Samir Shah
Centre for Intelligent Machines
McGrill University
3480 University St.
Montreal, Quebec, H3A 2A7
Canada

Dear Mr. Shah:

This is in response to your letter of September 10 in which you have requested permission
to reprint, in your upcoming thesis, one IEEE copyrighted figure. We are happy to grant
this permission.

Our only requirements are that you credit the original source (author, paper, and publica-
tion), and that the IEEE copyright line (© 1985 IEEE) appears prominently with the
reprinted figure.

Sincerely yours,

William J. Hagen, Manager
Copyrights and Trademarks
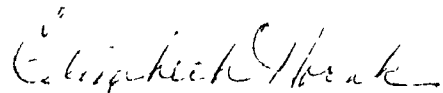
WJH:kl

21 September 1993

Dear Mr. Shah:

   We shall be glad to grant you permission for the reproduction
of the material referred to in your letters of 10 September 1993.

   Our only requirements are that you also obtain permission from
the author(s) and give suitable acknowledgement to the source in
the following manner: Reproduced from the Journal of Experimental
Medicine, year, vol., pp., by copyright permission of the Rockefeller
University Press.

                              Sincerely yours,

                              THE JOURNAL OF EXPERIMENTAL
                              MEDICINE

                              Elizabeth Horak
                              Permissions

Mr. Samir Shah
Centre for Intelligent Machines
McGill University
3480 University Street
Montreal, Quebec, H3A 2A7
Canada

P.S. Kindly write to us each time for permission concerning future
editions and translations, as we do not grant blanket permission.

Samir Shah,
Centre for Intelligent Machines,
McGill University,
3480 University St,
Montreal, Quebec, H3A 2A7
tel. (514) 398-8093
fax. (514) 398-7348

Sept 10,1993

Permissions and Copyright officer,
Rockefeller University Press,
222 E.70th St.,
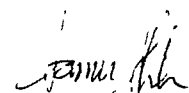New York, NY 10021

Dear Sir/Madam,

As part of my Master's thesis requirements, my thesis titled "An adaptive model of information processing in the primate retina" will be microfilmed and made available in the National Library of Canada and at McGill University.

I would like your permission to reproduce a few figures from the following sources in my thesis, and in any future journal articles based on the thesis:

Authors: R.A. Normann, F.S. Werblin, and D.R. Copenhagen
Article: The Control of Sensitivity I,II,and III   (3 articles)
Journal: Journal of General Physiology, vol. 63, pg.37-110, 1974
Figures: fig. 4,   pg. 46   (cone flashed background responses)
           fig. 1-4, pg. 66-67, (bipolar and horizontal cell responses)
           fig. 8,   pg. 98,   (ON-OFF ganglion cell response)

It is understood, of course, that full credit will be given to the author and publisher as a refrence within the figure text. A release form is given below for your convenience. The duplicate copy of this request is for your files.

Your's sincerely,

Samir Shah

Permission is granted for use of the material as stipulated.

Date:_____   Signature: _____

                                    Title: _____

Dear Samir Shah,

I am sorry you didn't receive the letter granting permission to reprint.
Please take this note as my permission to reprint the figures you wish to
use.

Frank Werblin

On Tue, 11 Jan 1994, Samir Shah wrote:

> Dec 11th, 1993
>
> Dear Prof. Frank Werblin,
>
> Hello again! I still have not recieved your letter granting permissiion
> to reproduce some figures from your 1974 J. Gen. Physiology articles
> titled "The control of sensitivity I,II, and III" in my masters thesis.
> Perhaps with the university closings over christmas things got misplaced.
> Could you please print this letter, sign it, and mail it back to me.
>
> Here is the info I sent to you before:
>
> The figures I would like to reproduce are the recordings of cell potentials
> you made in Necturus and Mudpuppy retinas in order to make qualitative
> comparisons between the outputs of my simple retinal model and biological
> retinal neurons when presented with similar stimuli. I have already
> obtained permission from Rockefeller University Press, the publisher for
> J. Gen Physiology but they require that I also obtain written permission
> from you.   I require this permission in order to submit my thesis titled
> "An adaptive model of information processing in the retina" which
> is then microfilmed and made available in the National Library of Canada.
>
> The specific figures used in my thesis are the following:
>
> Articles: "The control of Sensitivity I, II, and III"
> Journal: Journal of General Physiology, vol. 63, pg. 37-110, 1974
> Figures: fig 4., pg.46 (cone flashed background responses)
>   fig 1-4, pg.66 (bipolar and horizontal cell responses)
>   fig 8 , pg.98 (ON-OFF ganglion cell response)
>
>
> I would appreciate a quick response by mail to the address below so
> that I can make my final submission. Thank you very much in advance
> (again) for your time in dealing with this request.
>

```
> regards,
> Samir Shah
>
>
>
>
> ------------------------------------------------------------------------
> Samir Shah                    .           tel#1   (514) 398-8093
> Centre for Intelligent Machines           tel#2   (514) 398-7493
> McGill University                         fax     (514) 398-7348
> McConnell Engineering Bldg. 4th Floor     email   samir@cim.mcgill.ca
> 3480 University Street
> Montreal, Quebec, Canada  H3A 2A7
> ------------------------------------------------------------------------
>
>
>
```

REQUEST FOR PERMISSION TO REPRINT MATERIAL FROM SCIENTIFIC AMERICAN

SCIENTIFIC AMERICAN, INC.
415 MADISON AVENUE
NEW YORK, NEW YORK 10017

DATE _Sept 24, 1993_

I request permission to reprint the following from **SCIENTIFIC AMERICAN** (*specify author, title, date of issue, page number, and fee as noted on covering letter herewith*):

Author: J.L. Schnapf and D.A. Baylor
Title: How photoreceptor cells respond to light;
Journal: Scientific American, vol. 156, no. 4, 1987, pgs 40-47

Figure: pg. 47, top right figure (Membrane Currents of cone)

to appear in the following volume:

Title and Author _____ Samir Shah, "An adaptive model of information processing in the primate retina".

Publisher _____ McGill University

Type of Publication (text, professional, trade) _____ M. Eng Thesis

The undersigned agrees:

1. Acknowledgment of an illustration shall be made on the page of the volume where the illustration appears. See form of acknowledgment below.

2. Payment of the required fee __N/A__ is enclosed herewith. The fee is nonrefundable; payment is not contingent on publication of the material.

3. Copies of the appropriate pages (illustration and acknowledgment) from your volume shall be mailed with a copy of this form to the Permissions Department of Scientific American, Inc.

4. This permission applies only to the edition specified above. A new application must be made for any additional use.

SIGNED _____ ADDRESS _____
Samir Shah
McGill University Centre for Intelligent Machines
3480 University Ave, Montreal, Quebec H3A 2A7
Canada
(514) 398-7348 Fax
(514) 398-8093 Office

≈ **Approval of Request** ≈

The foregoing application is hereby approved, subject to the conditions stated above, and provided that the following form of acknowledgment and copyright notice is used as specified above:

From (title of article and author). Copyright © (date) by Scientific American, Inc. All rights reserved.

DATE _29 Sept, 1993_

APPROVED by _____
Linda Hertz, Permissions & Rights Manager
for SCIENTIFIC AMERICAN, INC.

McGill
University

Research Centre for Intelligent Machines
McConnell Engineering Building

November 8, 1993

The Physiological Society
Admin. and Publications Office
P.O. Box 506
Oxford OX1 3XE, U.K.

Dear Sir/Madam,

As part of my Masters Thesis requirements, my thesis titled "An adaptive model of information processing in the primate retina" will be microfilmed and made available in the National Library of Canada and at McGill University.

I would like your permission to reproduce in my thesis the figures from the following source(s):

Authors: A.M. Derrington and P. Lennie
Article: "Spatial and temporal contrast sensitivities of neurones..."
Journal: Journal of Physiology, vol. 357, pp.219-240, 1984
Figures: fig 3a and fig 10a (P and M cell spatial freq. sensitivity)

It is understood, of course, that full credit will be given to the author and publisher as a refrence within the figure caption. A duplicate copy of the request letter is enclosed for your files.

Yours sincerely,

Samir Shah

A M. Derrington's address
Dept of Physiological Sciences
The Medical School
Newcastle - Upon - Tyne.
NE2 4HH   UK

PERMISSION GRANTED

PROVIDED the author's consent is first obtained

15/11/93

Postal Address: 3480 University Street, Montréal, Québec Canada H3A 2A7   FAX: (514) 398-7348
Telephone: (514) 398-8093   email: samir@cim.mcgill.ca

McGill University

Research Centre for Intelligent Machines
McConnell Engineering Building

November 30, 1993

Prof. A.M. Derrington, Dept. of Physilogical Sciences
The Medical School
Newcastle-Upon-Tyne
U.K. NE2 4HH

Prof. Derrington,

As part of my Masters Thesis requirements, my thesis titled "An adaptive model of information processing in the primate retina" will be microfilmed and made available in the National Library of Canada and at McGill University. I would like your written permission to reproduce in my thesis two figures from one of your papers. I use the figures to compare the outputs of my model to those you recorded in Macaque monkeys. I would also like your permission to use the figure again in an article which will be a condensed version of the thesis results to be submitted to IEEE SMC.

Authors: A.M. Derrington and P. Lennie
Articles: "Spatial and temporal contrast sensitivities of neurones in the LGN of ..."
Journal: Journal of Physiology, vol. 357, pg.219-240, 1984
Figures: fig. 3a, P-cell spatial freq. sensitivity
. fig. 10a, M-cell spatial freq. sensitivity

I have already obtained permission from The Physiological Society, the publisher for J. Physiol. They requested that I also obtain written permission from you. Full credit will be given to all the authors and the publisher as refrences within the text. If you agree to this, please sign and date this letter with "permission granted" and return it to me. The duplicate copy is for your files.

Yours sincerely,

Samir Shah

Samir Shah

Permiss ion granted

Anthony Derrington

7 Dec 1993

Postal Address: 3480 University Street, Montréal, Québec Canada H3A 2A7 FAX· (514) 398-7348
Telephone: (514)398-8093 samir@cim.mcgill.ca

Samir Shah,
Centre for Intelligent Machines,
McGill University,
3480 University St.,
Montreal, Quebec, H3A 2A7
tel. (514) 398-8093,
fax. (514) 398-7348

Sept 10,1993

Permissions and Copyright officer,
Cambridge University Press,
40 W.20th street, New York, NY 10011

Dear Sir/Madam,

As part of my Master's thesis requirements, my thesis titled "An adaptive model
of information processing in the primate retina" will be microfilmed and made
available in the National Library of Canada and at McGill University.

I would like your permission to reproduce a few figures from the following
sources in my thesis, and in any future journal articles based on the thesis:
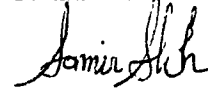
[1]   Authors: K. Purpura, D. Tranchina, and E. Kaplan,
       Article: Light adaptation in the primate retina: Analysis ....
       Journal: Visual Neuroscience, vol.4, no.1, pg.75-93, 1990,
       Figures: pg.80, fig. 1A - P-cell TMFT
                  pg.81, fig. 2A - M-cell TMFT

[2]   Authors: E.A. Benardete, E. Kaplan, and B.W. Knight,
       Article: Contrast gain control in the primate retina: P cells ...
       Journal: Visual Neuroscience, vol.8, pg.483-486, 1992,
       Figure: pg.485, fig. 1 - P and M cell contrast gain

[3]   Authors: A.M. Derrington and P.Lennie
       Article: Spatial and temporal contrast sensitivities of neurones...
       Journal: Journal of Physiology, vol.357, pp.219-240, 1984,
       Figures: pg.225, fig. 3a - P-cell spatial freq. sensitivity
                  pg.233, fig. 10a - M-cell spatial freq. sensitivity

It is understood, of course, that full credit will be given to the author and
publisher as a refrence within the figure text. A release form is given below
for your convenience. The duplicate copy of this request is for your files.

Yours sincerely,

Samir Shah

 Permission is granted for use of the material as stipulated.

Date:_____   Signature: _____

                                          Title: _____

October 31, 1993

Samir Shah
Centre for Intelligent Machines
McGill University
3480 University St.
Montreal, Quebec   H3A 2A7
Canada

Dear Samir Shah:

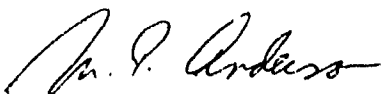Thank you for your request for permission to include

Fig. 1a and Fig. 2a, from Purpura, et al.,
Visual Neuroscience, Vol. 4, No. 1 (1990),
and
Fig. 1, from Benardete, et al.,
Visual Neuroscience, Vol. 8 (1992),

in your forthcoming thesis, ONLY, to be microfilmed and made available in the National Library of Canada and at McGill University.

Permission is granted for this use only, subject to full acknowledgement of our material and clear indication of the copyright notice as it appears in our publication, followed by the phrase "Reprinted with the permission of Cambridge University Press." This permission does not authorize the use of our material in any future publications, for which separate permission must be requested.

Please note that this permission does not allow reprinting any material copyrighted by or credited to another source; to use such material, permission must be obtained directly from the owner of that material. Cambridge disclaims all liability in connection with the use of such material without proper consent. We cannot provide additional information or addresses other than that which appears in our publication.

Sincerely,

M. P. Anderson
Manager
Rights and Permissions

Thank you for your permission request. Rights to material from the
Journal of Physiology are controlled by:

       The Physiological Society
       Administration and Publications Office
       P.O.Box 506
       Oxford OX1 3XE
       United Kingdom

Please contact them directly.

Sincerely,

Rights and Permissions Dept.

Samir Shah,
Centre for Intelligent Machines,
McGill University,
3480 University St,
Montreal, Quebec, H3A 2A7
tel. (514) 398-8093
fax. (514) 398-7348

Sept 10,1993

Permissions and Copyright officer,
Academic Press,
1250 Sixth Ave,
San Diego, CA 92101

Dear Sir/Madam,

As part of my Master's thesis requirements, my thesis titled "An adaptive model of information processing in the primate retina" will be microfilmed and made available in the National Library of Canada and at McGill University.

I would like your permission to reproduce a figure, from the following source, in my thesis, and in any future journal articles based on the thesis:

Author: J.P. Thomas
Article: Spatial resolution and spatial interaction
Book: Handbook of Perception, volume 5
Editors: E.C. Cartertette and M.P. Friedman
Publ: Academic Press, New York, 1979
Figure: chap. 7, fig 3, pg. 237   (visual acuity vs. illumination)

It is understood, of course, that full credit will be given to the author and publisher as a refrence within the figure text. A release form is given below for your convenience. The duplicate copy of this request is for your files.

Yours sincerely,

Samir Shah

Permission is granted for use of the material as stipulated.

Date:_____   Signature: _____

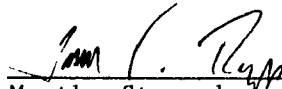   Title: _____

September 30, 1993

PERMISSION GRANTED, provided that 1) complete credit is given to the
source, including the Academic Press copyright notice; 2) the material
to be used has appeared in our publication without credit or
acknowledgement to another source and 3) if commercial publication
should result, you must contact Academic Press again.

We realize that the National Library of Canada must have permission to sell copies
of your thesis, and we agree to this. However, we must point out that we
are not giving permission for separate sale of your article.

Martha Strassberger
Contracts, Rights and Permissions
Academic Press, Inc.
Orlando, FL 32887

ABSTRACT

At the retinal level, the strategies utilized by biological visual systems allow them to outperform machine vision systems, serving to motivate the design of electronic or "smart" sensors based on similar principles. Design of such sensors in silicon first requires a model of retinal information processing which captures the essential features exhibited by biological retinas. In this thesis, a simple retinal model is presented, which qualitatively accounts for the achromatic information processing in the primate cone system. The *computer retina* model exhibits many of the properties found in biological retinas such as data reduction through non-uniform sampling, adaptation to a large dynamic range of illumination levels, variation of visual acuity with illumination level, and enhancement of spatiotemporal contrast information. The model is validated by replicating experiments commonly performed by electrophysiologists on biological retinas and comparing the response of the *computer retina* to data from experiments in fish and monkeys. In addition, the response of the model to synthetic and real images is shown. The experiments demonstrate that the model behaves in a manner qualitatively similar to biological retinas and thus may serve as a basis for the development of an "artificial retina"

RÉSUMÉ

Au niveau de la rétine, les stratégies utilisées par les systèmes visuels biologiques leur permettent de surpasser de loin les systèmes de vision artificielle. Ceci motive donc la conception de senseurs électroniques ou "intelligents", basés sur des principes similaires. La conception en silicone de tels senseurs nécessite d'abord un model du traitement de données représentant les charactéristiques essentielles se manifestant au sein des rétines biologiques. Cette thèse décrit un modèle simple de rétine qui tient qualitativement compte du traitement de l'information achromatique au sein du système de cones chez les primates. Le modèle de *rétine artificielle* manifeste plusieurs des propriétés retrouvées dans les rétines biologiques tel que la réduction de l'information grâce à un échantillonnage non-uniforme, une adaptation *locale* à des niveaux d'illumination couvrant plusieurs ordres de grandeur d'intensité, une variation de l'acuité visuelle avec le niveau d'illumination et le rehaussement des contrastes spatio-temporels. Le modèle est validé en répétant des expériences réalisées communément par les électro-physiologistes sur des rétines biologiques et en comparant la réponse de la *rétine artificielle* avec des données obtenues dans des expériences sur les poissons et les singes. La réponse du modèle lorsque soumis à des images synthétiques et réelles est également examinée. Les expériences démontrent que le modèle répond d'une manière qualitativement similaire à la rétine et peut donc servir de base au dévelopement d'une "rétine artificielle".

ACKNOWLEDGEMENTS

I would like to thank many people. I would first like to thank my advisor M.D. Levine for his direction and many invaluable comments throughout this project. His enthusiasm and support made this project a truly enjoyable experience.

I would also like to acknowledge all those people which made it possible for various aspects of the *computer retina* program to be assembled. In particular, I would like to thank Marc Bolduc for technical assistance in interfacing the *computer retina* program to his *foveated* retinal mapping program. I would also like to thank Hiro Yamamoto for the use of a ray-tracing package for the generation of synthetic images used to test the *computer retina*.

Other people who also deserve thanks are those who commented on the preparation of different parts of this thesis: Anna Lin, Michael Kelly, James Elder, Marc Bolduc and Gérard Blais. I would especially like to thank Diane Kampen, who not only read my thesis several times but supported me emotionally during the entire writing stage.

Table of Contents

List of Figures

1.1 Background

Of the five senses, vision is perhaps the one upon which humans rely the most. We depend on visual feedback for tasks such as navigation, motor control, object recognition, and building scene descriptions. The brain receives its visual information through approximately one million nerve fibers carrying visual signals from the retina in each eye. These fibers from both eyes account for nearly half of all the sensory nerve fibers streaming into the brain, and a considerable portion of the cortical machinery is used to process the transmitted information[32]. There are some estimates that, for every nerve fiber carrying signals out from the retina, there are over 2000-4000 cortical neurons involved in processing its signals [32].

Vision capabilities are also quite important in many computer-controlled applications such as mobile robot navigation, parts inspection and object recognition tasks, just to name a few. To be able to see and understand what one observes seems to be very simple for humans. Although much research effort has been expended on understanding vision, the computer vision community has discovered that practical applications of machine vision are exceedingly difficult. Traditional computer vision techniques which have for the most part ignored strategies employed by biological visual systems have not been very successful. Some current research efforts are thus focused on studying biological visual systems in an attempt to understand not only how these visual systems function, but also to guide the design of future machine vision systems.

Many of the properties of the human visual system are ultimately limited by the fidelity of image sampling within the retina and the strategies used to preprocess the sampled information before further processing in the cortex. Even at the retinal level, the performance of the human visual system far exceeds the capabilities of commercially available visual sensors and machine vision systems, thereby motivating the study of the human or primate retina [10][32].

Commercially available visual sensors typically have poorer sampling densities and dynamic range than the human retina. Although commercially available charge-coupled-device (CCD) cameras are beginning to approach a million or more uniformly distributed pixel outputs (1024 by 1024 resolution), this number is still small compared to the over 5 million cone and over 100 million rod photoreceptors used to sample the image in the human retina. Furthermore, the capacity to process all of this information in real-time is beyond the ca-

pabilities of today's machine vision systems. While such uniform high-resolution sensors are ideal for applications such as TV, a nonuniform sampling scheme combined with data reduction such as that employed in many biological retinas may be more appropriate for many machine vision applications [32][82].

The dynamic range of commercial camera photosensors is typically less than 3 log units of illumination intensity. Even quite sensitive cameras (such as the super-HARP camera [80]) only have dynamic ranges of slightly over 4 log units of illumination intensity. The retina, by contrast, has an operational range covering over 12 orders of magnitude in intensity. Another major difference between the retina and commercial cameras is the ability to deal with a large *variation* in intensity levels in a single scene. In order to be sensitive to small variations in contrast, many camera systems use photosensor arrays with very narrow dynamic ranges (≈ 2 log units) and a high contrast gain. A measure of the global ambient illumination level may then be used to extend the operating range of the camera by globally shifting the operating point or gain of the entire receptor array. However, when confronted with scenes containing a very wide range of illumination levels (> 3 log units), many parts of the scene appear washed out or underexposed in the camera output but remain perfectly visible to the naked eye. Again, although restricted dynamic range cameras are adequate for certain applications in which the lighting conditions are controlled, they may not be appropriate for applications that require operation in both indoor and outdoor environments where a wide range of illumination may be encountered.

It is apparent that the human retina has superior imaging fidelity and a larger dynamic range than commercial camera systems. Furthermore, uniform resolution camera systems may also be inappropriate in many machine vision applications that require real-time processing of visual information (such as for navigational and object recognition tasks in mobile robotics). For such applications, it is advantageous to extract or enhance the specific information which is useful for the particular visual task and reduce or compress peripheral data, thereby greatly reducing the computational requirements at higher levels. For such applications, new sensors need to be developed. Our approach is to base the design on some of the same principles utilized by biological vision systems. Knowledge of the retinal architecture, along with a model of the processing performed in the retina, can serve as a basis for the development of "artificial retinas" for machine vision. Towards that end, this thesis presents a simple retinal model which incorporates various adaptation mechanisms used to deal with large changes in illumination level, and also mimics the nonuniform sampling scheme used in the primate cone system. It is hoped that this model will ultimately serve as the foundation for a silicon implementation for an adaptive foveated sensor.

In order to develop a model of information processing in the retina useful for machine vision applications, it is necessary to study the strategies employed by the primate retina.

The properties of the retina pertinent to our model are very briefly summarized here and a more detailed review of retinal structure and models of information processing are presented in a later chapter.

1.2 Overview of Retinal Information Processing

At a first glance, one may be tempted to compare the retina to a TV camera which simply converts an optical image to electrical signals for further processing in the brain. However, the retina does considerably more than that. Each retina contains millions of photoreceptor cells (rods and cones) which sample the image projected onto it by the optics of the eye. Photoreceptor cells convert optical information in the image into *graded potentials* which then drive further processing in the retina. Intermediate cells in the retina enhance certain features of the visual signal while discarding other information, until at the last stage, ganglion cells convert the graded potential signals into *action potentials* for transmission to the brain via the optic nerve.

The principles utilized by the retina in processing visual information in the cone system may be summarized as follows:

- Significant data reduction is achieved through a foveated sampling scheme at the receptor level and increasing convergence of cone inputs into ganglion cell outputs with increasing eccentricity [32][23][49]. Such sampling schemes have been modelled using log-polar mappings [50][76].

- The cone transduction function is described by a log-like function with saturation nonlinearities and a dynamic range of 3 log units in intensity [21][8].

- Mechanisms within the cone itself and network feedback from other retinal cells *locally* adapt the sensitivity of cone photoreceptors so that their response range is centred around a *local* spatiotemporal ambient intensity.[1] These mechanisms extend the cone operating range by several orders of magnitude.

- Circularly concentric centre-surround receptive field (RF)[2] structures emerge at the *bipolar* cell level. The bipolar cell essentially performs a difference operation between the centre and surround portions of the signal. This serves to strip the 'dc' background

---

[1] *Local* in the above context means a small neighbourhood or area around a given photoreceptor

[2] The extent of a cell's receptive field (RF) is defined here as the region on the retina which, when stimulated, influences the cell response. The structure of a cell's RF is defined by the degree to which regions within the RF influence the cell output. Bipolar and ganglion cells have RF profiles with two circularly concentric regions (labeled centre and surround) which are most often modeled by a difference of two Gaussians weighting profile.

intensity information from the visual signal and allows the bipolar cell to be sensitive to *local* variations in contrast [28].

- The retina appears to adapt the size of its receptive fields as a function of illumination level in an effort to maintain a good balance between high visual acuity and contrast detectability [1][62][75][81]. At dim photopic illuminations levels, the input signal-to-noise ratio (SNR) is relatively low; the retina compensates for this by averaging information over larger receptive fields to improve absolute contrast detectability at the expense of slightly poorer visual acuity [81]. With increasing illumination levels, the input SNR increases, facilitating improvements in both visual acuity and absolute contrast detectability [65].

- We hypothesize that feedback mechanisms within the retina adapt the spatiotemporal sensitivity in regions of high spatiotemporal contrast by reducing the relative size of the surround field of bipolar and ganglion cell receptive fields. This mechanism acts to sharpen spatial edges in the retinal output and improve sensitivity to temporal change in the visual input. This hypothesis, which is supported by data on the effects of *interplexiform* cell feedback on *horizontal* cell RF sizes [68], will be discussed in more detail in Chapter 3.

- Two major classes of ganglion cells (P-cells and M-cells) account for 90% of the retinal output and represent the two distinct channels of information from the retina [23]. P-cells are more numerous (80% of all ganglion cells), have smaller receptive fields and respond to higher spatial frequencies than M-cells. M-cells have larger receptive fields, higher contrast gain, and are more responsive to temporal stimulation [33].

In summary, the biological retina is more than just a simple TV camera. The retina not only converts optical information to electrical signals but performs considerable processing on the visual signal itself before transmitting it to higher levels. Various local adaptation mechanisms extend the retina's dynamic range by several orders of magnitude. In order to meet the transmission bottleneck at the optic nerve, the retina extracts only those features required in later stages of visual processing while employing many data reduction strategies such as nonuniform sampling.

1.3 Summary of Thesis Contributions

Many researchers are interested in modelling the retina or building artificial retinas. A few groups have already fabricated silicon chips to model certain aspects of the retinal function [36][39] [53][66]. In addition, many computer models of the retina have also been proposed

[5] [10][25] [58][77][82]. All of these models mimic some parts of the retinal function but ignore others. Some implementations model the nonuniform sampling occurring in the retina [53][66]. Others simulate the nonlinear transduction and adaptation occurring at the cones but ignore the nonuniform sampling [10][36][58]. Furthermore, existing computer models or silicon implementations do not account for the changes in visual acuity associated with changing illumination level and adaptation to spatiotemporal contrast.

The contributions of this thesis are in three main areas. First, the work presented here consolidates variations of existing models with different features of the retina into a single, more cohesive model. The effects of nonuniform sampling, nonlinear transduction at the cones, and a difference of Gaussians operation at the bipolar cell level are incorporated into a *computer retina* model. In addition, the effects of local cone and network feedback mechanisms in adapting the cone sensitivity are modelled. The *computer retina* implementation also accounts for the spatial and temporal aspects of retinal processing, and similar to the retina, provides outputs at two scales to represent the outputs of P-cells and M-cells.

Secondly, adaptive features of the retina which have not previously been modelled are incorporated here. The changes observed in human visual acuity over the cone system's operating range are accounted for by assuming that the degree of coupling between cells in the cone and horizontal cell layers is a function of illumination. In addition, it is speculated that *interplexiform* cells in the retina alter the retina's sensitivity in regions of high spatiotemporal contrast [68], and the effects of such a mechanism are incorporated into the *computer retina*.

The third contribution consists of verifying the behaviour of the *computer retina* model with known data on biological (principally primate) visual systems by replicating a few typical experiments performed by electrophysiologists. The model responses are shown to be qualitatively similar to the biological retina despite the model's simplicity. Furthermore, as the *computer retina* allows its response to be monitored at all stages of processing and for the entire visual field, it serves as a useful tool in visualizing what the outputs of the biological retina may look like in response to complex visual stimuli.

1.4 Model Simplifications

It is beyond the scope of this thesis to present a model of all visual processing occurring within the primate retina. Thus, the scope of the model is limited as follows:

- Only the cone system is modeled. Over much of the retina's response range, the cone and rod systems function fairly independently [70]. The cone system with its high resolution fovea is responsible for our high acuity daylight vision and is thus more appropriate for modeling when considering a potential silicon implementation.

- Only achromatic intensity information is considered. Even though the cone system codes chromatic as well as achromatic information, many visual tasks can be accomplished with pure intensity information. It has also been theorized that, although the chromatic and achromatic information is carried in the same pathway, the two signals may be processed separately at higher levels [33].

- In the biological retina, ganglion cells come in two varieties, *on*-centre and *off*-centre, to code positive and negative contrast signals, respectively. Unlike the biological retina, the computer can represent positive and negative signals equally well in the same output. Thus only *on*-centre type ganglion cell outputs are generated in the model here and are implemented to be able to code both positive and negative signals. This effectively reduces the required number of retinal outputs by a factor of two.

- Many model simplifications are motivated by the desire to implement an "artificial retina" in silicon in the future. However, it is not the objective of this thesis to present a design for a silicon retina.

1.5 Organization of Thesis

This chapter has provided the motivation for studying and modelling the primate retina. Chapter 2 provides a summary of retinal biology and a review of existing models used to explain the flow of information through the retina. Chapter 3 summarizes the various adaptation mechanisms in the retina and the models used to describe them. Chapter 4 presents the adaptive retinal model of achromatic information processing in the primate cone system as developed in this thesis, and discusses some implementation aspects of the *computer retina*. Chapter 5 presents the results of a few experiments which illustrate the behaviour of the *computer retina* and allow a comparison with published data on biological retinas. The final chapter summarizes the contributions of this thesis and provides suggestions for future research.

This chapter presents a summary of the primate retina structure and function and a survey of existing models used to describe retinal functions.

Although a great many types of retinal neurons may be distinguished on the basis of morphology, retinal cells can all be broadly classified into six cell types. These are photoreceptor cells, bipolar cells, horizontal cells, amacrine cells, ganglion cells, and interplexiform cells. Excellent surveys of the anatomical structure of the retina are given by Rodieck [49][48], Dowling [21] and Hubel [28].

The retinal cell bodies are found in three distinct layers. The synaptic contacts between these layers are confined to two interposed synaptic layers which are termed the inner and outer plexiform layers. All visual input to the retina is received first by the photoreceptor cells and then processed by other cells. Likewise, ganglion cells are the only cells in the retina that convey output signals through the optic nerves to the visual cortex of the brain. The outer plexiform layer contains the processes of receptor cells, horizontal cells, and bipolar cells. The inner plexiform layer contains the processes for bipolar cells, interplexiform cells, amacrine cells, and ganglion cells. In general, all signals passing from the the outer to the inner plexiform layer pass through the bipolar cells and exit the retina through the ganglion cells. The lateral networks of horizontal and amacrine cells form indirect pathways which modify and modulate the signal flow through the bipolar and ganglion cells. Figure 2.1 shows schematically the layering of different cells found in the human retina.

2.1   Photoreceptors

As in most other vertebrates, there are two types of photoreceptor cells in the human retina, rods and cones. Anatomically, rods are shaped like thin cylinders, whereas the cones are tapered at one end, and wide and flat at the base. Rods are far more numerous than cones. In the human retina, there are approximately 100 million or more rods compared to between three and five million cones [49].

The rods and their associated circuitry are specialized for operating in low light conditions. By pooling the responses of many rods, the rod system is able to detect single photon events at the expense of a loss of fine spatial resolution. The cones, together with the neural pathways of the cone system, are specialized to operate in brighter illumination conditions and to sample the image at a higher spatial resolution. There are three types of cones (red, green, and blue), each with a different peak spectral sensitivity. Utilizing
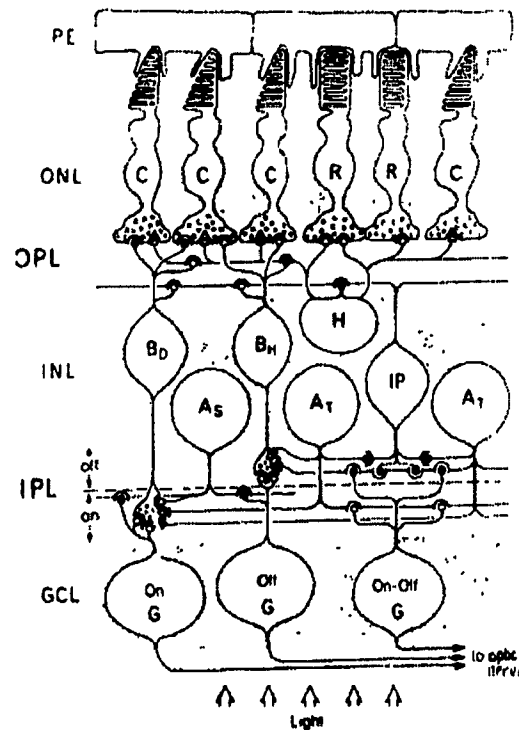
LEGEND

PE — Pigment Epithelium	C — cone
ONL — Outer Nuclear Layer	R — rod
OPL — Outer Plexiform Layer	B_M — midget bipolar
INL — Inner Nuclear Layer	B_D — diffuse bipolar
IPL — Inner Plexiform Layer	H — horizontal cell
GCL — Ganglion Cell Layer	IP — interplexiform cell
	G — ganglion cell
	A — amacrine cell

Figure 2.1: Retinal Cells: Schematic layering of cells in the retina. From Dowling [20], ©1983 MIT Press.

the different spectral sensitivities of each cone type, the cone system encodes chromatic information allowing colour vision to be possible.

Why does the retina require more than one receptor cell type? Rodieck argues that this is likely because the requirement to respond both to very low-energy signals, consisting of a very few quanta, and to relatively high-energy signals lead to conflicting requirements [49]. The rods are about 20 times more sensitive than the cones, and by pooling their outputs, they are even able to detect the reception of single photons during dark adaptation [49]. Maintaining this sensitivity however causes the rods to quickly saturate at increasing light levels. The cones have a much higher level of intrinsic noise, such that their signal output is distinguishable from the noise only at higher light levels [70]. On the other hand, cones continue to adapt their sensitivity to the ambient illumination and operate over many orders of magnitude. Thus, the cone system is responsible for our high acuity chromatic vision in normal daylight conditions, while the rod system is primarily responsible for vision under scotopic (low light) conditions. Separate parallel pathways appear to be used by the rod and cone systems for much of retinal processing, leading researchers to study one system or the other for simplicity [49][31]. The emphasis here will be on the cone system which is responsible for our high acuity vision.

2.1.1 Transduction Process

The primary function of photoreceptors is the transduction of the captured light energy into electrical neural signals. Photon catch is controlled by the amount of visually sensitive pigment contained in the outer segment of the cell. Without any visual pigment, the energy barrier would be too high to permit a receptor cell to capture photons. The visual pigment molecules lower the energy barrier required to catch a photon. The photon capture boosts the pigment molecule into an "excited" state leading to a molecular rearrangement from an 11-cis isomer to the all-trans isomer form. This initiates a chain-reaction of molecular changes and other intermediate products which eventually results in the closure of some channels permeable to Na^+ and Ca^+ on the plasma membrane [49][21].

The closure of sodium channels while potassium channels remain open results in the transmembrane potential moving toward the K^+ equilibrium, thus hyperpolarizing the cell. This potential passively spreads to the synaptic terminals where it alters the rate of release of the transmitter substance. Both rods and cones are known to release transmitter in the dark. Cell hyperpolarization in response to light causes a decrease in this release rate. Although much is known about the rod and cone transduction process today, the nature of the transmitters is still uncertain for most vertebrate species [49][9].

2.1.2 Spatial Distribution

The distribution of the rods and cones is not uniform over the retina. In the center of the retina (called the fovea), there is a rod-free area consisting of densely packed red and green cones. Blue cones comprise only about 8 percent of the total cone population and are found outside the central foveal region regularly interspersed between the two other cone types. The concentration of cones rapidly diminishes with increasing distance from the fovea, while the concentration of rods rises and peaks in the parafovea (area surrounding the fovea) and then also decreases. Figure 2.2 shows the density of rods and cones across the retina as a function of eccentricity (distance from the center of the fovea).
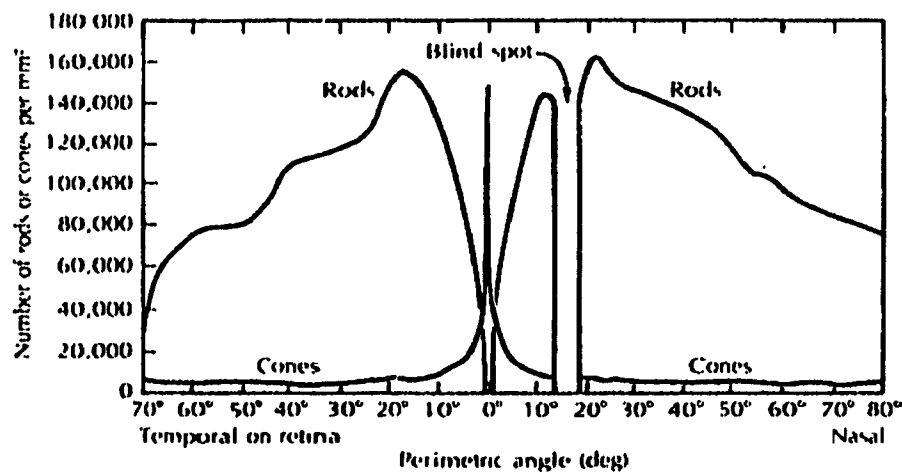
Figure 2.2: Distribution of Photoreceptors: Variation in density of rod and cone photoreceptors with retinal eccentricity. The cone density drops off almost exponentially from a maximum of 140,000 cones/mm^2 in the fovea to about 5,000 cones/mm^2 in the far periphery. Figure from Pirenne [45], © 1967 Methuen & Leo.

Why are the photoreceptors distributed in such a nonuniform manner with very high resolution cone sampling in the center and progressively coarser sampling in the periphery? One of the constraints on the sampling and processing of information in the retina is the fact that only a million or so fibers exit from the retina to the brain. The nonuniform sampling scheme used by the retina is an important data reduction scheme that complies with the transmission bottleneck while still retaining a small central area of high resolution sampling. Attentional and saccadic movements may then be employed by the visual system to scan points of high interest at high resolution [79][23]. Van Essen argues that the exponential drop in photoreceptor density and linear increase in receptive field size of ganglion cells with

retinal eccentricity is evidence for the retina using a scale-invariant sampling strategy in the foveal region [23]. In machine vision, such a retinal sampling scheme is often modelled by space-variant visual sensors with complex-logarithmic geometry [50].

It is puzzling why the biological visual system limits itself to only a million fibers exiting the retina. Why not double that number? It has been suggested that the limit on the number of fibers leaving the retina is not due to the physical constraints of the fibers but rather a constraint imposed by the limited size of the cortex and its ability to process visual information [33][23][32]. As a considerably large fraction of our brain is devoted to visual processing (on the order of 4000 cortical neurons processing visual information for every ganglion cell), doubling the retinal output would also double the cortical machinery required to process it.

Quantitatively, the cone density is the highest in the center of the fovea and approaches 140,000/mm^2. This corresponds to about 7 cones per min^2 of arc. It drops quickly to 25,000/mm^2 within 0.4 mm (1.4 degrees), eventually declining to about 5000/mm^2 in the far periphery [49]. The dropoff in cone density is usually modelled as exponential outside the fovea. If the cone density in the retina were as high everywhere as in the fovea, it would require about 100 times more cones than the number that actually exist!

Although the density of cones is not uniform, the arrangement of the cones follows a very regular hexagonal sampling pattern. There are three types of cones, broken down by their spectral sensitivities (red, green, and blue). The blue cones, which are more sensitive to shorter wavelengths, are much less common than the other two cone types. Because of chromatic aberrations of the eye-lens system, not all wavelengths of light are in focus on the retina simultaneously. In fact the retinal image is quite blurry for the shorter wavelengths that blue cones are sensitive to [49]. Thus this part of the spectrum of the visual signal may be sampled more coarsely and explains the sparsity of blue cone cells. Lennie in fact suggests that colour information as a whole is coded at a fairly low resolution compared to luminance information [33].

2.1.3 Photoreceptor Coupling

In the rod system, coupling between adjacent rods extends the summation area to almost 200μm diameter around the rod. Rod coupling is believed to be part of a mechanism for preventing the saturation of individual rods when they capture a photon. Rather than saturating the response of the rod when a photon is captured, the rod coupling spreads the signal to many rods which all signal the same event together. This signal is then amplified at later stages of processing, thereby increasing the rod system's overall sensitivity [49]

The coupling of cones to neighbouring cones and the presence of gap junctions between

cones is well documented in the periphery [49][70]. Recent anatomical evidence shows that the basal processes of the cone pedicles project laterally to contact nearby cone pedicles of between 6 and 12 cones through gap junctions both within the fovea and outside the fovea [67]. For cones, the effective summation area of coupling has been estimated to have a diameter of $50\mu m$ around the cone [20][70][49]. The coupling is much stronger for cones of the same spectral type than for mixed types [70]. The function of cone coupling is not very well understood, although it probably plays a role similar to noise reduction in the rod system. Psychophysical data shows that visual acuity varies over an order of magnitude in photopic range of light levels reaching a maximum plateau only at moderately bright illuminations [75][65]. At these levels, the acuity closely matches the receptor sampling and ganglion cell densities and rules out extensive cone coupling [2]. However, for dimmer photopic illuminations, visual acuity is much lower and is likely attributable to increased cone coupling [67]. Extensive cone coupling would improve the signal to noise ratio and aid in absolute contrast detection at the expense of slightly lower resolution.

There have been several recent attempts at incorporating some form of receptor coupling in silicon retinas as a means of noise reduction. Yagi et al. [77] and Brill [9] both model receptor coupling with a resistive network that passively spreads the receptor potentials of receptors to neighbouring receptors. The extent of the coupling, and hence relative spread of the receptor signal, is mainly controlled by the relative conductivities of the network interconnecting the receptors as compared to the conductivity of connections from receptor layer to other layers. However, in these models, the degree of coupling does not vary as a function of the illumination level and thus the summation areas are invariant with illumination level.

2.1.4 Horizontal Cell Feedback

In several lower order vertebrates, there is physiological evidence of feedback signals from horizontal cells which inhibit the cone responses [3][17][40][49] and rapidly adapt the cone sensitivity to match the local[1] ambient intensity [21][58]. Feedback from horizontal cells to rods has not been found except for the rods of the gecko[2], which have many cone-like properties and are believed to be "transmuted" cones [21]. Figure 2.3 shows the response of a gecko rod to a flash stimulus with horizontal cell feedback present (left) and the response again (right) when the horizontal cell feedback is inhibited by aspartate treatment [21]. Studies in the tiger salamander by Skrzypek also indicate that the horizontal feedback

---

[1] By local, we imply only information from a small neighbourhood or patch of the retina, centred around the cone, is used to compute the local ambient intensity. The size of this neighbourhood is comparable to the size of horizontal cell receptive fields.

[2] A type of a lizard.
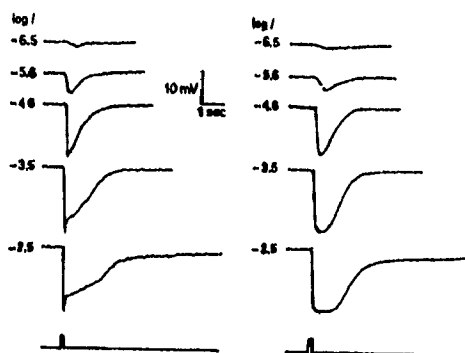
Figure 2.3: Horizontal Cell Feedback: The figure shows the response of a gecko "cone-like" rod cell in response to a flash of light first with inhibitory horizontal cell feedback present (left) and again when the feedback signal is dampened by the application of aspartate (right). Note that the feedback signal is slightly delayed with respect to the receptor signal response and thus serves to sharpen the response. From Dowling [21] ©1987 Harvard University Press.

signal acts to almost instantaneously adapt the sensitivity of the cone response curves to match the local ambient illumination level [60].

There is a small time lag in the feedback signal from the horizontal cells as compared to the receptor signal because of the synaptic delay through the longer feedback path. The horizontal cell feedback sharpens the transient response of the receptors but is not strong enough by itself to drive the receptor response back to its resting potential.

Although physiological evidence for horizontal cell feedback to receptors has been measured in many retinas such as those of the gecko, perch, and goldfish, it is not yet certain that it is present in the human retina. However, it is certainly anatomically feasible [70]. In general, the function of inhibitory horizontal cell feedback is still poorly understood.

A neural network model of the reciprocative excitatory and inhibitory connections between receptors and horizontal cells is presented by Yagi et al. [77] and implemented in VLSI by Boahen [5]. In this model, both the receptor cell layer and horizontal cell layers are modeled as resistive networks. Each neuron in a layer sends a signal to and receives a signal from a corresponding cell in the other layer. Skryzpek presents a different model in which the horizontal cell feedback signal nonlinearly modifies the cone sensitivity and thus forms the basis of a fast cone adaptation mechanism [58].

2.1.5 Adaptation

Over moderate and bright illumination conditions, the rod system saturates, and it is mainly the cone system which signals visual information to the cortex. The cone photore-
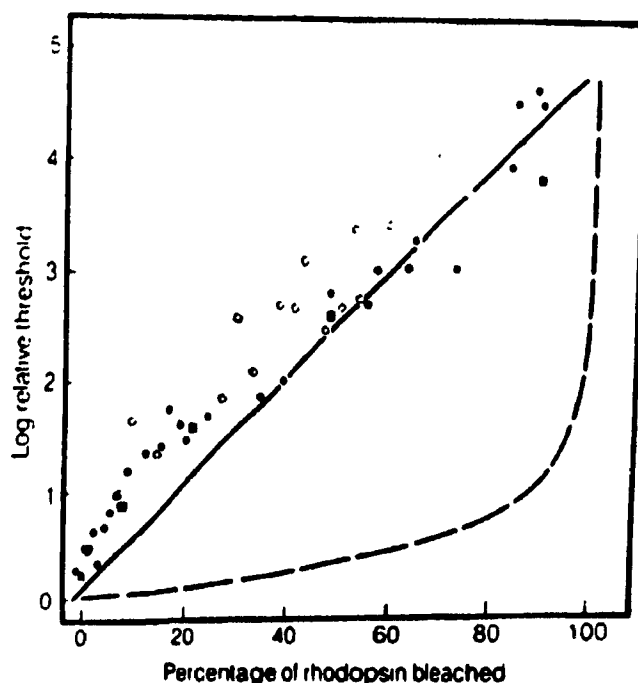
Figure 2.4: Visual Threshold vs. Percentage of Pigment Bleached: The figure indicates the rise in the log visual sensitivity compared to the amount of visual pigment bleached. The data shown here is actually for rods of the skate retina but a similar curve is obtained for cones as well. The dashed line shows the expected rise in visual threshold for rods if reduced photon catch were the only effect of rhodspin pigment bleaching. From Dowling [21] ©1987 Harvard University Press.

ceptors continue to function under illumination conditions spanning an additional five to six log units of illumination intensity right up to their light damage level. The cones operate by continuously adapting their gain to match the ambient background illumination so that the cone outputs remains close to the center of their useful voltage range [71].

A large part of this adaptation mechanism is intrinsic to the cones themselves and is believed to be mainly a result of pigment bleaching. As the light level increases in brightness past a certain point, the photopigment molecules in the cone cells being to bleach. Initially, the cone response may saturate in response to a bright stimulus causing increased bleaching. However, bleaching of the pigment reduces the photon catching ability of the cone so that an equilibrium is eventually reached where the pigment bleaching rate equals the rate of regeneration of pigment. Thus, the cone system does not saturate and is able to operate in increasing levels of illumination. Figure 2.4 shows the rise in visual threshold as a fraction of pigment bleached.

Although pigment bleaching is a major component of sensitivity control in cones at

high illumination levels, psychophysical studies have shown that the cone system adjusts its sensitivity even for illumination intensities that do not cause significant pigment bleaching. These other components are due to several other factors, including neural and synaptic network feedback mechanisms in the retina [21]. These mechanisms (such as the effects of horizontal cell network feedback) are discussed in more detail in chapter 3.

2.1.6 Model of Cell Response

The cone photoreceptors adapt their sensitivity continuously to the ambient background illumination I_a through a mechanism which tends to keep the steady state receptor potential v_a at the middle of its response range ($v_{max}/2$) [12][84]. Figure 2.5 shows the cone response curves at various adapting intensities I_a. For transient changes in intensity I about the adapting level, the receptor potential can be modeled by the following simple saturation equation [32][21][48][84] [12][8]:

$$\frac{v_r}{v_{max}} = \frac{I^n}{(I^n + k(I_a)^n)} \tag{2.1}$$

where
v_r = receptor potential
v_{max} = maximum receptor potential
I = flashed stimulus intensity
n = exponent which is very close to 1 for cones
I_a = ambient illumination intensity
$k(I_a)$ = function value is semi-saturation intensity

The semi-saturation function k is a highly compressive function of the local ambient intensity I_a and is the intensity value at which the receptor potential $v_r = v_{max}/2$. When the local ambient illumination I_a is very high so that v_a is very close to $v_{max}/2$, then $k(I_a) \approx I_a$. Boynton [8] suggests a linearized semi-saturation $k(I_a)$ function based on a best fit of the quantitative data and related to pigment bleaching:

$$k(I_a) = \frac{k_r}{k_b}I_a + k_r \tag{2.2}$$

where
k_r = half-saturation constant (833 trolands)
k_b = half-pigment bleach constant (1000 trolands)
I_a = local ambient illumination intensity

Other photoreceptor models include one by Curlander [17] who presents a dynamic model of photoreceptors in which the receptor potential is the output of an N-stage reaction equation. Inhibitory feedback from horizontal cells is also incorporated into this model. However, for our purposes, the simple saturation function given above is a reasonably

CONE RESPONSE vs FLASH INTENSITY
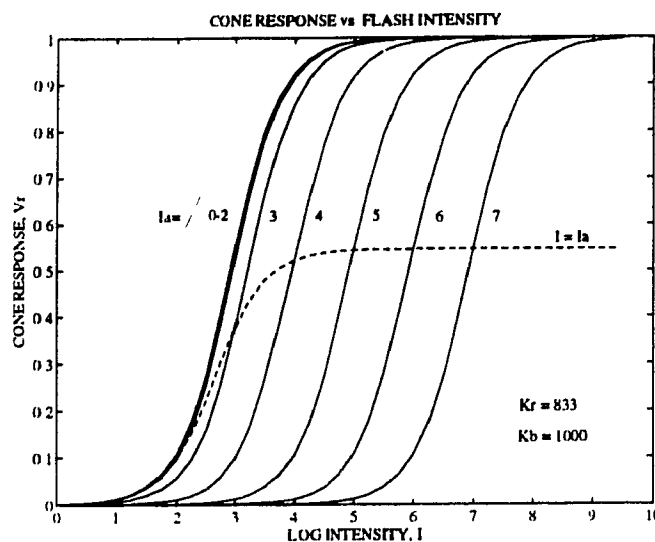
Figure 2.5: Cone Response Curves: The figure shows the expected response of cone photoreceptors v_r with variation of flash intensities I superimposed on various background illumination intensities I_a. The log of the background intensity I_a is indicated at the top of each curve At any one given background intensity I_a, the cone response saturates with a 2 5 log unit change in flash intensity. However, the entire curve shifts to the right to match any I_a, thereby allowing the cone to adapt to any ambient illumination level. The dashed curve shows the steady state response of the cones when the local intensity matches the ambient intensity I_a All intensities are in units of trolands.

accurate model of the receptor response.

2.2 Horizontal Cells

2.2.1 Cell types

At least two types of horizontal cells have been found in every vertebrate studied so far. In primates, two morphologically different horizontal cells are found and these are termed 'HI' and 'HII' [49].

The HI horizontal cell has a tiny cluster of dendritic processes near the cell body which contact several cones and a long axon which extends several millimeters before branching into an extensive teleodendritic [3] arborization connecting to a number of rods. Although the electrophysiology of horizontal cells has not been studied in primates, in all species in which it has been studied, the cells are found to generate graded potentials which spread

---

[3] Dendritic like processes on the end of an axon.

17

passively through the cell. In addition, because of the very long length of the axon, it has been shown that signals generated at the two ends of the horizontal cell do not interact [49]. HI horizontal cells contact all the cone pedicles within their dendritic fields regardless of the cone type and thus carry only brightness information. These horizontal cells are also sometimes classified as luminosity (L-type) horizontal cells.

The HII horizontal cell differs from the III horizontal cell in a number of ways. The IIII cell does not contact every cone within its dendritic field but may make contact with only cones of the same spectral type. In addition, the axon of this type of cell is much shorter, so that about 15% of the amplitude of a signal generated by the cell body (from cone input) spreads to the end of the axon [49]. The HII horizontal cell is also sometimes referred to as a chromaticity (C-type) horizontal cell.

It appears that each cone makes at least one or more connections to each type of horizontal cell. The horizontal cells also synapse onto bipolar cells and are known to form the antagonistic surrounds of the bipolar cell receptive fields.

2.2.2 Receptive Fields

In almost all species studied so far, the receptive field sizes of the horizontal cells are much larger than their actual dendritic spread, often being 40-100 times larger [21]. The very large receptive field sizes are the result of gap junctions between horizontal cells with relatively low resistance, which passively spread current from one horizontal cell to neighbouring horizontal cells. The extent of this electrical spread is controlled by the relative conductivity of the gap junctions compared to that of the horizontal cell walls.

The dendritic spread of horizontal cells grows linearly with eccentricity so that in the far periphery, hundreds of rods and cones may be contacted by a single horizontal cell. This scaling of dendritic field size with eccentricity seems to be a general principle used in the retina. It is a means of data reduction at the expense of progressively coarser resolution with eccentricity.

2.2.3 Horizontal Cell Function

Like the cone, the steady-state horizontal cell response may also be fit to the Michaelis-Menton saturation equation with the exponent $n = 0.7$ (see equation 2.1) [21]. Compared to the cone receptors, horizontal cells have a much shallower response curve and thus are able to signal up to 4 log units of change in input illumination intensity from threshold to saturation as compared to only 2.5 log units for cones.

Electrophysiological measurements of horizontal cell potentials in fish and other lower vertebrates show the horizontal cell layer to act like a purely resistive network for signals of

up to 100 Hz [40]. The horizontal cell layer behaves like a resistive sheet that spreads and diffuses signals received from the receptors and thus computes some sort of spatial average of these signals.

Mead [39] and Curlander [17] model the horizontal cell layer as a resistive network with a small capacitance, driven by inputs from many photoreceptors at discrete points. The horizontal cells then spread the current collected from the receptors and derive a spatially and temporally averaged signal. The extent of spread of the signals, and thus the effective size of the receptive fields of the horizontal cells, is controlled by the conductance of the gap junctions modelled by the resistivity in the network. This kind of operation is usually modelled by a Gaussian-weighted averaging operation or a diffusion process in computer vision [32][51][82]. It has also been shown that the conductance of these gap junctions is modified by signals from interplexiform cell; this may be another sensitivity control employed by the retina [21][68][78].

Due to the peculiar nature of contacts made by the horizontal cell, it is not always possible to know where the output of the horizontal cell goes or in which direction information is flowing. There exists fairly convincing evidence that the horizontal cells form the antagonistic surround portion of the bipolar cell receptive fields. In some species, such as the rabbit retina and the carp, it appears that the bipolar cell surround field is partially mediated through an inhibitory feedback from the horizontal cells to the cones [40]. In other mammals, there are instead direct ribbon synapses from horizontal cells to bipolar cells [49]. In humans, the exact nature of the information flow from horizontal cells remains uncertain.

Experiments done by Naka [40] on catfish retinas indicate that there is some signal transmission directly from horizontal cell axons to ganglion cells [40]. Information on the mean luminance level is required by the brain for tasks such as pupillary control and a rough judgement of brightness. It is possible that these horizontal cells with axons to the innerplexiform layer could be serving this function. However, there is no mention of such horizontal cells with axons in Rodieck's authoritative anatomical description of the primate retina [49].

In summary horizontal cells have large receptive fields which sum information from a large number of photoreceptors. The outputs of the horizontal cells play a role in influencing the information flow at the bipolar cell level as well as sensitivity control at the cone cell level.

2.3 Bipolar Cells

2.3.1 Bipolar Cell Classification

In primates, there are several anatomically distinguishable types of bipolar cells. Many of these bipolar cells either have their cell bodies in distinctly different layers, or selectively make contact with only rods or only cones, or synapse in the inner plexiform layer in different sub-layers and thus connect to different types of ganglion cells.

Rod Bipolars

In mammals, there is only one type of bipolar cell making direct contact with rods and it is aptly named the rod bipolar. There is likely a secondary pathway for rod information through inter-photoreceptor contacts as well, although it is not well understood. Each rod bipolar cell contacts between 15 and 45 rods in the central area, while each rod contacts an average of 2.5 bipolar cells [49]. Adjacent rod bipolar cells thus have dendritic fields overlapping by about 20 percent. The dendritic field size increases with eccentricity, and in the far periphery, many hundreds of rods may converge onto a single bipolar cell.

Cone Bipolars

In contrast to the single type of rod bipolar, there are at least six types of cone bipolars in the primate retina. Anatomically, Polyak has classified them into four different clusters based solely on their dendro-dendritic spreads [49]. Recently, Boycott has distinguished yet another subclass of bipolar cell named 2C [7]. Figure 2.6 shows the clustering of bipolar cell types based on Polyak's classification and these are described below:

- **Midget cluster:** These bipolar cells have small dendritic fields. In the central area, each midget bipolar cell contacts on average only one cone. There are two varieties of midget bipolars; those with invaginating ribbon synapses and those with flat connections to the cone photoreceptors.

- **Diffuse cluster:** Each diffuse bipolar contacts six or seven cones in the central area. It is not known if these contact cones of the same spectral type only or mix signals from different cones. However, considering the tight bottleneck of transmittable information through the optic nerve, these cells may be extracting information not readily extracted from the midget bipolar pathway. Like the midget cluster, the diffuse cluster contains bipolar cells with either invaginating or flat connections to the cone photoreceptors.
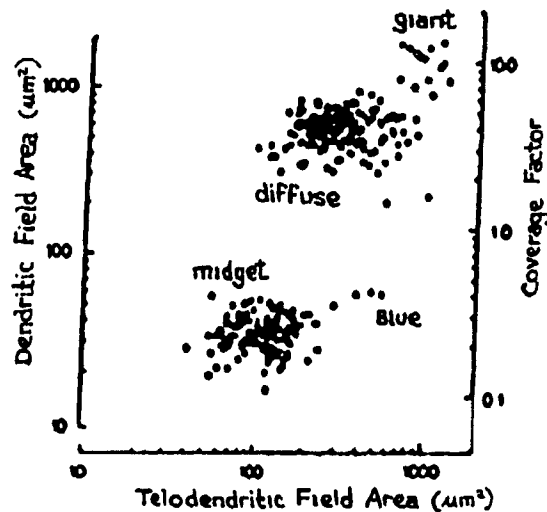
Figure 2.6: Bipolar Cell Types: Scatter diagram of dendritic field area versus teleodendritic field area of bipolar cells lying in a 1.4mm^2 strip 6.2-8.0 mm from the fovea in a whole-mounted *Macaca nemestrina* retina. Using this classification, four natural clusters of bipolar cells are observed and are labeled as midget, diffuse, blue, and giant. Data from Rodieck [49].

- **Blue cone cluster:** The complexity of connections made by the blue cones remains unclear; they connect to a few cones but skip over many cones to do so. The spread of blue cone bipolars closely matches the spacing of blue cones at all eccentricities in the retina.

- **Giant cluster:** This cluster contains bipolar cells having much larger dendritic fields (50μm - 100μm) which contact approximately 20 cones in the central region.

- **2C cluster:** These cells are similar to the midget bipolar cells except that they contact two or more cones. They are very rare in the central fovea but become much more frequent outside the fovea. Boycott suggests that these may be functionally similar to midget ganglion cells [7].

2.3.2 *On*-centre and *Off*-centre Pathways

There are at least four distinct bipolar cell information pathways for the more common red and green cones. The midget and diffuse bipolar cells split cone information into two pathways. In addition to this, in both the midget bipolar and diffuse bipolar clusters, there is a dichotomy of cells that depolarize with centre field illumination (*on*-centre) and those that hyperpolarize with centre illumination (*off*-centre). The *on*-centre cells correspond

anatomically to the bipolar cells with invaginating terminations at the photoreceptors. The hyperpolarizing, *off*-centre bipolar cells make flat connections onto the receptors.

This *on/off* dichotomy is also exhibited anatomically in the inner plexiform layer where the axons of the bipolar cells terminate and contact ganglion cells. The inner plexiform layer is divided into different sublaminae. The axons of the *on*-centre bipolar cells terminate in what is called sublamina "b" in the lower part of the inner plexiform layer (IPL) where they make contact with *on*-centre ganglion cells and amacrine cells. The axons of *off*-centre bipolar cells terminate in the upper part of the IPL in sublamina "a" where they synapse with *off*-centre ganglion cells and amacrine cells. Richter [17] and Rodieck [49] cite evidence that different transmitters are involved in the *on* and *off* pathways, and that the *off* pathway is slightly slower than the *on* pathway. The connectivity of bipolar cells to amacrine and ganglion cells in the inner plexiform layer and its significance will be covered in the description of the amacrine and ganglion cells.

Why are there both *on* and *off* pathways in the retina? It is well known that neurons reliably code information only by increasing their firing rate from their resting rate. For firing rates lower than the resting rate, the inter-spike interval times become significantly long, and the signal to noise ratio is reduced. Thus to signal the presence of dark features on bright backgrounds as effectively and quickly as bright features against darker backgrounds, two pathways are required. In addition, by utilizing both the *on* and *off* pathways, the effective dynamic range of signals coded by the ganglion cells is doubled [2][32].

2.3.3   Bipolar Cell Function

The bipolar cells form one part of the direct pathway for information flow from the photoreceptors to the ganglion cells. The bipolar cell's receptive field consists of a circular center field driven directly by the photoreceptors and a much larger antagonistic surround field that is driven by signals from horizontal cells. The bipolar cell is generally assumed to compute a difference function between receptor and horizontal cell signals feeding into it.

The bipolar cell signals only differences of the receptor inputs as measured against the local background average signal provided by the horizontal cells. The bipolar cell illumination response curve is much steeper than that of the photoreceptors and goes from threshold to saturation within a little more than one logarithmic unit change of centre field intensity [71]. Thus, the bipolar cell effectively indicates contrast in the image with a high gain.

As the antagonistic surround signal from the horizontal cell is slightly delayed compared to the center inputs from the cones, the bipolar cell is also responsive to temporal changes in the signal [24].

In addition, since each midget bipolar cell connects to only one cone photoreceptor in the fovea, this is likely the pathway for high visual acuity. These bipolar cells are also color opponent, with the center and surround of the receptive fields having different spectral sensitivities. The most prominent are those with red/green (R/G) opponency, with a much fewer number of blue/yellow (B/Y) opponent cells. The antagonistic receptive field structure of midget bipolar cells permits it to code both achromatic and chromatic information on the same channel [23][33]. The midget bipolar cells provide input to parvocellular (P) ganglion cells which form the high acuity visual pathway (described in a later section).

The role of the diffuse cluster of bipolar cells that contact several cones in the fovea is not as clear. It is possible that these bipolar cells contact cones of only a single spectral type and receive antagonistic surround input from the HIII horizontal cells. The other alternative is that they receive information from cones of mixed spectral types and form the basis of the magnocellular (M) ganglion cell pathway. This pathway is characterized by cells with large receptive fields, little colour sensitivity, and properties significantly different from the parvocellular (P) ganglion cells.

The blue cluster is much more sparse and is again likely involved with one of the colour pathways. The giant bipolar cells are also much less common than the midget and diffuse bipolar cells and have very large receptive fields. Consequently, these cells are not likely part of the direct high acuity visual pathway, but rather are used for extracting information at a much coarser grain.

2.3.4 Bipolar Cell Summary

- Most results show the bipolar cell to perform a difference function between receptor signals and an antagonistic horizontal signal [39].

- The ratio of diameters of the center field to the diameter of the surround field ranges from 1:5 to 1:10 in most vertebrates [21]. The size of the surround field correlates well with the size of the horizontal cell receptive fields at all eccentricities [28].

- Fleet [24], Richter [47], Naka [40] and Dowling [21] all give biological evidence that the antagonistic horizontal cell input to the bipolar cell is delayed compared to the receptor inputs. This gives the bipolar cell a small transient spike which can be thought of as a crude time differentiation operation [47].

- Rodieck [48] shows that the bipolar cell dynamic range is very narrowly tuned and goes from threshold to saturation with only about a 1.6 log unit change in center intensity. The antagonistic horizontal signal serves to center the response range around the local average signal, thereby maximizing the available response range [39]. This subtractive

process is an important factor in the transformation of the visual signal from intensity to contrast [26].

- Curlander [17] and Richter [47] both model the bipolar cell response $V_b(r,t)$ as a temporal low pass filter characteristic, and spatially, as a high pass filter using a linear model:

$$V_b(r,t) = [k_{br}V_r(r,t) - k_{bh}V_h(r,t)] * h_b(t) \qquad (2.3)$$

where k_{br}, k_{bh} are constants whose sign and value depend on the type of bipolar cell. $V_r(r,t)$ and $V_h(r,t)$ are the receptor and horizontal cell potentials, respectively, with r being the radial spatial variable and t being time. The spatial differencing operation performs the spatial high pass operation which is then convolved with the temporal low pass impulse response of the bipolar cell $h_b(t)$. This equation may be used to model both the midget and diffuse class of bipolars by appropriately adjusting the receptive field sizes and constants k_{br} and k_{bh}.

2.4 Interplexiform Cells

The interplexiform cells are unique in the retina in that, although their cell bodies lie in the inner plexiform layer, they act pre-synaptically and post-synaptically in both the outer and inner plexiform layers, making contact with both horizontal, bipolar, and amacrine cells. Not much is known about the distribution or physiological function of the interplexiform cell, and in fact, it has only been relatively recently that these cells have been studied at all [21][68].

From studies in fish, it has been found that interplexiform cells release dopamine which locally reduces the conductivity of the gap junctions between horizontal cells and thus diminishes the size of their receptive fields [21][28][49][68]. This also tends to increase the sensitivity of bipolar cells to centre illumination as the size of the inhibitory surround is reduced. Studies in fish indicate that interplexiform cells release dopamine under extreme dark adaptation, at the threshold of vision when only the rod system is active, and also in the photopic illumination range in regions of high spatiotemporal contrast (flickering lights, spatial edges) [68].

No models of the interplexiform cell function have been proposed to date. However, the ability of interplexiform cells to vary the receptive field (RF) size of other cells is clearly advantageous from a retinal information processing point of view [62][81]. Srinivassan [62] puts forth an argument on the need for modulating the RF size of the inhibitory surround field of ganglion cells based solely on tradeoffs between signal-to-noise ratio and acuity in the coding of information. He suggests that the horizontal cell RF size (which accounts for

the ganglion cell inhibitory surround field) should diminish as the illumination level rises and the signal-to-noise ratio improves. A similar argument is used in a very different model applicable to the rod system put forth by Yellott [81]. Zeevi [83] also suggests that the interplexiform cell could provide this feedback in the retina for gain and sensitivity control.

In summary, the interplexiform cell collects signals from a large area in the inner plexiform layer, likely from many bipolar and amacrine cells. It feeds this signal back to the horizontal cells in the outer plexiform layer where it locally modifies the effective horizontal cell receptive field size. It is predominantly involved in a regulatory function and is an important mechanism of gain and sensitivity control employed in the retina.

2.5 Amacrine Cells

2.5.1 Amacrine Cell Types

Amacrine cells are generally defined as those cells lying in the inner plexiform layer which lack an axon. All vertebrate retinas studied so far show amacrine cells with a dazzling diversity of morphological forms and an impressive number of different neurotransmitters [49]. It has been estimated that there are about 20 types of amacrine cells in the human retina [38].

No one knows why there are so many types of amacrine cells. They may be partly responsible for many of the more complex receptive field properties such as orientation selectivity and movement detection found in some vertebrate retinas. However, this does not explain why cats or primates, with their much simpler centre-surround receptive field properties, need such a rich diversity of amacrine cells. Some of the amacrine cells have been implicated in the rod pathway, linking signals from the rod bipolar cells to ganglion cells [63]. They also may be involved in the centre-surround organization of change-sensitive ganglion cells [71]. However, this still does not explain the need for such a large number of amacrine cell types.

Despite this rich diversity, Masland [38] indicates that if one groups the amacrine cells based on the density of their dendritic fields over the retinal surface, they fall naturally into three groups:

1. Frequent, narrowly-branched cells

2. Sparse, widely-branched cells

3. Densely overlapping cells
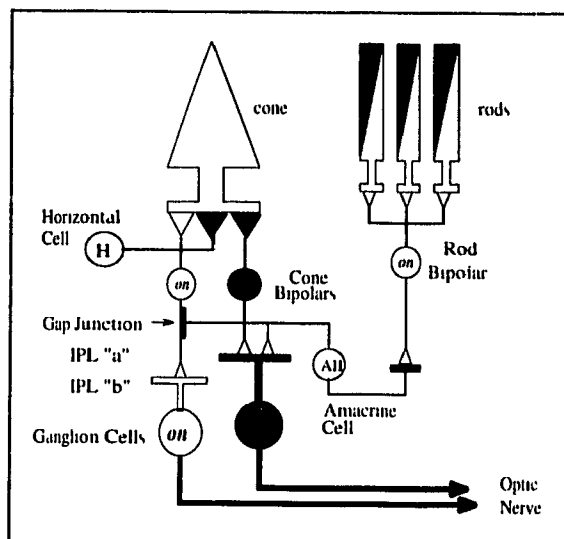
Figure 2.7: Schematic of AII Amacrine Cell Wiring: The figure shows schematically how the AII amacrine cells signal rod information to ganglion cells. The gap junction made by the AII amacrine cells with *on* cone bipolar cells produces responses in the cone bipolar cells that mimic the responses of the *on* rod bipolar cells and the AII amacrine cells. The AII cells also make synaptic junctions with *off* ganglion cells. Thus the AII cells allow both *on* and *off* ganglion cells to be excited by the rod system

Frequent narrowly-branched cells

These amacrine cells are densely packed with narrow dendritic fields. They include the type AII amacrine cells which have been extensively studied in the cat. Kolb and Sterling have implicated the AII amacrine cell as an obligatory pathway for information flow in the rod system of the cat [49][63]. Rod bipolar cells appear only to make direct contact with *on*-centre ganglion cells in sublamina "b". However, it is known that the *off*-centre ganglion cells also receive both rod and cone inputs. The AII amacrine cell is believed to communicate the rod signals from the terminations of rod bipolars in sublamina "b" to sublamina "a", where they form an inhibitory input either directly onto *on*-centre ganglion cells or via some of the cone bipolars that also terminate there. Figure 2.7 shows a schematic diagram of this geometry.

The fact that the AII cells are part of the direct pathway of information flow is consistent with the finding that they are densely packed with very little spread of their dendritic fields. Other similar amacrine cells that synapse with the cone bipolars have also been found but little is known about them or their function[38].

Sparse, widely-branched cells

These amacrine cells are much more sparsely distributed but have very wide-spreading dendritic fields enabling them to cover the entire retina. Due to their small number and the large spread of their dendritic fields, it is postulated that these cells play a global or regulatory function which modulates the information flow in the retina, but do not form a direct pathway for this information.

An example of such a cell is the dopaminergic cell known to make synaptic contacts with type AII amacrine cells [38][49]. A single dopaminergic cell may contact several AII amacrine cells. Thus a relatively sparsely-distributed amacrine cell is able to become a control point which can influence the direct pathway of rod information throughout the AII amacrine cells.

Densely overlapping cells

This class contains numerous amacrine cells with wide and densely overlapping dendritic spreads. Examples of these are the cholinergic cells and indoleamine-accumulating cells [38]. In the rabbit retina, there are approximately 290,000 cholinergic cells compared to about 350,000 ganglion cells. These cells have dendritic fields ranging from 250 μm in the central retina to 800μm in the periphery. The indoleamine-accumulating cells are a second group in this class that have dendritic field sizes ranging from 300μm in the central retina to 1000μm in the periphery, with dendritic overlap factors of 30 to 60 [38]. Again, the function of these cells is poorly understood.

2.5.2 Cell Function and Models

Except for the AII amacrine cells implicated in the rod pathway, very little is known about the functional role of any of the amacrine cells in primates or any other vertebrate species [49].

Werblin suggests that some amacrine cells play an inhibitory role in forming the centre-surround type receptive fields of change-sensitive or transient ganglion cells [71]. In his experiments, the response of change-sensitive ganglion cells to changing centre input was reduced or inhibited if there were corresponding changes also presented in the surround field of the ganglion cell. He attributed this inhibition as coming from the amacrine cells. Thus in his model, the amacrine cell layer provides inhibitory input to the ganglion cells from a large diffuse area, one that matches the ganglion cell receptive field surround size. These amacrine cells are somehow sensitive to changes in illumination in their receptive fields due to either a spatial or temporal change in the visual image.

Richter and Ullman [47] also implicate the amacrine cells in cats to be computing tem-

poral derivatives of the visual signals through inhibitory recurring synapses feeding from these amacrine cells back to bipolar cells which drive them. The outputs of these amacrine cells are then assumed to feed into the Y-type ganglion cells of the cat which are more sensitive to transient inputs.

In summary, no satisfactory model exists for any of the amacrine cells for any of the cone pathways.

2.6 Ganglion Cells

2.6.1 Cell Types

Ganglion cells are the only retinal cells that provide signals carried on the optic nerves leaving the retina. In fact it is the ganglion cell axons which comprise the optic nerve. This fact also makes them one of the easiest cells to study and ganglion cells have been extensively examined by recording responses to various stimuli and measuring the activity of optic nerve fibers [22][27][61][52].

Ganglion cells, like bipolar cells, come in a variety of morphological forms. However, in primates, midget and parasol class ganglion cells constitute 80% and 10% of the population, respectively. These two classes of cells form two distinct streams of information which flow from the retina to the lateral geniculate nucleus (LGN) and diversify further in the cortex. The midget ganglion cells project to the parvocellular layers of the LGN and are termed P-cells. The parasol ganglion cells project mainly to the magnocellular layers of the LGN and are termed M-cells.

The remaining 10% of the ganglion cells come in a variety of forms and do not project to the LGN but instead project primarily to the superior colliculus. Some of these include cells such as shrub ganglion cells, ganglion cells of the blue-cone pathway, and biplexiform ganglion cells. The biplexiform ganglion cells are truly surprising as they not only make conventional synapses with rod bipolars and amacrine cells but also have some erratic dendritic arborizations which branch and directly connect to about 25 rod spherules [49]. These ganglion cells appear to serve very specialized functions and provide the necessary information to the superior colliculus for such things as pupillary control and eye movements. They will not be considered further here.

Anatomically, the midget ganglion (P) cells are small, closely spaced and have narrow dendritic fields. In the foveal region, each midget ganglion cell likely connects to only one cone bipolar and thus preserves the private pathway for each cone [33][49]. The parasol ganglion (M) cells have much larger dendritic fields (approximately 3-4 times larger) than the P-cells at all eccentricities [33]. The anatomical differences between the midget (P) and parasol (M) ganglion cells is further supported by their different electrophysiological

responses to various stimuli.

The P-cell and M-cell class of ganglion cells are further divided into two subclasses based on their response to illumination presented to the centre of their centre-surround receptive fields. Separate *on*-centre and *off*-centre pathways exhibited at the bipolar cell level are maintained at the ganglion cell layer. The *on*-centre ganglion cells have their dendritic fields synapsing with *on*-centre bipolar cells in sublamina "b" of the IPL and the *off*-centre ganglion cells connect to *off*-centre bipolars in sublamina "a" [63]. The implications of this are that in the central foveal region, there are about two ganglion cells serving every cone which split the information into signals of opposite polarity.

2.6.2 X/Y Classification

There is a very large body of literature describing the properties of cat ganglion cells [22][27][52][61]. Thus primate ganglion cells are often compared to or categorized based on the classifications used for cat ganglion cells [57].

Cat ganglion cells are classified into X, Y and W type cells based on their physiological properties [22]. X-cells account for about 55% of the ganglion cells in the rod-dominated retina of the cat while Y-cells account for 5% of the population. All other cells are lumped into W-type ganglion cells. X-cells basically behave linearly with respect to summation of subunit inputs while Y-cells are quite nonlinear. Both X and Y cells have high contrast gains and simple centre-surround receptive fields. X-cells respond better in a sustained manner to stimuli, whereas Y-cells show a more transient response.

For primates, P-cells are often compared with or classified as X-cells, while M-cells are classified as Y-cells. However, Shapely [57] shows that this grouping has many inconsistencies and thus may really not be valid.

2.6.3 Spatial Distribution

It has been estimated that there are between 1.1 and 1.3 million ganglion cells in the human retina. This compares to approximately 5 million cones and 100 million rods which initially sample the visual image.

Although in total, cones outnumber ganglion cells by a factor of five, the number of ganglion cells serving the foveal region actually exceeds the density of cone photoreceptors as there are two midget ganglion cells for virtually every cone in the fovea: one serves the *on*-centre pathway, and the other the *off*-centre pathway. In addition, the cone spacing in the fovea very closely matches the resolution of the image projected by the optics of the eye-lens system. Thus acuity in the fovea is neither limited by the cones nor the ganglion cells [2].

However, outside the fovea, ganglion cell density falls off much faster than the cone density. Figure 2.8 shows the density of ganglion and cone cells with variation in eccentricity [32]. The psychophysically measured acuity in the periphery is much worse than the image quality available to the retina and the acuity that could be expected with the cone spacing in the periphery [2]. In the periphery, the ratio of cones to ganglion cells increases sharply and thus visual acuity is limited by the ganglion cell spacing rather than the optics of the eye or the cone sampling [23].
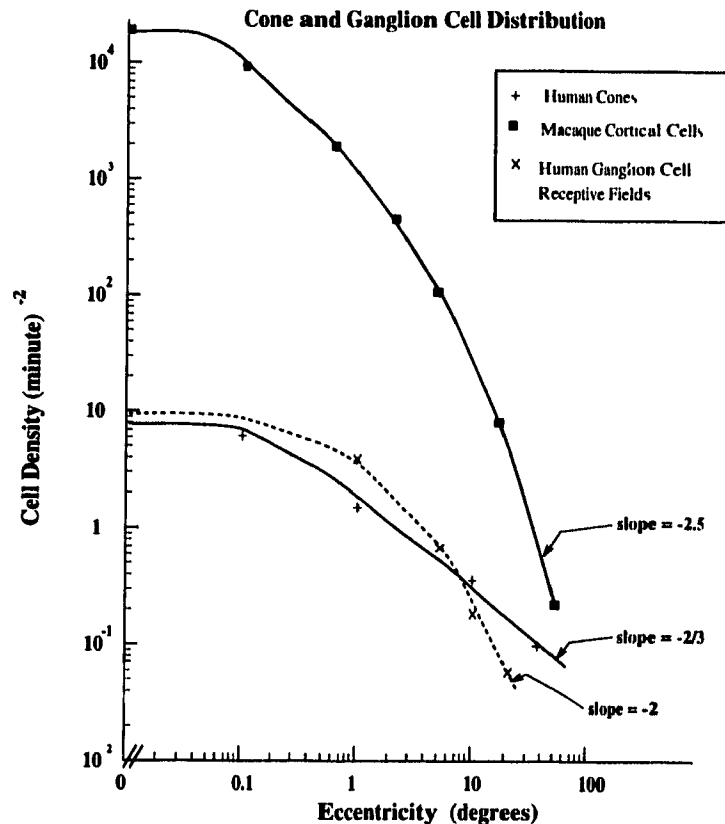
Figure 2.8: Cone and Ganglion Cell Densities: The figure shows the distribution of human ganglion cells and cone receptors with respect to retinal eccentricities. For humans, the ganglion cell density slightly exceeds the cone density for eccentricities less than 8 degrees. For retinal eccentricities greater than 5 degrees, the ganglion cell density decreases much faster than the cones. The figure also shows the density of cortical neurons in a Macaque monkey that are processing visual information at a given eccentricity. Figure adapted from Kronauer [32] ©1985 IEEE.

Although M-cells represent 10% of the ganglion cell population, there are some studies which indicate that in the very central foveal region, the M-cell population is much sparser than this [33]. Outside the fovea, M-cells are uniformly distributed in a regular sampling lattice which accounts for 10% of the ganglion cells.

The ganglion cell dendritic spreads and thus their receptive field diameters increase almost linearly with eccentricity for both P-cells and M-cells. Figure 2.9 shows the variation of receptive field size of P-cells and M-cells with eccentricity [23]. The receptive field size of M-cells increases about 3 times faster than the P-cells. The percentage overlap factor of receptive fields is approximately constant outside the fovea [23] and is estimated to be 50% based on macaque monkey data[76].

GANGLION CELL DENDRITIC FIELD SIZES vs. RETINAL ECCENTRICITY
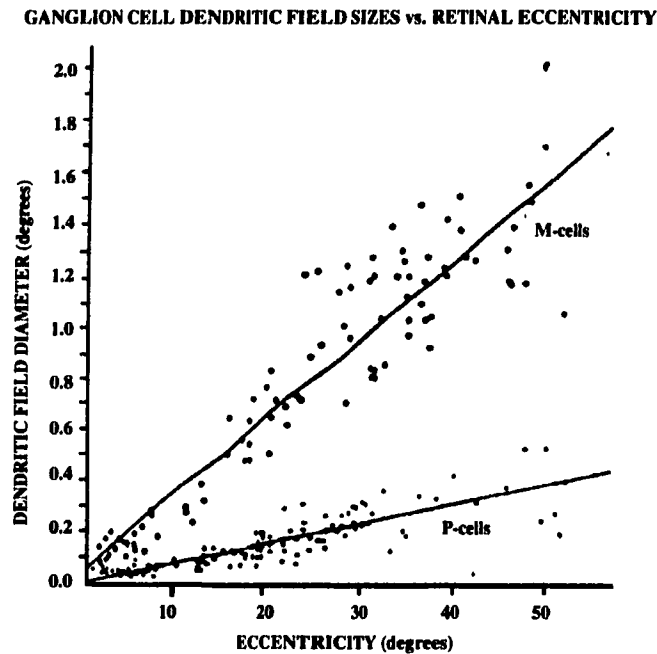
Figure 2.9: Ganglion Cell Dendritic Field Sizes: The figure shows the variation with eccentricity of ganglion cell dendritic field sizes of parasol (M) cells and midget (P) cells. At all eccentricities, the diameters of dendritic fields of M-cells are about 3 times larger than those of P-cells. Data re-plotted from Van Essen [23].

Van Essen and Anderson[23] argue that the retina employs a scale invariant sampling strategy with linear increase in ganglion cell spacing. Using linear degradation in resolution with eccentricity, they argue that the image can effectively be represented by 350,000 sampling nodes. Next, they define the functional multiplicity of ganglion cells or equivalently the "retinal coverage factor" to be the number of ganglion cell receptive fields of a given class which overlap one another at each sampling node in the retina. Using this as a basis, in the fovea the functional multiplicity of ganglion cells is about 2 per sampling area corresponding to the on and off pathways of the P-cell lattice [23]. As one moves further out into the periphery, the sampling regions become much larger with widely overlapping receptive fields. Thus for P-cells, for a given sampling node in the periphery, there may be as many as 3-5 ganglion cells whose receptive fields fall into that region. For M-cells, which have

a much larger and widely overlapping receptive fields, the functional multiplicity starts at about 2 per area just outside the fovea and increases to as much as 6-10 per area in the periphery. This may contribute to the increase of sensitivity to peripheral motion.

2.6.4 Receptive Field Properties

The receptive field properties of ganglion cells have been studied quite extensively in both cats and primates [16][22][27][35][47] [57][61][63][69][47][71]. Both P-cells and M-cells have simple centre-surround receptive fields which are usually assumed to be circularly symmetric. This is in contrast to some lower vertebrates such as the frog or rabbit retinas whose ganglion cells exhibit some fairly complex receptive field properties such as direction selectivity, and motion selectivity [21]. However, by extracting and coding such specialized information in the retina, much of the original visual information is discarded in the retina and cannot then be recovered by the cortex. For much more sophisticated visual systems, it seems that the retina is relegated to performing more basic signal processing on the initial visual signal, leaving as much raw information as possible for further processing in the cortex.

The receptive field of a ganglion cell is usually represented mathematically in the literature by a difference of two Gaussian functions, one computing the response due to the centre and the other, much wider Gaussian responsible for the antagonistic surround (see Figure 2.10). The output of the ganglion cell is represented as the convolution of this "difference-of-Gaussians" function with the input image sampled by the cones. This operation results in enhancement of local contrast or edges and the suppression of uniform background signals. This of course ignores all of the intermediate processes previously described.

Marr and many others looked on such an operation as evidence that the retina was extracting and coding *edge* information about the visual image [37]. Others have considered it as the coding of local *contrast* by the retina rather than absolute luminance. Cleary, *edge* and *contrast* information concern spatial properties in the image and are thus related. It is doubtful that the purpose of the ganglion cells is just to extract edge information in the image or to code contrast since the retina also codes information regarding the dynamic and spectral components of the visual image. It is more likely that the information coded by the ganglion cells is a result of the constraints imposed by the dynamic range mismatch at the input and output to the retina on the one hand, and the transmission bottleneck imposed by the optic nerve on the other. The multiple parallel pathways of information in the retina suggest that several different types of information are extracted by the retina and coded onto the same channels at the ganglion cell level [33].
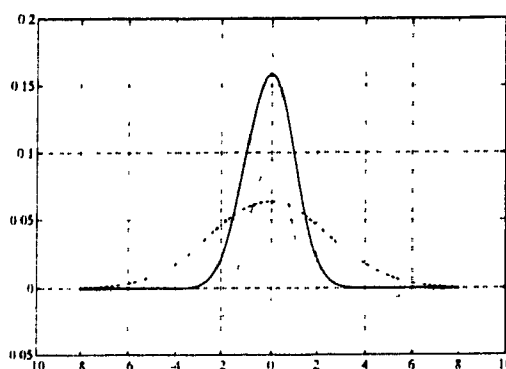
Figure 2.10: Ganglion Cell Receptive Field: The figure shows how the summation of inputs to the ganglion cell are weighted. The receptive field consists of two regions The centre circular region consists of a narrow Gaussian-weighting of direct inputs from bipolar subunits (solid line). The inhibitory surround region is represented by a much wider Gaussian (dashed line) and is the result of indirect input from horizontal cells onto the bipolar cells and amacrine cell input to ganglion cells. The result is a "Mexican hat" function used very extensively in computer vision (dotted line).

2.6.5 The P-cell Pathway and Functional Role

As these cells account for 80% of all ganglion cells in the primate retina, P-cells likely form the basis of our high spatial acuity vision. In the fovea, they have very small dendritic spreads, matching the width of the narrow dendritic termination of a single midget bipolar. Electron microscopy studies by Kolb [30] have shown that P-cells in the fovea receive direct input mainly from a single midget bipolar cell and a very small number of synapses from other bipolar cells. However, the bipolar cell providing most of the central input does not make contact with any other ganglion cells. Kolb's data indicate that the midget bipolar cells make exclusive contact with single midget ganglion cells in the fovea. In addition, it appears that midget ganglion cells also receive input from amacrine cells as there is an equal number of synapses from amacrine cells as from bipolar cells.

As a result of the centre field being derived from a single cone, and the surround consisting of mixed inputs from cones of all different spectral types, the P-cells also exhibit color opponency. Most P-cells are red/green opponent cells, with a much smaller proportion of yellow/blue opponent cells. The yellow/blue opponent cells represent about 7% of the P-cells matching the proportion of blue cones in the retina. Kolb argues that the yellow/blue pathway is served not by midget ganglion cells, but by a separate class of giant ganglion cells which also project to the Parvocellular region of the LGN [30]. This differs from the

views put forth by Rodieck [49] and Sterling [63] who include the yellow/blue pathway as part of the P-cell path.

The red-green opponent P-cells are well suited to respond to achromatic spatial contrast at moderate and high spatial frequencies and to low frequency chromatic patterns modulated in time. Although P-cells carry most of the color information about the image, psychophysical studies indicate that this is only a small percentage of the information relayed by P-cells [33]. Acuity for isoluminant gratings is only about one-tenth of that for luminance gratings at all eccentricities [33]. However, the contrast sensitivity is approximately eight times higher for isoluminant chromatically opponent gratings than achromatic gratings [11].

P-cells generally give sustained responses to a maintained stimulus. Their response is best for patterns modulated at 10 Hz, and they are often unable to follow stimulus modulations more rapid than 20-30 Hz. P-cells in the fovea can resolve gratings of 50 cycles/degree which closely matches the psychophysically measured acuity [23].

The P-cell response is fairly linear with respect to summation of inputs from bipolar and amacrine cell subunits. In this respect, it is very similar to the X-type ganglion cells in the cat [33][24]. In fact, in much of the literature, primate ganglion cells are often classified using the X- and Y- type dichotomy used for cat ganglion cells.

Fleet and Jepson [24] model the ganglion cell receptive field properties as the difference of two Gaussians with different spatial and temporal characteristics. The centre and surround Gaussians have different time constants of integration; the surround is slightly delayed with respect to the centre. This agrees with the physiologically known data and is similar to the model used by Richter and Ullman[47]. Using Fleet's spatiotemporal centre-surround (CS) filter, both the spatial and temporal characteristics of the P-cell can be modelled by adjusting the ratio of time and space constants between the centre and surround inputs.

The linear centre-surround spatiotemporal filter (CS) is defined by the following equations:

$$CS(\mathbf{r}, t) = \alpha_c K(t; \tau_c) G(\mathbf{r}; \sigma_c) - \alpha_s K(t - d; \tau_s) G(\mathbf{r}; \sigma_s) \tag{2.4}$$

$$G(\mathbf{r}; \sigma) = \frac{1}{2\pi\sigma^2} \exp \frac{-|\mathbf{r}|^2}{2\sigma^2} \tag{2.5}$$

$$K(t; \tau) = \begin{cases} \frac{1}{\tau} \exp \frac{-t}{\tau} & \text{if } t \geq 0, \tau > 0 \\ 0 & \text{if } t < 0 \end{cases} \tag{2.6}$$

where

τ_c	= centre time constant (ms)
τ_s	= surround time constant (ms)
σ_c	= centre Gaussian width (μm)
σ_s	= surround Gaussian width (μm)
d	= surround time delay (ms)
$K(t; \tau)$	= low pass impulse response
$G(r; \sigma)$	= 2D Gaussian spatial filter

In the model, the P-cell output is the product of the spatially radially symmetric centre-surround (CS) filter with the visual input image. The P-cell output amplifies both the local spatial contrast and temporal change in the visual signal. A block diagram of this process is shown in Figure 2.11.
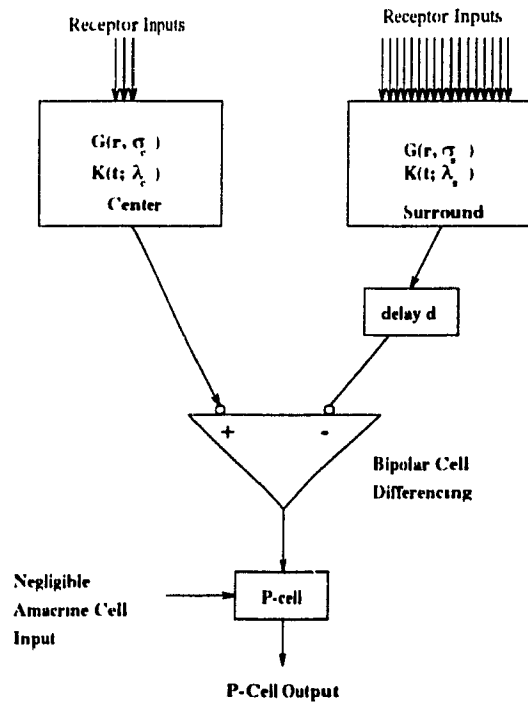
Figure 2.11: Centre-Surround Spatiotemporal Filter:

2.6.6 The M-cell Pathway and Functional Role

M-cells are slightly more complex than P-cells. Although the majority of M-cells behave as linear filters over most spatial and temporal frequencies, some M cells have nonlinear responses.

M-cells have much larger cell bodies and receptive fields than P-cells and scale in size linearly with eccentricity just like P-cells. Their receptive field diameters are approximately

35

3 times larger than P-cells at all eccentricities. The M-cells (parasol ganglion cells) receive direct input from the diffuse bipolar cells which contact several cones. It is not clear if the M-cells receive centre input from only one diffuse bipolar cell or several bipolar cells. However, due to the large size of their receptive fields, they likely receive input from several bipolar cells. M-cells also possess many reciprocal synapses between amacrine cells, diffuse bipolar cells and the ganglion cells.

As such, M-cells are tuned to respond more to temporal changes in the visual input and code spatial information at a coarser level. M-cells account for only 10% of the ganglion cells in the retina and thus form a much sparser sampling lattice than the P-cells. As a result, M-cells are only able to spatially resolve gratings with spatial frequencies less than 20 cycles/deg. Temporally, they respond best at patterns modulated at 20 Hz but can follow modulations as high as 60-80 Hz [33].

M-cells do not show much colour opponency and for the most part respond only to achromatic contrast. They are very sensitive to low contrast but begin to saturate in the presence of higher contrast signals.

M-cells are often compared to the nonlinear Y-type cells in the cat. Shapely [57] shows that this analogy is valid only for a small fraction of the M-cells. For primates, most M-cells (95%) have simple receptive fields and sum inputs linearly like the cat X-cells and primate P-cells and thus may be labelled M_X. Only about 5% of M-cells sum inputs nonlinearly and behave like the cat Y-cells and are thus labelled M_Y.

Fleet and Jepson[24] propose that much of the temporal characteristics of M_Y-cells can be modelled by the same spatio-temporal filters that are used to model P-cells but with the parameters tuned more specifically for temporal differentiation (see equations 2.1-2.6).

For Y-type cells, Richter and Ullman [47] model the response as being a nonlinear summation of inputs from bipolar cells and amacrine cells. The amacrine cells in their model form reciprocal synapses with the bipolar cells to achieve a temporal derivative of the bipolar cell signal. The nonlinearity of subunit summation is achieved by separating positive and negative contrast signals and weighting them differently.

Shapely suggests that the primate M-cells have properties of both the X-type and Y-type cells in the cat [57] and that P-cells are an additional system in primates which accounts for our high acuity chromatic vision. M-cells have also been explained in terms of multiple channel theory as being the coarse resolution *on* and *off* channels, while P-cells form the fine resolution channels [34]. To summarize, M-cells signal visual features at a coarser spatial grain and respond better to high temporal frequencies as compared to P-cells. The properties of P-cells and M-cells are summarized in Table 2.1.

Table 2.1: P-type and M-type Ganglion Cell Properties

P-cell properties	M-cell properties

- midget class ganglion cell
- small cell bodies,
  small axons, dendritic arbors
	- parasol class ganglion cell
	- larger cell bodies, axons.
	  and larger dendritic arbors
	- faster axon conduction vel.

- 80% of ganglion cells - projects to Parvo LGN - response peak at 10 Hz - cutoff freq at 20-30 Hz	- 10% of ganglion cells - projects to Magno LGN - response peak at 20 Hz - cutoff freq at 60-80 Hz
- sampling multiplicities: - fovea: 2 per sampling area - periph: 3-5 per area	- sampling multiplicities: - fovea : 2 per sampling area - 15 deg: 4 per area - periph : 10 per area

- small receptive fields
 	
- linear increase in size of
  rec. field with eccentricity
	- receptive fields 3-4 times
	  larger than P-cells.
	- linear increase in size of
	  rec. field with eccentricity

- linear summation of subunit inputs to P-cell - low contrast sensitivity - large contrast range - respond to high spatial freq - can resolve 50 cycles/deg - color opponent - fine sampling lattice - code contrast well	- 80% of M-cells are linear - 20% of M-cells are nonlinear - high contrast amplification - low saturation threshold - sensitive at lower spatial freq. - can resolve 20 cycles/deg - little color opponency - coarser sampling lattice - saturate with high contrast
- high spatial acuity	- fast flicker detection - fast low contrast motion

2.7 Overall Summary of Retinal Structure and Function

The retina is a highly structured neural network that extracts and pre-processes visual information from the image projected upon it by the optics of the eye. The processed information is subsequently transmitted to the cortex through the optic nerves. The style of processing performed by the retina is dictated by two main requirements. One requirement is that the retina must function in an environment where the ambient illumination intensity changes over several orders of magnitude. The second requirement is that all information extracted by the retina must be transmitted through a limited number of optic fibers by ganglion cells with a very limited dynamic range of firing rates. This limitation on the amount of data that may be transmitted requires the retina to perform considerable data reduction and is one of the reasons for a foveated retinal sampling scheme.

The retinal structure has been well mapped through anatomical studies. However, the functional nature of many of the retinal cells is still a mystery or at best poorly understood. In simplest terms, retinal cells can be classified as falling into one of six types. However each one of these comes in various subtypes and reflects the multiple parallel pathways of information processing in the retina.

To meet the input dynamic range requirements, the retina uses two photoreceptor types, rods and cones, to subserve different regions of the image intensity domain. The rod system provides low resolution but high sensitivity vision down to the threshold of photon detection. The cone system consists of a high resolution fovea with rapidly decreasing sampling density in the periphery. The cone system operates at higher light levels, and is able to continuously adapt its sensitivity to the ambient background illumination up to the light-damage limit.

The output of the receptor cells is next processed by bipolar and horizontal cells. Each horizontal cell connects to many receptor cells and computes some sort of an averaging or summation function. The receptive field size of these horizontal cells is many times their dendritic field size by the virtue of passive conduction of current across gap junctions between adjacent horizontal cells. The conductivity of these gap junctions is controlled by feedback received from interplexiform cells. It is the horizontal cell that is believed to account for the surround fields of the bipolar and ganglion cell receptive fields.

The bipolar cells essentially compute a difference operation between the receptor signal and the horizontal cell signals. Their receptive field consists of two parts; the centre is stimulated by inputs from the receptors; the much larger surround reflects the input from horizontal cells. The different time constants of integration in the photoreceptor and horizontal cell layer, in addition to a small delay of the horizontal cell inputs, results in temporal as well as spatial differentiation.

The splitting of visual information into different streams is readily observable at the

bipolar cell level. An *on*-centre and an *off*-centre receptive field split of information is started at the bipolar cell level and continued to the ganglion cell level. In addition, the scale at which information is extracted is further subdivided by two major classes of bipolar cells. Midget bipolar cells connect to a single cone thus maintaining high resolution pathways, while diffuse bipolars contact several cones and thus likely code information at a coarser level.

The outputs of bipolar cells feed into amacrine cells, interplexiform cells, and ganglion cells. The function of amacrine cells, which come in a large variety of forms, is still very poorly understood. Some of the amacrine cells have been implicated in the rod system pathway, while others are known to have a diffuse, regulatory function which controls how other neurons in the retina process visual information. In addition, inhibitory input from amacrine cells is believed to be responsible for the transient nature of responses of change-sensitive ganglion cells. One of the functions of the interplexiform cells seems to be to adapt the nature of the bipolar and ganglion cell receptive fields by modifying the conductivity of gap junctions in the horizontal cell layer.

The ganglion cells form the output of the retina. They receive input from bipolar cells and amacrine cells. Two major classes of ganglion cells account for about 90% of the ganglion cell population.

Midget ganglion cells (P-cells) receive input mainly from midget bipolar cells and project to the parvocellular layers of the LGN. These cells account for 80% of the ganglion cell population and form the high spatial acuity, chromatic pathway. They exhibit simple circular centre-surround receptive fields which increase in size linearly with eccentricity. P-cells respond to both chromatic and achromatic signals.

The parasol ganglion cells (M-cells) have larger receptive fields than P-cells at all eccentricities and their outputs project mainly to the magnocellular layers of the LGN. These cells account for only 10% of the ganglion cell population. It is not clear whether the M-cells receive input only from diffuse bipolars or a mix of midget and diffuse bipolar cells. These cells respond better to higher temporal frequencies at the expense of lower spatial resolution. Amongst other things, these cells form the pathway for fast, low contrast motion detection.

This chapter has summarized the structure and function of biological retinas. The next chapter addresses and summarizes adaptation mechanisms within the retina that enable it to operate over a wide range of illumination conditions.

At any one ambient illumination level, the physiological response range of individual photoreceptors spans only 3 log units of intensity from threshold to saturation (see Figure 3.1) [21][8]. However, various adaptation mechanisms present in the retina which shift the operating range of the receptors to match the background illumination level allow the visual system to function over an impressive 12 orders of magnitude of illumination intensity [48]. The narrow response range of individual photoreceptors permits the visual system to respond with high gain to local variations in contrast, while the adaptation mechanisms which shift the operating point of the individual photoreceptors extend the overall dynamic range of the visual system. Most of these facts have been mentioned in the previous chapter on retinal structure and function but are summarized in this chapter.
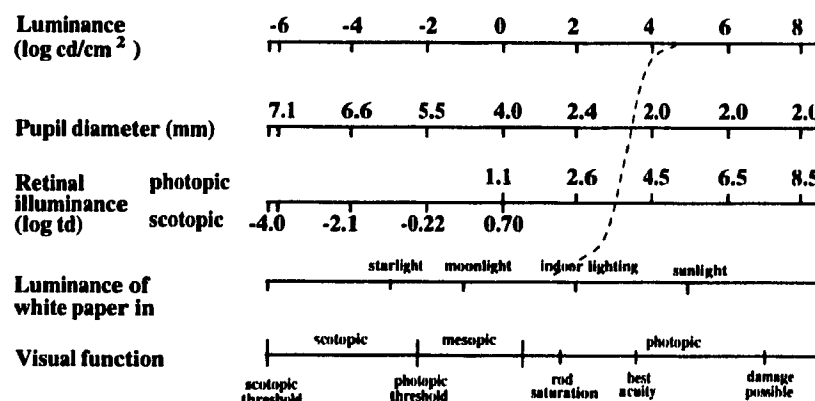
Figure 3.1: Visual System Operating Range: The figure shows schematically the operating range of the visual system. The dashed curve represents the cone stimulus-response function of a single cone at one background intensity. Around this background illumination level, the cone has a response range of about 3 log units. The overall cone system response range is achieved by adaptation mechanisms that shift the entire stimulus-response curve along the intensity axis to match the ambient illumination level. Retinal illuminance for the cone system is measured in photopic trolands which are defined as the product of luminance (cd/cm^2) and pupil diameter (mm). Data from Walraven et al. [70].

One way in which the retina accomplishes this task is by trying to maintain lightness constancy over most of its dynamic range: "One aspect of lightness constancy is to maintain uniformly high sensitivity at the receptor stage regardless of variations in local or global ambient light level" [58]. The overall retinal response range is facilitated by adaptation mechanisms that shift the response range of photoreceptors to be centred around the local ambient illumination level. This extends the receptors' operating range while still main-

taining high contrast sensitivity. In addition, receptoral and post-receptoral mechanisms discard much of the dc-like background illumination information. Thus, they primarily process contrast information and thereby make better use of the limited transmission bandwidth available at the optic tract.

Certain camera systems are also able to function over a wide range of illumination levels [64]. However, there are key, differences between the two in the manner of their operation and in their response to scenes containing a very wide range of intensities. The clarity with which the retina is able to process visual scenes with illuminations that span several log units of intensity is due to the very **local** sensitivity control exhibited by the retina starting right at the photoreceptor level. In contrast to the retina, the sensitivity of photosensing elements in commercial camera systems is controlled by a measure of the **global** ambient illumination level. Around this illumination level, individual camera photoreceptors respond only to a small dynamic range of intensities. In a scene containing a very wide range of intensities, many regions would be either washed out (saturated sensors) or too dark (below sensor threshold) for a globally adaptive camera system but would be handled easily by a retina with local gain control. Clearly, locally adaptive control at the photosensing stage is a desirable feature in machine vision systems and has sparked some recent research interest: one actual implementation includes Mahowald's silicon retina with adaptive photoreceptors [36].

In addition to local gain control, other adaptation mechanisms adjust receptive field sizes of various retinal neurons in response to the prevailing local ambient illumination level. These mechanisms trade off visual acuity against absolute contrast detectability. At low illumination levels when the input signal-to-noise (SNR) ratio is fairly low, larger receptive fields improve the output SNR ratio and thus aid contrast detection. At much higher illuminations, when the input SNR is already high, receptive field sizes are shrunk in order to improve the acuity of the system.

It is apparent that several mechanisms are employed by the retina to achieve its impressive dynamic range. These may be broken down into the following categories:

- Pupillary Control

- Separate Rod and Cone systems

- Receptoral Mechanisms

- Post-Receptoral Mechanisms

Each of these items is discussed in turn in the following sections.

3.1 Pupillary Control

One manner in which the visual system controls the amount of light entering the retina is by adjusting the eye's pupil size. As the light level increases, the pupil diameter decreases. However, the pupil size is only controllable to a factor of sixteen [70]. This still leaves over 10-11 orders of magnitude of illumination intensity with which the retina must contend.

3.2 Separate Rod and Cone Systems

To cope with the still large range of retinal illuminations encountered, two separate photoreceptor systems are used. Individual rod photoreceptors are about 25 times more sensitive than cones. Still higher sensitivity is achieved in the rod system by pooling the responses of many hundreds of rods to so that even the detection of a single photon is possible [70]. In response to increasingly brighter illuminations, the rod system exhibits response compression and saturation. In the presence of daytime illumination, the rod system saturates. This is where the cone system functions the best. Cones are much less sensitive than rods but are able to adapt their sensitivity no matter how bright the illumination is, even right up to their light damage limit.

For much of retinal processing, the rod and cone systems are relatively independent systems. The rod system serves the lower seven orders of magnitude of the visual system's dynamic range while the cone system serves the upper seven orders. Figure 3.1 illustrates this fact. It is only in the the mesopic region (twilight conditions) that rod and cone systems are both contributing to the visual signal leaving the retina. Anatomical studies of the merging of rod and cone pathways have been performed in the cat [63], but in general these interactions are still poorly understood and for simplicity are ignored in this work.

3.2.1 Rod System Adaptation

Rod adaptation has been studied in considerable detail and summaries of this topic may be found in [41][21][43]. Rod light and dark adaptation is controlled largely by the degree of pooling, not only at the receptor level through rod coupling, but also at a post-receptoral site, likely the horizontal cell layer [49][81]. In addition, as the rod system is normally functioning at very low light levels, photon statistics and background noise play a large factor in governing the sensitivity of the rod system [81][84].

The arrival of photons is statistically Poisson distributed [81]. The level of noise due to random photon arrival times grows as the square root of ambient intensity. As a result, the signal-to-noise (SNR) ratio also grows as the square root of the ambient intensity (SNR $\propto \sqrt{I}$) [81]. Yellott shows that the reliability of absolute contrast detection depends on the

total "photon catch" [81]. Thus, at very dim illuminations, when the noise is comparable to the signal, absolute contrast detection is improved if the rod signals are summed over a much larger area. Some estimates indicate summation of several hundreds or thousands of rods signals may be occurring at dim illuminations [49][70].

A model proposed by Cornsweet and Yellott [14][81] based on photon statistics and adaptive pooling of signals models many aspects of the rod system very well. According to this model, as illumination levels increase, the signal-to-noise ratio also increases and the area of summation or pooling in the rods system is decreased. This results in improved acuity with increasing illumination. The features of rod adaptation will not be discussed further here as we are primarily concerned with the cone system.

3.2.2 Cone System Adaptation

At photopic illumination levels, the input signal-to-noise ratio is sufficiently high that photon noise is not a large factor in determining the cone system sensitivity [70]. The system must instead contend with intrinsic noise such as spontaneous cone pigment isomerizations, often called "dark noise". This dark noise likely sets the absolute threshold for the cone system.

In contrast to the rod system, a large part of the sensitivity in the cone system is controlled right at the photoreceptor level. Adaptation mechanisms within the cone shift its response curves laterally to be centered around the local ambient illumination level, thus allowing the limited response range of the photoreceptor to signal local intensity variations with a higher gain. This makes functional sense as it removes the burden of having to cope with a large range of signals for all subsequent retinal neurons. This local control is due to both the effects of cone photopigment bleaching and feedback from horizontal cells.

In addition to these receptoral mechanisms, there are several post-receptoral mechanisms which modify the input signal adaptively. Both receptoral and post-receptoral mechanisms will be summarized in the following sections.

3.3 Receptoral Mechanisms

3.3.1 Weber's Law and Lightness Constancy

Over the photopic range of light levels, the human visual system obeys Weber's law. This law states that at any given background illumination level, the added stimulus intensity required for a change to be just noticeable is proportional to the background illumination level. This kind of behaviour results in lightness constancy [59]

This behaviour is due in large part to multiplicative and subtractive cone photoreceptor adaptation mechanisms which cause the entire cone stimulus-response curves to shift

laterally while leaving the shape of the curves virtually unchanged along the background intensity axis (see Figure 2.5). An example of a multiplicative mechanism is pigment bleaching. Subtractive mechanisms are exhibited both at the photoreceptor level (through horizontal cell feedback) and at the bipolar cell level. All of these mechanisms will be briefly discussed in the following sections.

3.3.2 Time Course of Adaptation

Studies of light and dark adaptation in cones have shown there to be several components that together contribute to the cone system sensitivity. The components may be grouped as either being photochemical in nature or as network mechanisms involving a feedback path either within the cone itself or from horizontal cells. The relative contributions of photochemical and network mechanisms over the dynamic range of the cone system are shown in Figure 3.2(a). Network mechanisms quickly adapt the cone system sensitivity even for illumination levels too dim to cause significant photopigment bleaching.

The different components of adaptation may also be distinguished by their time course during cone light and dark adaptation [21][42]. There are both fast and slow components to cone light and dark adaptation. Light adaptation is very rapid and the cone potential reaches a steady state within 1-2 seconds, with most of the potential change complete almost instantaneously [21]. It is believed that this fast adaptation is mediated by network feedback to the cones from horizontal cells [60]. Dark adaptation is much slower and more readily observable. Figure 3.2 (right) shows schematically the time course of cone dark adaptation while (left) shows the relative contributions of network and photopigment mechanisms to the steady state cone potential in cone light adaptation. The initial recovery of sensitivity in dark adaptation occurs relatively quickly (within 200 ms) and is likely limited by "receptor persistence"[1] rather than horizontal cell feedback [21]. The slower component of cone dark adaptation is generally attributed to regeneration of photopigment within the cone and is noticeably slower (taking 5-7 minutes to reach a plateau).

3.3.3 Photochemical Adaptation

The effects of photopigment bleaching have been studied extensively [18]. Pigment bleaching controls the sensitivity of the cone system for all light levels bright enough to bleach a significant portion of the photopigment [8][21]. The efficiency of photon catch of a photoreceptor is controlled by the amount of photo-sensitive visual pigment present in the receptor. Absorption of a photon starts a chain-reaction of events which results in the breakdown of

---

[1]receptor persistence is the phenomenon of continued perception of a visual signal to a stimuli that has been removed for a short instant
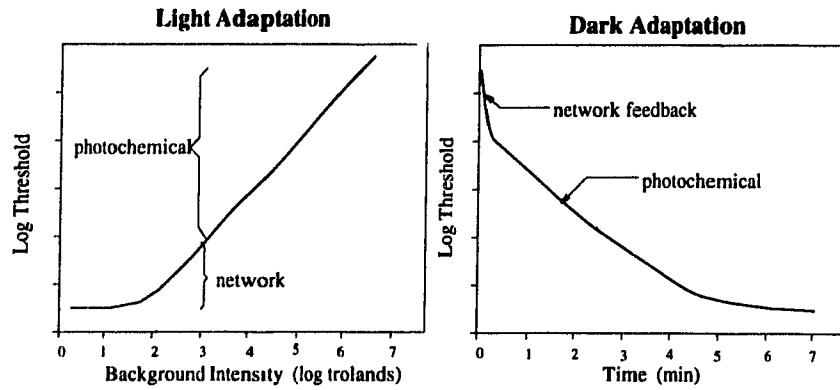
Figure 3.2: Light and Dark Adaptation: The figure on the left shows schematically the relative contributions of the photochemical and network feedback mechanisms in cone sensitivity adaptation. At low background intensities, network mechanisms cause cone thresholds to rise despite the absence of photopigment bleaching. At higher illumination levels, pigment bleaching is more prominent and controls the overall sensitivity. The figure on the right shows the time course of the recovery of sensitivity in dark adaptation. The initial fast recovery drop in cone thresholds is due to fast network mechanisms such as horizontal cell feedback to the cones. Subsequent recovery of sensitivity is due to the much slower photopigment regeneration. From Dowling [21] ©1987 Harvard University Press.

the pigment molecules. These are also constantly being regenerated. Equilibrium is reached when the rate of pigment bleaching equals the rate of pigment regeneration. This mechanism allows the cone photoreceptor to continuously adjust its photon catching ability to match any illumination level, even one that is energetic enough to damage the receptor.

The effects of pigment bleaching are approximated by assuming that the efficiency of quantum catch is logarithmically proportional to the remaining amount of (un-bleached) visual pigment. This implies that the effects of pigment bleaching would be similar to the effect of a neutral density-filter that scaled down the original image intensity levels [70].

The equations modeling bleaching-type adaptation are summarized by Chang [10] and are repeated here for completeness. The model includes two stages: (1) The "adaptive process" which involves bleaching-type kinetics, and (2) the "response function" which is the Michaelson-Menton equation used to model response saturation. The dynamics of photoreceptor bleaching-type kinetics are described by the following first-order differential equations:

$$\frac{dp(t)}{dt} = -[k_1 I(t) + k_2]p(t) + k_2 \tag{3.1}$$

$$Q(t) = k_3 I(t)p(t) \tag{3.2}$$

$$p(I_T) = p(t \to \infty) = \frac{k_b}{I_T + k_b} \qquad (3.3)$$

where I(t) is the light intensity, p(t) describes the fraction of unbleached pigment and the sensitivity of the photoreceptor at time t, and Q(t) is the rate of quantal absorption. k_1, k_2 are rate constants, and k_3 is a constant of proportionality. The steady-state fraction of unbleached pigment is given by equation (3.3) where I_T is the local temporal ambient illumination level and k_b is the half-bleach constant (the illumination level at which half the pigment is bleached). The cone "response function" is described by the Michaelson-Menton saturation equation:

$$v_r(I(t)) = \frac{Q(t)^n}{Q(t)^n + (k_r)^n} v_{max} \qquad (3.4)$$

where $v_r(I(t))$ is the response voltage of the receptor, v_{max} is the saturation voltage of $v_r(I(t))$, k_r is the half-saturation constant, and n is a positive constant which determines the slope of the nonlinear function. Upon substitution of equations (3.2) and (3.3) into equation (3.4), with $k_3 = 1$, one obtains

$$\frac{v_r(I(t))}{v_{max}} = \frac{I(t)^n}{I(t)^n + (\frac{k_r}{k_b} I_T(t) + k_r)^n} \qquad (3.5)$$

Boynton [8] reports a good fit of the curves obtained by equation (3.5) for recordings of receptor potentials in monkey cones using values for k_r and k_b of 833 and 1000 photopic trolands for k_r and k_b respectively with $n \approx 1.0$.

The effects of pigment bleaching alone are insufficient to explain the very fast adaptive properties of the retina or adaptation in lower light levels. The retina adapts its sensitivity even for illumination levels that do not cause significant bleaching of the photopigment [21]. This fast and powerful adaptation process is generally attributed to network feedback mechanisms (such as feedback from the horizontal cell layer).

3.3.4 Horizontal Cell Feedback

Network feedback adaptation mechanisms operate even in dim lighting conditions where pigment bleaching is negligible. One such mechanism that operates at the photoreceptor level is a fast inhibitory feedback from the horizontal cells to the cones.

The horizontal cells compute a local spatiotemporal average of the cone signals [40]. The contacts made by horizontal cells onto cone "pedicles" serve not only as the signal source for the horizontal cells but also act as a feedback path from the horizontal cells back to the

cones. The difference between the horizontal cell signal and the individual cone potential nonlinearly modifies the cone sensitivity to match the local ambient intensity. Skrzypek [58] presents an approach in which inhibitory horizontal cell feedback may be used to *iteratively* estimate an effective local spatial ambient illumination I_S. In addition to this multiplicative effect, there may also be a small degree of subtractive inhibitory feedback from horizontal cells to the cones. Evidence for this has been found in many fish retinas [3][21][40] and is anatomically feasible in the primate retina[49]. Figure 3.3 shows schematically the bidirectional connection between cones and horizontal cells.
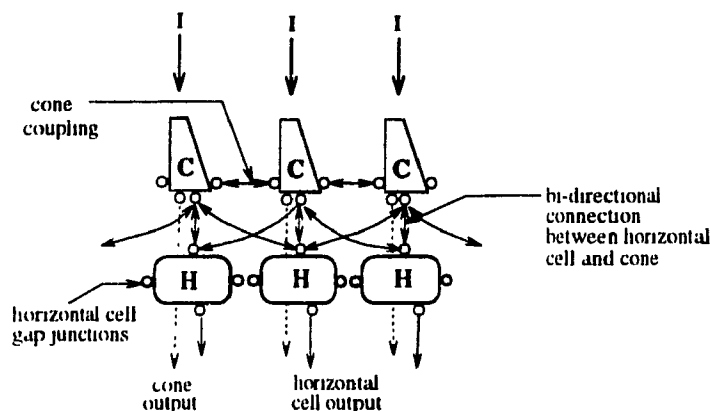
Figure 3.3: Horizontal Feedback to the Cones: The figure shows schematically the wiring of the feedback loop between horizontal cells (H) and cones (C) The arrows show the direction of information flow The cones convert light intensity (I) information into electrical signals used by the rest of the network Each cone is coupled to neighbouring cones. The contacts made with horizontal cells are bi-directional Each cone provides a signal to several horizontal cells which in turn slightly inhibit the neighbouring cone responses and alter the adaptation state of the cones by returning the cone potential to near the centre of its operating range Cones also provide signals to bipolar cells (represented here by dotted lines).

Chang [10] shows that the estimated spatial ambient illumination I_S (using Skryzpek's model [58]) can be used to adapt the cone sensitivity function in the same manner as pigment bleaching (I_S replaces I_T in equation (3.5)). The horizontal cell signals are used to iteratively compute an effective spatial ambient intensity I_S which then drives the adaptation of the semi-saturation function in equation (3.5). Skrzypek's model ignores temporal factors such as the feedback signal delay introduced by the relatively slow integration time constant within the horizontal cell layer. This delay in the feedback loop introduces pronounced transient oscillatory behaviour on the cone output signal in response to a step input. However, intracellular recordings of cone and bipolar cell potentials only show a single small dip in the output potential following the peak step response [41][47][55][72]. This effect can be attributed to a small inhibitory effect of horizontal cell signals on the cone output (see Figure 2.3). Skrzypek avoids the oscillation problem by iterating the

computation until the cone sensitivity stabilizes and then re-computing the outputs of the cone and horizontal cells. Although the *manner* in which cone cells adjust their sensitivity may be different than the simple iterative scheme proposed by Skrzypek, anatomical and electrophysiological evidence still points to horizontal cell feedback as the most likely source for the fast sensitivity adjustment by cones.

Subtractive inhibitory feedback from the horizontal cell signal has little effect on the cone adaptation state but serves to sharpen the cone signal to transient changes in the input while reducing the cone output by a small fraction (see Figure 2.3) [21]. Judging by eye from the figure, the horizontal cell signal appears to diminish the cone response by no more than 10-20%.

In summary, two mechanisms (pigment bleaching and horizontal cell feedback) act to modify the cone sensitivity to match the local spatio-temporal ambient intensity. The horizontal cell feedback signal acts to provide information about the spatial ambient intensity while pigment bleaching, localized to single cones, provides information about the temporal ambient intensity. The spatial and temporal ambient intensity signals may then be combined to adjust the semi-saturation parameter in the cone saturation function.

In addition to gain changes within the cone photoreceptors which adjust sensitivity to illumination and contrast, other adaptation mechanisms trade off visual acuity for absolute contrast detectability. Some of these mechanisms are believed to occur at the cone level and will be discussed next.

3.3.5 Visual Acuity and Adaptive Cone Coupling

The presence of gap junctions between cones and the direct coupling of neighbouring cones is well documented in the periphery [13][49]. Recent anatomical evidence indicates that there are gap junctions between cones (and thus cone coupling) in the fovea as well [67].

The function of cone coupling is still not well understood. One speculation is that cone-coupling plays a role in maintaining a certain minimum output signal-to-noise ratio (SNR) in the cone system over a wide range of input illumination levels. At illumination levels near the *cone threshold* (≈ 1 troland), the noise due to fluctuations in the photon catch and spontaneous cone pigment isomerizations ("dark noise") is comparable to the signal level [70][81]. Coupling of cone signals at these illumination levels would improve the reliability of spatial contrast detection but at the expense of degraded visual acuity. The input SNR increases with rising illumination levels so that at bright illumination intensities, improvements in both visual acuity and contrast sensitivity are possible with a reduced degree of cone coupling.

Although the largest changes in visual acuity occur at scotopic illumination levels (when

the rod system is active), visual acuity improves by an additional order of magnitude in the photopic range (when the cone system is active) [65][75]. Psychophysically measured visual acuity for the cone system using "Landolt ring" stimuli is shown in Figure 3.4(a) [65]. With increasing illumination levels, visual acuity quickly reaches a plateau of about $2.6 \ min^{-1}$ [65]. This corresponds to an ability to resolve a Landolt ring gap width as small as 23 sec (2.4 μm) and is comparable to the spacing of foveal cones ($\approx$ 2.5-2.7 μm). However, Figure 3.4(b) shows that at low photopic illuminations, the minimum resolvable gap may need to span several cone widths before it can be detected. Tsukamoto suggests that the improvements observed in visual acuity within the photopic illumination range may be partially due to changes in the degree of cone coupling [67].

Barlow suggests that visual acuity at the retinal level is inversely related to the size and spacing of the receptive fields (RF) used to sample the image [2]. In the fovea, there is a one-to-one correspondence between cones, midget bipolar cells, and midget (P) ganglion cells and thus the spacing of their receptive fields is determined by the cone spacing. At its input, each midget bipolar synapses onto a single cone while contacting a single P-type ganglion cell at its output [49]. This suggests that the diameters of the centre portions of bipolar and ganglion cell RF's are primarily determined by the effective RF size of cones which is in turn controlled by the degree of cone coupling. The smallest primate P-type ganglion cell RF centres measured to date (at bright illuminations) have diameters of 10 μm (3-4 cone spacings) [28]. This indicates that even at bright illuminations cones may be coupled to immediate neighbouring cones of the same spectral type. As the spacing of the receptive fields is fixed, Barlow's hypothesis implies that visual acuity at the retinal level is inversely related to the size of the ganglion cell receptive fields. The drop in visual acuity in the cone system for illumination levels below 1000 trolands may thus be explained by an increase in the coupling of cones leading to larger ganglion cell RF's[67]. It has been reported that peripheral cones may be coupled for distances up to 50μm (equivalent to 20 foveal cone widths) [70], and thus it is not unconceivable that foveal cones may also couple extensively at low photopic illumination levels.

3.4 Post-Receptoral Mechanisms

Although it is evident that a large part of the gain control in the retina is performed at the photoreceptor level, other retinal neurons also play a vital role. The non-receptoral mechanisms involved in retinal adaptation include modulation of horizontal cell receptive field sizes, lateral inhibition at the bipolar cell level, and amacrine cell feedback for modification of ganglion cell outputs.
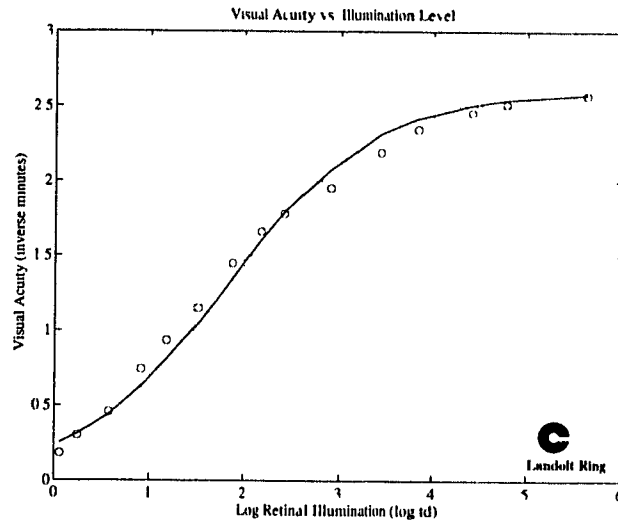
(a)
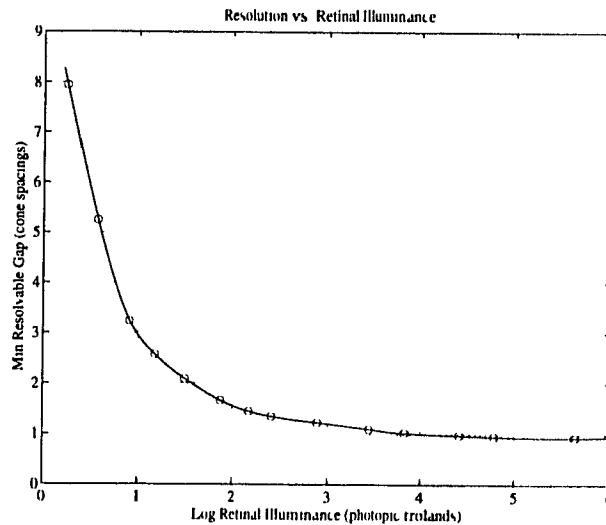
(b)

Figure 3.4: Visual Acuity vs. Illumination Level: Figure (a) shows the variation of visual acuity with respect to the log ambient illumination level for "Landolt ring" visual stimuli. Visual acuity is measured in inverse minutes of an arc subtended by the gap in the Landolt ring. The peak acuity value of $2.6\ min^{-1}$ corresponds to being able to detect a Landolt ring gap size equal to the cone spacing in the fovea. Data (unfilled circles) re-plotted from Thomas [65] (with permission of Academic Press ©1979). The same data is shown again in (b), with the minimum resolvable Landolt ring gap spacing (measured in terms of cone spacing) plotted against illumination level.

3.4.1   Lateral Inhibition at the Bipolar Cell Level

Each bipolar cell essentially performs a difference operation on the cone and horizontal cell inputs. Since the horizontal cell signal is a spatio-temporal average of the local cone signals, the bipolar cell operation apparently serves to suppress the "dc" signal from the input. This permits the bipolar cell to be very sensitive to small contrasts in the scene and to signal this information with a high gain [71]. It is at the bipolar cell level that the center-surround antagonistic receptive field properties emerge.

In addition to coding spatial contrast, the bipolar cells also code temporal contrast. Horizontal cells have a larger integration time constant than cones [17][40]. In addition, horizontal cell signals are slightly delayed with respect to the cones at the bipolar cell level [47]. This results in a spatio-temporal difference signal being computed at the bipolar cell. It is likely that the degree of spatial and temporal contrast tuning of the bipolar cell adapts with time and prevailing signal levels. Over most of its range, the bipolar cell is linear but exhibits saturation for large contrast signals.

3.4.2   Modulation of Horizontal Receptive Field Sizes

The horizontal cell receptive field size is greatly extended to beyond its dendritic spread by electrical coupling of signals through gap junctions between neighbouring horizontal cells [40]. At least two components seem to contribute to the modulation of horizontal cell receptive field sizes by modifying the conductivity of their gap junctions. Dopamine released by interplexiform (IPX) cells which feed back to horizontal cells is one factor known to reduce the horizontal cell receptive field size [68][78]. Increases in background illumination are second factor known to cause reduction in horizontal cell coupling although the exact mechanism is unknown [1]. Figure 3.5 shows schematically the anatomical wiring of the interplexiform cells in the retina.

IPX cells have fairly large receptive fields and receive their input from the outputs of several bipolar cells. As discussed above, the bipolar cell's output primarily represents a spatio-temporal contrast signal by virtue of the differencing operation performed on the cone and horizontal cell signals. Thus both flickering light (large temporal contrast) and spatial edges (large spatial contrast) elicit large bipolar cell outputs. Consequently, IPX cell activity and the release of dopamine by these cells is also likely increased in these regions, resulting in the reduction of horizontal cell coupling. This hypothesis is supported by studies that show increased release of dopamine by interplexiform cells in fish in response to flickering visual stimuli [68].

A rise in background illumination is another factor known to reduce the size of horizontal cell receptive fields [1]   Interplexiform cells appear to release dopamine under flickering
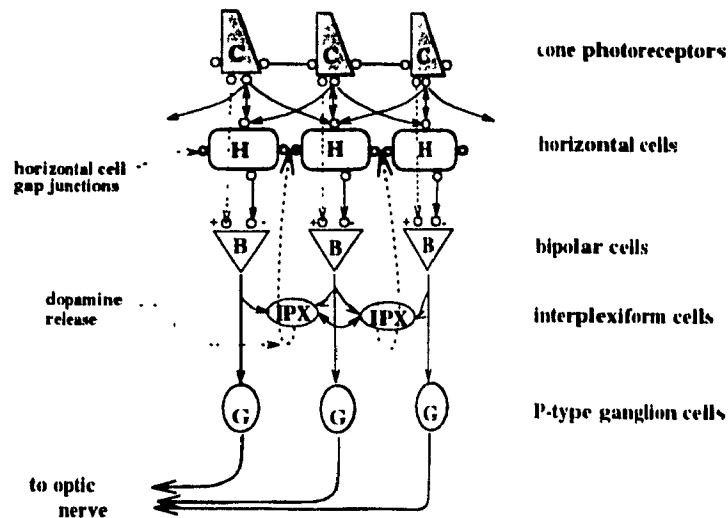
Figure 3.5: Interplexiform Cell Feedback: The figures shows schematically how interplexiform cells receive input from bipolar cells and have feedback paths to horizontal cells. Stimulation of interplexiform cells releases dopamine which reduces the conductivity of gap junctions between horizontal cells. The reduced spread of signals in the horizontal cell layer effectively, reduces the size of the horizontal cell receptive fields.

stimuli (or high spatio-temporal excitation) and under prolonged dark adaptation but not for steady background illumination [68][78]. Psychophysical tests also support this notion as visual acuity is known to rise slowly with rising illumination levels [75] [65]. The exact mechanism which causes this effect on horizontal cell gap junction conductivity is still unknown.

We can thus predict that a horizontal cell's receptive field size should be a function of both the local spatio-temporal contrast and the local background illumination. Increase in either of these two signals causes a reduction in local horizontal cell coupling. Figure 3.4 shows how visual acuity varies with background illumination level. As acuity is inversely related to the size of the cone and horizontal cell receptive fields, this implies that both cone coupling and horizontal cell coupling adapt to the local background illumination level.

3.4.3 Amacrine Cell Effects

Although little is known about the functional roles of the many varieties of amacrine cells found in the primate retina, it is clear that they play an important role in signal modulation in the inner plexiform layer judging from the large number of synapses amongst amacrine cells and ganglion cells of the Magnocellular pathway (M-cells).

The situation is complicated by the incredibly large variety of anatomically distinguishable amacrine cell types. Furthermore, there are possible pitfalls of generalizing amacrine cell function from studies performed on other species to primates due to large interspecies
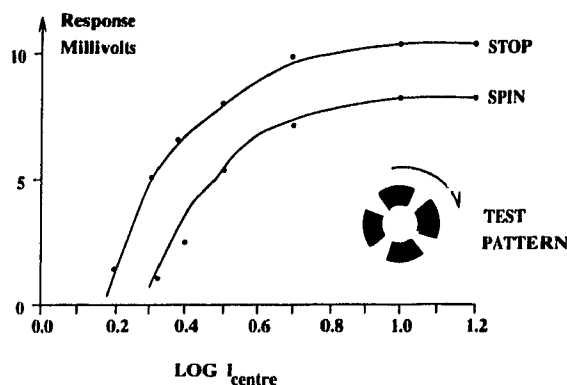
Figure 3.6: Motion Stimuli and *on-off* **Ganglion Cell Output:** The figure shows *on-off* ganglion cell response to variation in centre spot intensity in the test stimulus under two conditions. The test stimulus consists of a bright centre spot surrounded by a windmill pattern. Spinning the windmill test pattern leads to increased amacrine cell activity (not shown) and decreased *on-off* ganglion cell activity as compared to a stationary windmill stimulus. The decrease in *on-off* ganglion cell activity is attributable to inhibitory signals from amacrine cells [74]. Figure from Werblin [74] ©Rockefeller University Press.

differences. Amacrine cell synapses to ganglion cells seem to be more prevalent in visual systems in which "exotic" properties are exhibited by ganglion cells. Thus, amacrine cells have often been implicated in the formation of complex receptive field properties at the ganglion cell level. In primates, the receptive fields of retinal ganglion cells are quite simple, with more complex visual processing occurring at later stages. In primates, there are relatively few synapses between amacrine cells and ganglion cells of the Parvocellular pathway (P-cells) as compared to the larger number found for some M-cells.

M-cells account for about 10% of the total ganglion cell population and are generally more sensitive to motion stimuli (higher temporal frequencies) than P-cells. M-cells may also be classified into two subtypes based on their response properties, M_X and M_Y [57]. The majority of M-cells (M_X, 80%) are like cat X-cells in that they perform a linear summation of signals. It is the remaining 20% of M-cells (M_Y) that exhibit nonlinear behaviour like that of cat Y-cells. It is likely that this small fraction of M_Y-cells receives the bulk of the amacrine-to-ganglion cell input [57][47].

Studies by Werblin in the mudpuppy [74] indicate that some amacrine cells respond to temporal changes in visual stimuli. Furthermore, these amacrine cells provide inhibitory surround input to *on-off* ganglion cells. Figure 3.6 shows the change in response of the *on-off* ganglion cell in the mudpuppy due to a spinning disk in its RF surround. Motion in the surround field of the *on-off* ganglion cell reduces the potential of these ganglion cells as well as their firing rates (not shown). This inhibitory effect is directly related to an increase in the amacrine cell output for the spinning wheel stimuli.

These *on-off* ganglion cells are in many respects much like the primate M_Y-cells. Both are tuned to temporally changing stimuli, and respond transiently to maintained visual stimuli with a high contrast gain. Both also have considerable input from amacrine cells.

The outputs of M_Y-cell ganglion cells are modulated by inhibitory surround mechanisms at two levels. In the outerplexiform layer, horizontal cells provide an inhibitory spatio-temporal "average" signal which removes the "dc" signal from the input. At the innerplexiform layer, the output of M_Y-cells is further modulated by inhibitory input from amacrine cells that respond to motion stimuli over their large receptive fields.

3.5 Summary

Adaptation mechanisms are found to act both at the photoreceptor level and at subsequent levels in the retina to locally modulate the sensitivity and acuity of the system to match the prevailing lighting conditions. Mechanisms that adjust the sensitivity of photoreceptors and centre their response range based on the background illumination level include photochemical pigment bleaching and fast neural feedback from horizontal cells. At the bipolar cell level, lateral inhibition serves to emphasize spatio-temporal contrast in the visual signal to suppress the output in homogeneous regions.

Adaptation mechanisms also act to adjust the acuity of the visual system to match the prevailing lighting conditions. As illumination levels increase, the signal-to-noise ratio of the system also improves. In response, the retina modulates the size of cone and horizontal cell receptive fields by modulating the cone-cone coupling and horizontal cell layer coupling. Horizontal cell receptive field size is also modulated by feedback from interplexiform cells which respond to high spatio-temporal contrast in the input signal.

The next chapter presents a simple retinal model which incorporates the adaptation features discussed in this chapter.

This chapter presents a retinal model which has been developed and based upon the retinal biology and retinal adaptation discussed in the previous chapters. The model fulfills the goals set out at the beginning of the thesis in that it mimics many of the adaptive properties found in biological retinas. The model is also fairly simple so that a silicon implementation may be considered in the future.

This chapter starts with a very brief summary of existing silicon implementations and computer models of the retina. The remainder of the chapter describes both the theoretical and implementational aspects of the *computer retina* model. The presentation of the model is in order of the information flow through the retina. For each layer of "cells" in the *computer retina*, the computations performed at that layer are described, as well as the assumptions and simplifications made in the model.

4.1   Existing Models

There has been much recent interest in developing artificial retinas, and a few groups have already fabricated silicon chips [36][39][53][66]. In addition, many computer models have been developed [5][10][25][58][77]. Each implementation models certain specific aspects of the retinal function and most incorporate nonlinear or logarithmic transduction at the photoreceptor level but not local adaptation. To date, Mahowald's *Adaptive Silicon Retina* [36] is the only device with locally adaptive photoreceptors. Lateral inhibition or a differencing operation at either the receptor or a subsequent level is another common feature found in most models [24][36][39][66]. One foveated sensor design approximates the nonuniform sampling scheme employed in the retina [53] but ignores further aspects of retinal processing. In general, most retinal model implementations, whether in software or in silicon, limit themselves to mimicking logarithmic transduction and lateral inhibition but ignore other aspects of retinal processing such as adaptation of receptive field (RF) sizes with illumination level or local spatio-temporal contrast. The exceptions to this are a rod system model by Yellott [81] and a model for an adaptive gain control camera by Zeevi [82]. In Zeevi's design, although the RF sizes of "cells" increase with illumination level, this is the reverse of what one would expect if visual acuity rises with brighter illumination levels. Table 4.1 shows the features of the biological retina that are incorporated in each model.

Retinal Feature	Model Characteristics	Models
Locally adaptive photoreceptors	Photoreceptor gain is adapted based on local changes in illumination level.	[Chang, 1991] [Mahowald, 1991]* [Skryzpek, 1990]
Cone coupling	Cones are coupled to neighbouring cones and can effect their output.	[Boahen, 1991] [Chang, 1991] [Yagi, 1989] [Curlander, 1982]
Horizontal cell coupling	Horizontal cell receptive field size is extended by passive spread of the signal through gap junctions to neighbouring horizontal cells.	[Boahen, 1991] [Mead, 1988]* [Mahowald, 1991]* [Curlander, 1982]
Modulation of receptive field sizes with changing illumination level	Cone and Horizontal cell receptive field sizes are adapted to changing illumination levels	[Yellott, 1987] [Zeevi, 1989]
Interplexiform cell feedback	Feedback from inner plexiform layer back to the outerplexiform layer driven by spatiotemporal contrast.	
Foveated sampling	Log-polar sampling and linear variation of receptive field size with increasing eccentricity.	[Wilson, 1983] [Yamamoto, 1992] [Sandini, 1989]* [Rojer, 1990]
Spatio-temporal properties	Incorporates spatiotemporal properties of both P and M type ganglion cells	[Fleet, 1982] [Richter, 1982]

Table 4.1: Summary of retinal features which are incorporated in published models of the retina Citations followed by * indicate those models which are implemented in silicon.

4.2 Implementation Overview

The *computer retina* model presented here is in part based on the spatiotemporal *Centre-Surround* operators (CS) presented by Fleet [24] and described in Section 2.6.5 of this thesis. The CS operator is essentially a spatiotemporal difference-of-Gaussians operator which describes some of the receptive field (RF) properties of ganglion cells but ignores the nonlinear transduction and adaptation occurring at earlier stages of retinal processing. The building blocks of the CS operator (a Gaussian operator (G) and an exponential lowpass temporal filter (K)) are referred to often in this chapter, and thus, for convenience, equations (2.4) - (2.6) describing the CS operator are repeated below:

$$CS(\mathbf{r}, t) = \alpha_c K(t; \tau_c) G(\mathbf{r}; \sigma_c) - \alpha_s K(t - d; \tau_s) G(\mathbf{r}; \sigma_s) \tag{4.1}$$

$$G(\mathbf{r}; \sigma) = \frac{1}{2\pi\sigma^2} \exp \frac{-|\mathbf{r}|^2}{2\sigma^2} \tag{4.2}$$

$$K(t; \tau) = \begin{cases} \frac{1}{\tau} \exp\left(\frac{-t}{\tau}\right) & \text{if } t \geq 0, \tau > 0 \\ 0 & \text{if } t < 0 \end{cases} \tag{4.3}$$

where

σ_c, σ_s	= RF centre and surround Gaussian widths (μm)
α_c, α_s	= weighting of centre and surround inputs (both set to 1.0)
τ_c, τ_s	= centre and surround RF time constants (ms)
d	= surround time delay w.r.t. centre (ms)
$\mathbf{r}, t$	= 2D spatial position vector $\mathbf{r}$ (μm), and time t (ms)

The use of a spatiotemporal difference-of-Gaussians operator to describe the structure and dynamics of bipolar and ganglion cell RF's is maintained in the *computer retina* as it is simple yet still describes many of the properties of these cells [22][24][37][47]. The distinguishing features of the present model are its various adaptive properties that deal with illumination conditions which may vary over several orders of magnitude. These features include local gain changes at the photoreceptor level as well as adaptation of cell RF sizes. The effects of illumination level and spatio-temporal contrast on the horizontal cell gap junction conductivity and cone coupling are hypothesized and incorporated into the model. Two output streams are produced at the ganglion cell level to represent the distinct spatiotemporal features of the P-cell (parvo) and M-cell (magno) pathways. Finally, the effects of nonuniform receptor sampling and linear variation of RF sizes with eccentricity are accounted for using a log-polar mapping scheme.

The model has been kept as simple as possible while still emulating many of the features

exhibited by the primate retina. To maintain simplicity, only the cone system is considered. The rod system and rod-cone interactions are ignored. Furthermore, although cones are responsible for colour vision, only the achromatic luminance information is considered in our model. In the biological retina, bipolar and ganglion cells come in two varieties, *on*-centre and *off*-centre, to code positive and negative contrast signals respectively. Because the computer can represent positive and negative values equally well, a further simplification is made. In the model, only *on*-centre type bipolar and ganglion cell outputs are generated, thus effectively reducing the required number of outputs by half. These *computer retina* *on*-centre cells respond to both positive and negative contrast equally well.

The remainder of this chapter presents both the theoretical and computational aspects of the *computer retina* model. Brief discussions of how log-polar mappings are useful for modelling the nonuniform sampling occurring in the retina, and the advantages of using of a diffusion process to generate Gaussian-weighted receptive fields are presented first. The remaining sections follow the computations performed at each layer of "cells" in the *computer retina* model. Wherever possible, the manner of computation or the parameters used are based on published data on primate retinas. Where insufficient data are available, any assumptions and simplifications that are made are explicitly stated. The main emphasis of the model presented here is to demonstrate how different adaptation mechanisms play a role in extending the operating range of the primate retina.

4.3 Nonuniform Sampling and Log-Polar Mappings

4.3.1 Variations in Retinal Information Processing with Eccentricity

The advantages of using a foveated sensor array are argued by Kronauer [32]. Such an approach offers a tremendous reduction in the data that must be processed by all subsequent levels of the system while still retaining a small high-resolution sampled fovea. In the biological retina, the concentration of cone photoreceptors is the highest in its centre (the fovea). This sampling density drops off exponentially for eccentricities up to 14° and then much more gradually further into the periphery. The density of other retinal cells also matches the cone photoreceptor distribution to some degree. In the central 1° region around the fovea, the number of ganglion cells match the number of cones 1:1 for each of the *on*-centre and *off*-centre pathways. The separate *on* and *off* pathways essentially form two overlapping sampling lattices which enable the biological retina to code both positive and negative contrast in the input signal, respectively. Outside the fovea, both the cone and ganglion cell densities drop off approximately exponentially with eccentricity (see Figure 2.8) [49]. The progressively coarser retinal sampling with increasing eccentricity is matched by linear increases in the size and spacing of receptive fields of most cells [49]. However, the

bipolar and ganglion cell density drops off much faster than that for cones in the periphery (see Figure 2.8), and as a result, the number of cone inputs converging into bipolar and ganglion cell RF's grows with eccentricity [23]. The nonuniform sampling scheme utilized by the retina results in a greater than one hundred-fold reduction in the number of outputs that would otherwise be required if the high-resolution cone and ganglion cell sampling found in the fovea was maintained uniformly over the entire retina [32].

4.3.2   Usefulness of Log-Polar Mappings

Although one VLSI foveated sensor has been developed, the number of photosensitive elements in that sensor is rather small [53]. Foveated sampling may also be simulated with uniform-sampling CCD cameras by using log-polar transformations on the input image before further processing is performed. In fact, log-polar mappings have been used by several researchers to model the receptive-field size and sampling density variations with retinal eccentricity [50][76][79]. The motivation for such mappings is based on the close fit of the log-polar mappings of the visual field into V1 of the cortex [50]. Using a foveated sampling scheme for data reduction not only reduces the computations required at the retinal or sensor level but has even greater savings for all further visual processing. We also use a similar technique for data reduction based on Wilson's model [76] and implemented by Bolduc [6]. Figure 4.1 shows schematically how the input image is transformed by the log-polar transformation used by the *computer retina*.

The log-polar transformation essential divides the image into two separate parts with the number of pixels in each region approximating the number of P-type ganglion cells in the fovea and the periphery (see Figure 4.1). An assumption is made here that the number of pixels in the original Cartesian domain image approximate the number of cones sampling the retinal image whereas the number of pixels in the two transformed images (fovea and periphery) match the number of P-type ganglion cells [76]. The foveal region is represented in the original Cartesian coordinates and is an area of uniform sampling, where for every pixel in the input image, there is one output pixel. This region models the 1:1 ratio of cones to *on-centre* ganglion cells in the central $1°$ of the retina.

The peripheral region is sampled along concentric rings of exponentially increasing diameter. The number of samples along each ring is constant, while the dimensions of the sampling regions grow linearly with eccentricity. These aspects of the log-polar mapping model the variations in size and spacing of receptive fields of most retinal cells with increasing eccentricity [76]. The values assigned to "pixels" in the log-polar domain periphery data structure may either be obtained from subsampling the original image (taking the value of only one pixel from the original image in each sampling region), or by computing a
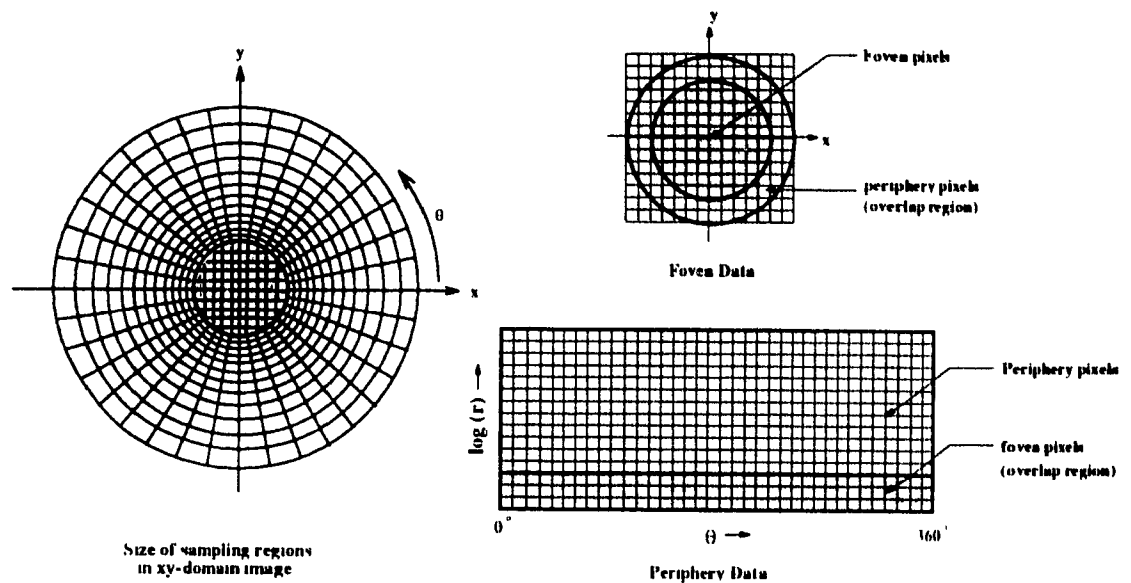
Figure 4.1: Log Polar Mapping: The figure shows schematically how the original image is broken down into foveal and peripheral regions using nonuniform sampling. The fovea (shaded region) is represented by a small circular region that is uniformly sampled. Outside the fovea is a peripheral region that consists of radially concentric rings whose diameters scale exponentially with eccentricity (r). The number of sampling regions per ring are fixed while the dimensions of the sampling regions grow linearly with eccentricity (r). This is equivalent to a log-polar transformation [76]. The peripheral data are represented in the log-polar domain while the foveal data are represented in the linear-Cartesian domain. To simplify the computations, both the fovea and periphery data structures are extended so that they slightly overlap each other.

weighted average of all the pixels from the original image contained in the sampling region. By "averaging" the original image pixel values over an entire sampling region, the convergence of cone inputs into ganglion cell RF's found in the primate retina periphery may be partially accounted for immediately at the input stage. The sampling regions may be non-overlapping annular segments (as shown in the Figure 4.1) or circular regions (not shown in Figure 4.1) which slightly overlap each other. Both sampling schemes are equivalent to a log-polar transformation [76][79] and thus result in a much more compact representation of the visual information. We utilize circularly shaped, Gaussian-weighted sampling regions to model the increasing convergence of cone information into ganglion cell receptive fields with increasing retinal eccentricity [49].

4.3.3   Computational Considerations

Using a log-polar transformation offers other advantages in addition to a reduction of data required to be processed by the *computer retina*. It allows for easy decoupling of the processing of foveal and peripheral information. By extending both the fovea and periphery data structures so that they overlap each other to some degree, information near the fovea-periphery boundary is available in both data structures. By making the overlap region larger than the size of the largest operators used in modelling the retinal function, the processing of the information in the two regions may be performed independently.

In the model, the computations performed to generate the output of each *computer retina* "cell" are strictly local, requiring information from only the immediately neighbouring "cells" (pixels). The lateral spread of information in the retina and the generation of cell receptive fields is modelled using a discrete, iterative, diffusion process in which a small "operator" using only local neighbourhood information is repeatedly applied (described in section 4.4). The local nature of information processing in the retina makes working in the log-polar domain advantageous and greatly simplifies the implementation of the *computer retina*. For example, in the biological retina, the diameters of ganglion cell RF's are known to scale approximately linearly with eccentricity [49]. To model this in the original image domain would require changing the size of all operators with eccentricity. However, in the log-polar domain, operator sizes are automatically scaled linearly with eccentricity [50][76]. Using the same operator in the log-polar domain as in the fovea leads to a slightly distorted operator shape in the original retinal image domain. However, it is assumed here that since all the computations in the model are spatially localized, distortions in the operator shape due to the log-polar mapping are minimal.[1]

4.3.4   Summary of Foveated Sampling

The use of a log-polar transformation to model the data reduction occurring in the retina splits the original image into two separate ones: the fovea and the periphery. The foveal image is represented in the original Cartesian-coordinate domain while the compressed peripheral information is represented in the log-polar domain. The transformation as implemented here decouples the processing of information in the fovea and the periphery and allows each region to be processed separately and transparently by the *computer retina*.

The retinal model presented in the rest of the chapter describes the retinal processing as it occurs in the fovea. However, the model is equally valid for computations in the periphery

---

[1]The distortions in an operator shape due the log-polar mapping may be minimized by re-adjusting the operator weights to give the desired weighting profile in the original retinal domain. This is discussed further in section 4.4.1

as all of the effects of the scaling of receptive fields and the pooling of cone information with increasing eccentricity are accounted for by the log-polar transformation and made transparent to the rest of the model.

4.4 Diffusion, Gaussian Convolution, and Receptive Fields

The summation of inputs within the circular receptive fields (RF) of most cells is usually assumed to be a Gaussian-weighted average of the inputs. The size of the Gaussian operator (G) used to describe such a RF profile is specified by its width parameter σ (see equation 4.2). The response of the receptive field is given by the convolution of the operator $G(\mathbf{r}; \sigma)$ with the input signal.

It can be shown that a Gaussian convolution is equivalent to a 2D diffusion process performed on the input signal [44][85]. Diffusion in two dimensions is defined by the following equation:

$$\frac{\partial u}{\partial t} = c\nabla^2 u \tag{4.4}$$

where $\partial u/\partial t$ represents the derivative of the input signal with respect to time, $\nabla^2 u$ is the Laplacian of the input signal u, and c represents the rate of diffusion or *diffusivity*. The solution to this diffusion equation for a given input signal and initial conditions is given by the convolution of the signal with a *source kernel* $K(\mathbf{r}, t)$, where $\mathbf{r}$ represents the spatial position, t represents time, and K is a Gaussian of the form:

$$K(\mathbf{r}, t) = \frac{1}{4\pi ct}\exp\frac{-|\mathbf{r}|^2}{4ct} \tag{4.5}$$

A discretized implementation of the diffusion process using finite differences is very simple. Equation (4.6) describes the discretized diffusion process in the fovea where $u_n[x, y]$ is the output at position [x,y] at iteration n with degree of diffusivity c [44] As the diffusion process proceeds, the value of a given pixel at iteration $n + 1$ depends only on its previous value and the previous values of its four immediate neighbouring pixels:

$$u_{n+1}[x, y] = (1 - 4c)u_n[x, y] + c(u_n[x - 1, y] + u_n[x + 1, y] + u_n[x, y - 1] + u_n[x, y + 1]) \tag{4.6}$$

Discretized diffusion is equivalent to repeated weighted averaging with the four nearest neighbours. In order to ensure that the weight given to the centre pixel is at least equal to the weights given to each of its four immediate neighbours, c must be less than 0.2

By replacing time t in equation (4.5) with the number of iterations n, it can be shown that the width (σ) of the Gaussian generated by discretized diffusion is related to the diffusivity parameter ϵ and number of iterations n by equation (4.7)[85]:

$$\sigma = \sqrt{2\epsilon n} \quad \text{where } 0 < \epsilon < 0.2 \tag{4.7}$$

4.4.1 Diffusion in the Fovea and the Periphery

In the fovea, equal weights are given to all the four neighbouring pixels and this results in circularly symmetric receptive fields. To ensure that diffusion performed in the log-polar mapped periphery also results in roughly circular receptive fields in the original retinal domain, the weights given to the radially neighbouring pixels are slightly modified for peripheral retina computations. In the periphery, the radial width of receptive fields from one sampling ring to the next varies by a constant factor, say κ (see Figure 4.1). Thus, for any given log-polar mapped peripheral pixel, the radial dimensions of the outer ring neighbour are κ^2 times larger than the inner ring neighbour. The dimensions of the the neighbours in the theta direction are all the same In order to partially compensate for the distortions in the radial direction, the weighting given to the inner radial neighbour is κ^2 times that of the outer radial neighbour. This is schematically shown in Figure 4.2. The use of such a template was experimentally found to generate reasonably circular shaped receptive fields in the periphery.

4.4.2 Computational Aspects of Diffusion

On a parallel machine, diffusion offers many implementational advantages. Although discretized diffusion requires multiple iterations, each operation is simple and only needs information from the immediate neighbouring pixels. The width of a Gaussian-weighted receptive field (RF) is controlled by both the diffusivity parameter ϵ and the number of iterations performed n. This allows for easy local adaptation of RF size by locally changing the diffusivity parameter ϵ while keeping the number of iterations n constant. This is ideal for VLSI implementation or execution on SIMD machines where the same operations must be performed at all pixel locations in order to achieve maximum parallelization and throughput

In what follows, diffusion is used extensively to model such processes as cone coupling, the summation and spread of potential through gap junctions in the horizontal cell layer, and the modeling of cell RF's. In many cases, the diffusivity parameter is a function of both the retinal position r and time t, thereby allowing for easy implementation of adaptive receptive

t = diffusivity coefficient
κ = ring diameter increase factor
γ = operator normalization factor

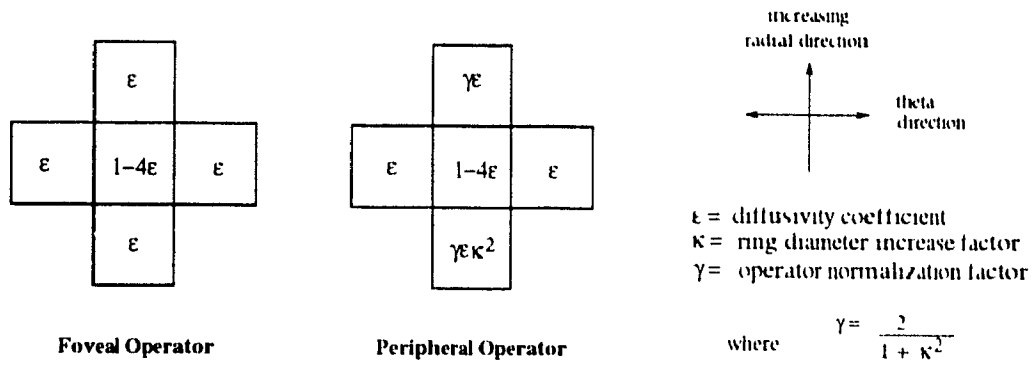where $\gamma = \dfrac{2}{1 + \kappa^2}$

Figure 4.2: Discrete Diffusion Weighting Templates: The figure shows schematically the weighting profile of discrete diffusion operators used in the Cartesian-domain foveal and the log-polar mapped peripheral images. For reference, see Figure 4.1 which illustrates how the foveal and peripheral images are generated by the log-polar transform. Discretized, iterative diffusion is equivalent to a weighted averaging operation performed using only nearest neighbour information. In the isotropic fovea, the weights given to each of the neighbouring pixels are equal and are as described by equation (4.6). Repeated application of this diffusion operator results in a Gaussian shaped receptive field profile. For operation on the log-polar mapped peripheral image, the weighting profile of the diffusion operator is altered in the radial direction as shown, so that repeated application of the operator results in approximately circular receptive fields in original retinal domain image.

field sizes. In order to minimize computation time, the number of diffusion iterations n that must be performed at a given layer is determined by the width σ_{max} of the largest Gaussian that must be generated at that level. By setting $t = 0.2$, and solving for n in equation (4.7), one obtains equation (4.8), which may be used to determine the minimum number of diffusion iterations (n) required to generate a Gaussian of width σ_{max}.

$$n \approx 2.5\sigma^2_{max} + 1 \qquad (4.8)$$

Although diffusion with parameters n and t is used to implement Gaussian shaped receptive fields, for comparison purposes, the sizes of the receptive fields in the remainder of the thesis are given in terms of the equivalent Gaussian width parameter σ.

4.4.3 Repeated Gaussian Convolution

In our model, receptive fields are generated using diffusion to obtain Gaussian-weighted circularly symmetric fields. The input signals to cells in any one layer of the model are in general fed from outputs of cells in one or more previous layers. Thus, the overall receptive

field size of a cell in any given layer must be at least as large as that of cells in any of the previous layer(s). In each layer, diffusion (equivalent to Gaussian convolution) may be used to further expand the size of the receptive fields of cells in that layer with respect to those in the previous layer.

In electrophysiology, the *receptive field* (RF) of a given cell is defined by the region at the input to the retina (photoreceptor sampling lattice), which when illuminated, elicits a change in the response of that cell. This receptive field may consist of excitatory and inhibitory regions as exhibited in bipolar or ganglion cell RF's.

In computer vision, it is common to specify the size of a Gaussian-shaped circular RF by the width σ of a Gaussian operator that would generate that RF from the input image. In our case, we are using the outputs of one layer of cells in the retina as inputs to the next layer. At each layer, there may be a diffusion / Gaussian blurring operation which increases the RF size of the cell at that layer in comparison to the previous layer. [2] In order to relate all the sequential Gaussian blurring operations at each layer and to estimate the overall receptive field size measured at the input to the retina, we need to know the effect of repeated Gaussian convolution. Using Fourier transforms, it can be shown that a Gaussian convolution with an operator of size σ_1 followed by convolution of an operator of size σ_2 is equivalent to Gaussian convolution with a single operator of size $\sigma_{effective}$ [29], where

$$\sigma^2_{effective} = \sigma_1{}^2 + \sigma_2{}^2 \qquad (4.9)$$

Thus, in the following sections where diffusion or Gaussian convolution is mentioned, the overall RF size for a cell in a given layer depends not only on the size of operators used in that layer, but also the amount of diffusion performed in all previous layers.

4.5 Cone Cell Output

4.5.1 Cone Transduction and Adaptation

The first stage of processing in the retina is the transduction of the input image intensities into signals that are used by the remainder of the network. Therefore, this stage must contend with the full range of intensities that may be encountered in any scene and adjust its sensitivity to match changing conditions. Each cone photoreceptor *locally* adjusts its sensitivity so that its operating range is centred around the *local* ambient illumination intensity in a small neighbourhood around the photoreceptor. This strategy allows the cone system to adapt to scenes containing a large dynamic range of illumination intensities.

---

[2] By increases in RF size, we imply that the number of original (retinal) image pixels that influences a given model cell's output increases with the number of sequential Gaussian convolution operations performed at that pixel location in all previous layers.

Figure 4.3a shows schematically the connectivity of the cone cells in the retina, while 4.3b shows the sequence of computations leading to the cone output as implemented in this model. The cone transduction and adaptation stage modifies the input intensity signal into a potential $v_r(I)$ that drives the rest of the retinal network. The gain or sensitivity of the retinal cones is controlled by two local mechanisms: pigment bleaching and horizontal cell feedback. The effects of these mechanisms are mimicked in the model by computing a *local* spatiotemporal ambient intensity I_a from a combination of two signals with different time constants and spatial extents. This ambient signal I_a is then used to adapt the gain of the cone transduction stage to match the local illumination level. The final cone output also includes the effects of cone coupling and the inherent temporal latency of cone cells. These aspects of the cone output will be discussed in the following sections. Only the transduction and adaptation stages are described here

The cone transduction function is modeled by the Michaelson-Menton saturation function in equation (4.10) [8][48][10].

$$\frac{v_r(I)}{v_{max}} = \frac{I^n}{I^n + (\frac{k_r}{k_b}I_a + k_r)^n} \tag{4.10}$$

where

v_r	= receptor potential before cone-coupling
v_{max}	= maximum receptor potential
I	= Input image stimulus intensity
n	= steepness of response curve (≈ 1.0) [8]
k_r	= half-saturation constant (833 trolands) [3] [8]
k_b	= half-pigment bleach constant (10^3 trolands) [8]
I_a	= spatio-temporal ambient illumination intensity

Figure 4.3(c) shows the cone response curves at various ambient illumination levels I_a. This nonlinear transduction function provides the cone cell with a dynamic range of ≈ 3 log units around any ambient illumination level I_a. Within this range, the response function is nearly logarithmic. In addition, shifting the ambient intensity value I_a shifts the entire cone response curve virtually unchanged along the intensity axis.

As shown in chapter 3, equation (4.10) may be used to account for the effects of pigment bleaching and horizontal cell feedback on cone sensitivity. When considering the steady-state effects of pigment bleaching alone, I_a is assumed to be the steady-state intensity impinging on the cone. Pigment bleaching is very localized and pigment bleached from one cone does not appear to significantly affect the sensitivity of neighbouring cones[13][49][70]. The *dynamic* properties of pigment bleaching may be roughly approximated by replacing I_a in equation (4.10) with a temporally lowpass filtered intensity signal I_T as given by equation
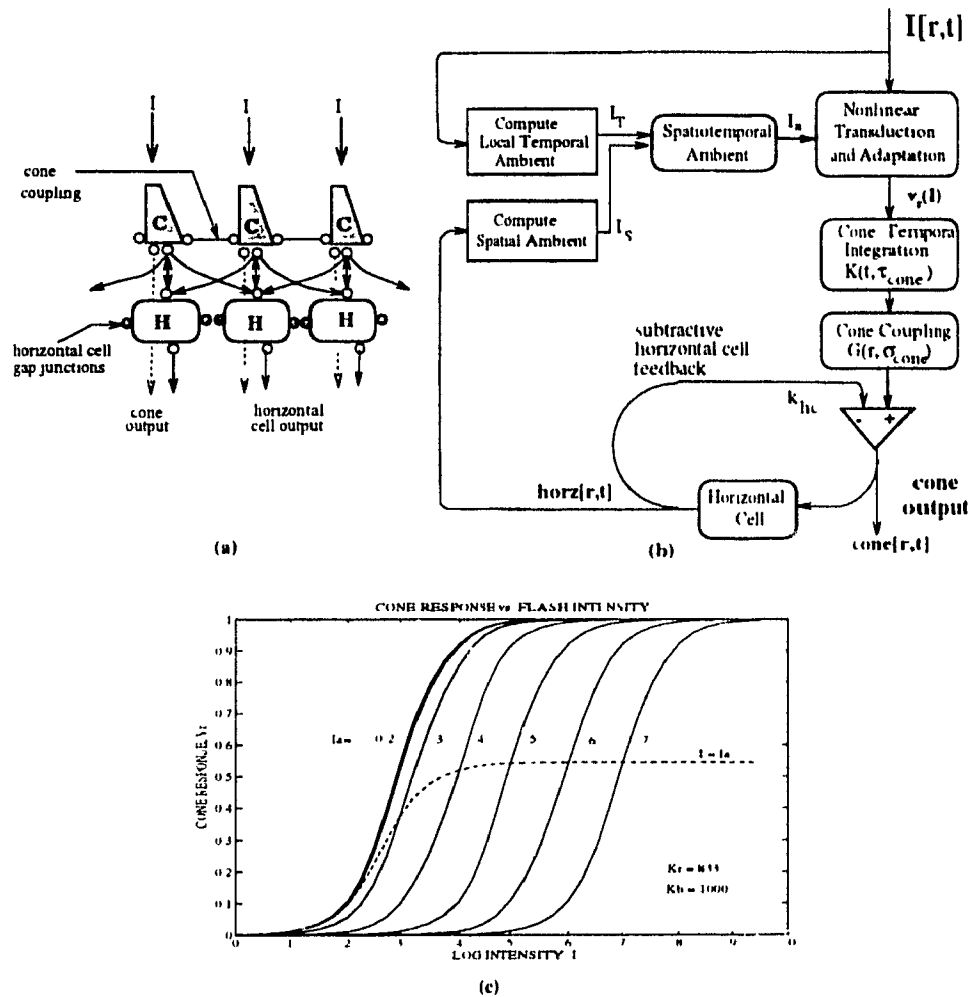
Figure 4.3: Cone Cell Output: Figure (a) shows schematically the connectivity of the cone cell in the primate retina. Each cone (C) is contacted by several horizontal cells (H), at least one midget bipolar, and several diffuse bipolars (not shown) In addition, cones are electrically coupled with neighbouring cones through gap junctions. Figure (b) shows schematically the computation of the cone output in our model The transduction stage converts input image intensities (I) into signals used by the rest of the network. Cone coupling is modeled using diffusion, while a temporal lowpass filter is used to account for the integration time of the cones The effects of pigment bleaching and horizontal cell feedback are accounted for by computing an effective spatiotemporal ambient illumination I_a which is then used in the transduction stage to adapt the cone sensitivity. Figure (c) shows the expected steady-state response of cones v_r with variation of flash intensity I superimposed on various log background illumination intensities I_a (indicated at the top of each curve). At any one given background I_a, the cone response saturates with a ≈ 3 log unit change in flash intensity I However, the entire response curve adapts to match any I_a by simply shifting along the intensity axis The dashed curve shows the steady state response of the cones when the local intensity matches the ambient intensity I_a. All intensities are in units of trolands

(4.11):

$$I_T[\mathbf{r}, t] = I[\mathbf{r}, t] * K(t; \tau_{bleach})\qquad(4.11)$$

where

$K(t; \tau)$ = lowpass temporal filter with time constant τ (see equation (4.3))

I_T = time-averaged local cone signal (for pigment bleaching)

$I(\mathbf{r}, t)$ = input intensity at 2D spatial position ($\mathbf{r}$) and time (t) in ms

τ_{bleach} = effective bleaching time constant $\approx 100ms$

Light adaptation due to pigment bleaching is known to be quite rapid and the cone sensitivity usually reaches a new plateau within 1-2 seconds of a step increase in intensity [21][70]. Since machine vision is not constrained by the limited rates of pigment bleaching or pigment regeneration it is possible to make this adaptation mechanism significantly faster while still maintaining robustness to photon shot noise caused by temporal fluctuations in the input signal. This allows the sensor to very quickly "adapt" to changes in illumination level. For implementation purposes, the *pigment bleach* time constant (τ_{bleach}) in the model was chosen to be shorter than that found in biological systems ($\approx$ 100ms). This is still about 10 times longer than the cone integration time and sufficient to filter any photon noise induced by temporal fluctuations in the intensity signal.

A much faster mechanism which modifies the cone sensitivity to match the local spatial ambient intensity almost instantaneously is mediated through horizontal cell feedback to the cones [21]. Chang [10] shows that if the horizontal cell feedback signal is used to compute an effective local spatial ambient intensity I_S, then equation(4.10) may be used to model the effects of this adaptation mechanism as well. Each cone is in contact with several horizontal cells having greatly overlapping receptive fields. Thus, the spatial ambient intensity must be computed over an area slightly larger than the receptive field size of a single horizontal cell ($\sigma_{I_S} \approx \frac{3}{2}\sigma_{horz}$). The spatial ambient I_s here is simply computed by diffusing the original image with operators slightly larger than the size of horizontal cell receptive fields and filtered by a temporal lowpass filter with the same temporal latency as horizontal cells in equation (4.12):

$$I_S[\mathbf{r}, t] = I[\mathbf{r}, t] * G(\mathbf{r}; \sigma_{I_S}[\mathbf{r}, t])K(t; \tau_{horz})\qquad(4.12)$$

where

$$G(\mathbf{r};\sigma) \quad = \text{Gaussian operator of width } \sigma \text{ as defined by equation (4.2)}$$

$$K(t;\tau) \quad = \text{lowpass temporal filter with time constant } \tau \text{ (see equation (4.3))}$$

$$I_S \quad\quad = \text{spatial average intensity estimated from horizontal cell feedback}$$

$$I(\mathbf{r},t) \quad = \text{input intensity at 2D spatial position } (\mathbf{r}) \text{ and time } (t) \text{ in ms}$$

$$\sigma_{I_S} \quad\quad = \text{spatial extent of ambient slightly larger than } \sigma_{I_S} \approx \tfrac{3}{2}(\sigma_{horz})$$

$$\tau_{horz} \quad\quad = \text{horizontal cell time constant} \approx 20ms \text{ [47]}$$

To model the effects of both pigment bleaching and horizontal cell feedback, an overall spatio-temporal ambient intensity I_a is computed and used to control the cone sensitivity. I_a is assumed to be a linear combination of the spatial ambient signal I_S (attributed to horizontal cell feedback) and a local temporal ambient signal I_T (used to account for the effects of pigment bleaching) (see equation (4.11)). Determination of the relative weights to assign to c_1 and c_2 is not easy. For simplicity, equal weighting is given here to both cone adaptation mechanisms ($c_1 = c_2 = 0.5$). Thus, we have:

$$I_a[\mathbf{r},t] = c_1 I_T[\mathbf{r},t] + c_2 I_S[\mathbf{r},t] \tag{4.13}$$

where

$$I_T \quad = \text{time-averaged local cone signal (for pigment bleaching)}$$

$$I_S \quad = \text{spatial average intensity estimated from horizontal cell feedback}$$

$$I_a \quad = \text{spatiotemporal ambient intensity}$$

In summary, equations (4.10)-(4.13) describe the cone transduction and adaptation function. However, the output of the transduction stage ($v_c(I)$) does not represent the final cone output since it does not account for the temporal latency of cone response, cone coupling, or inhibitory horizontal cell feedback. These are discussed next.

4.5.2 Cone Temporal Latency

Both cone and horizontal cells have a short temporal latency in responding to changes in the input signal [21][47]. This is reflected in many models by incorporating temporal exponential lowpass filters $K(t;\tau)$ (see equation (4.3)) with time constants τ_{cone} and τ_{horz} through which the cone and horizontal cell signals pass [24][17][47]. In the mudpuppy, cone and horizontal cells have time constants of approximately 100ms and 200ms, respectively [47]. Precise estimates of the time constants for these cells in mammals are not available but are believed to be about 10 times shorter. Richter [47] reports a good qualitative fit using time constants of $\tau_{cone} = 10ms$ and $\tau_{horz} = 20ms$ for primate cone and horizontal cells. We use similar values in our model.

4.5.3 Cone Coupling

As discussed in the previous chapter, anatomical evidence of gap junctions between cones indicates that cones may be coupled both within the fovea and in the periphery [67]. Psychophysical data show that the acuity of the visual system improves with increasing illumination levels and reaches a plateau only at moderately bright illumination levels ($I \approx 10^4$ trolands) [75][65]. At these illumination levels, the measured acuity approaches the maximum theoretically possible acuity, given the cone and ganglion cell sampling in the fovea and implies only a small degree of coupling. However, under dimmer photopic illumination conditions, measured acuity may be as much as an order of magnitude lower (see Figure 4.4). At these illumination levels, increased coupling of signals at the photoreceptor level makes functional sense since trading off acuity in favour of noise reduction may result in improved contrast sensitivity. This suggests that the degree of cone coupling may be a function of both ambient illumination intensity and eccentricity.

Some existing retinal models do incorporate photoreceptor coupling, but the degree of coupling is invariant with respect to the illumination level [5][10][17][77]. In the model developed here, the degree of cone coupling is assumed to vary with the illumination level and is designed to match the data on psychophysically measured visual acuity (see Figure 4.4) [65]. The data in Figure 4.4 (top) show that the visual acuity improves by an order of magnitude within the photopic range of light levels [65]. We fit the data in Figure 4.4 with equation (4.14) for photopic illumination levels with exponent $n = 0.55$ and constant $A_o = 65$ trolands:

$$Acuity = \frac{2.6 I_a{}^n}{I_a{}^n + A_o{}^n} \ min^{-1} \qquad (4.14)$$

At the retinal level, visual acuity is inversely related to the size of receptive field (RF) centres of midget bipolar cells and midget ganglion cells [2][23]. In the fovea, a single cone feeds the centre input to a midget bipolar cell which in turn is connected to a single midget ganglion cell [49][54]. Consequently, the midget (P-type) ganglion cell RF centre size is primarily determined by the RF size of individual cones which is dependent upon the degree of cone coupling. Cone coupling is modeled in the *computer retina* by a diffusion process in which the cone diffusivity ϵ_{cone} (and thus σ_{cone}) is a function of the local ambient intensity I_a and the retinal position **r**. For illumination intensities above 1000 trolands (td), visual acuity quickly reaches a plateau. At these illuminations, the Gaussian-weighted ganglion cell RF centres have sizes as small as 10 μm (4 cone spacings) which corresponds to a Gaussian width parameter of $\sigma_{cone} = 1.5$ cone spacings [28]. We assume that σ_{cone}
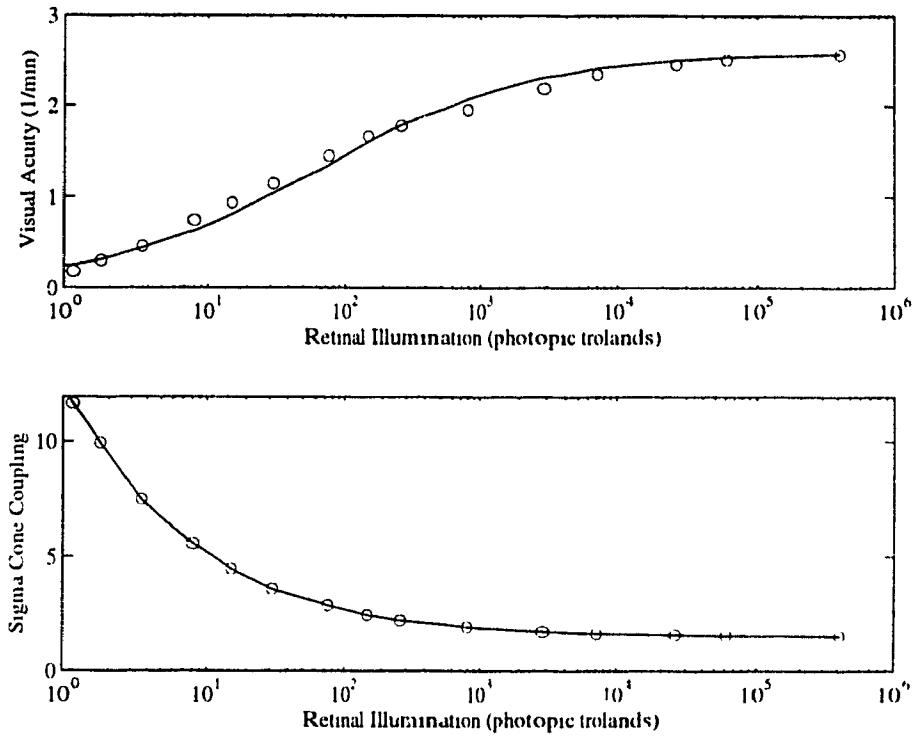
Figure 4.4: Visual Acuity and Cone Coupling: The top figure shows psychophysically measured visual acuity from Thomas [65] (open circles) and the curve given by equation (4 14) used to fit the acuity data (solid line) The bottom figure shows the variation of the cone coupling (σ_{cone}) with illumination level as modelled in the *computer retina* by equation (4 15).

which controls the cone coupling (and is a measure of the cone RF size) is approximately inversely related to equation (4.14) used to fit the human acuity data and has a minimum value of $\sigma_{cone} = 1.5$. The *computer retina* thus models σ_{cone} by equation (4.15) with $n = 0.5$, $\delta = .01$, and I_a measured in trolands:

$$\sigma_{cone}[\mathbf{r}, t] = 1.5 \frac{I_a[\mathbf{r}, t]^n + A_o{}^n}{I_a[\mathbf{r}, t]^n + \delta^n} \qquad (4.15)$$

The parameter $\delta = .01$ was added to equation (4.15) to ensure that σ_{cone} remains bounded for all illumination levels. As the illumination level increases from cone threshold (≈ 1 td) over the photopic range, the cone RF size described by σ_{cone} varies from a high of 12 down to 1.5 foveal cone spacings. At high illumination levels ($I > 10^4$ td), this corresponds to a RF diameter of 4 pixels (cone spacings). At 10 td, the lowest illumination used in our

71

experiments, the RF diameter is approximately 12 pixels.

To summarize, adaptive cone coupling allows for some degree of noise-filtering on the original image and allows the acuity of the system to be adjusted to match the prevailing lighting conditions. The degree of coupling in our model diminishes with increasing illumination in a manner consistent with the published data on variation of visual acuity with illumination.

4.5.4 Inhibitory Horizontal Cell Feedback

The connection between a cone and a horizontal cell not only provides the the horizontal cell with the cone output signal, but also serves as a feedback path allowing the horizontal cell signal to influence the cone output. The effect of this feedback path on the cone sensitivity has already been described in the transduction stage. In addition to this, the horizontal cell signal imparts a small inhibitory influence on the cone signal.

Such inhibitory feedback effects have been modeled by several researchers [17][77][5]. We use the simplest approach here. The weighted horizontal cell signal is simply subtracted from the cone output. The strength of this feedback path was chosen experimentally to be $k_{hc} = 0.15$ as it gave close agreement with the responses of monkey cones for flash experiments [55] and gecko photoreceptors (see Figure 2.3) [21]. Values smaller than this produce negligible effect on the cone output while much larger values result in large oscillations.

4.5.5 Summary of Cone Cell Output

The output of the cone cell includes the effects of nonlinear transduction, adaptation, horizontal cell feedback, cone coupling, and cone temporal integration. The final cone output $cone[\mathbf{r}, t]$ is described by equation (4.16), where v_r represents the nonlinear transduction and adaptation as given by equation (4.10). Cone coupling and temporal integration are represented by convolution with the product of a Gaussian operator G (equation (4.2)) and an exponential temporal lowpass filter K (equation (4.3)). Inhibitory horizontal cell feedback is modeled by simply subtracting out the horizontal cell signal weighted by k_{hc} from the cone output.

$$cone[\mathbf{r}, t] = v_r[\mathbf{r}, t] * G(\mathbf{r}; \sigma_{cone}[\mathbf{r}, t])K(t; \tau_{cone}) - k_{hc} horz[\mathbf{r}, t] \qquad (4.16)$$

The computations performed by the remainder of the retinal network are based upon the outputs of the cone cell layer. The outputs of the cone cells feed into horizontal and bipolar cells. The computations in the horizontal cell layer shall be described next.

4.6 Horizontal Cell Output

This section describes the computations performed by the horizontal cell which are represented by the box "horizontal cell" in Figure 4.3(b). The primate horizontal cells which are of concern here are the type HI cells. These horizontal cells are believed to be achromatic and receive inputs from many cones within their receptive fields [49]. The sizes of their dendritic fields scale up linearly with eccentricity [23][49]. In addition, passive conduction of signals through gap junctions between neighbouring horizontal cells greatly extends the size of their receptive fields (RF) in comparison to their dendritic spreads [40][1]. The function of the horizontal cells is usually modeled by a diffusion process or a resistive network which results in a Gaussian-weighted spatial and temporal averaging of the cone inputs over the cell's RF [17][40][73]. The connectivity of horizontal cells and the computation of their outputs is shown schematically in Figure 4.5. The outputs $horz[\mathbf{r}, t]$ of the horizontal cell layer feed into bipolar cells forming the surround portion of bipolar cell RF's. In addition, the bidirectional horizontal-cone cell connections serve as a feedback signal path to the cones.

The horizontal cell output may thus be given as the convolution of the cone signals with a spatiotemporal lowpass filter (the product of a spatial Gaussian G and an exponential lowpass temporal filter K). Horizontal cells typically have time constants 2-3 times larger than cones and thus the horizontal cell time constant in the model is set to be $\tau_{horz} = 20$ ms [47]. The overall horizontal cell output is given by the following equation:

$$horz[\mathbf{r}, t] = cone[\mathbf{r}, t] * G(\mathbf{r}; \sigma_{horz}[\mathbf{r}, t]) K(t; \tau_{horz}) \qquad (4.17)$$

where the cone output $cone[\mathbf{r}, t]$ is given by equation(4.16), G by equation(4.2), and K by equation (4.3). The Gaussian width $\sigma_{horz}[\mathbf{r}, t]$ represents a measure of the local spread of signals in the horizontal cell layer and thus locally controls the size of the horizontal cell RF.

Most researchers agree that the centre-surround RF structures observed at the bipolar and ganglion cell level are due to RF's of cones and horizontal cells [49][28]. The cones provide the centre input while the surround fields are attributable to and match the RF size of horizontal cells. The ratio of the centre field diameter to surround diameter is usually in a range between 1:3 and 1:10 in most mammals [21][49]. The summation of signals in the centre and surround portion of a ganglion cell RF is generally modeled by a convolution with a difference-of-Gaussians operator. In most primate models, the ratio of sigmas of the centre (σ_c) to surround (σ_s) Gaussians is approximated to be between 1:1.75 and 1:2 as this gives reasonable agreement with physiologically measured values [24][37][47]. Using a
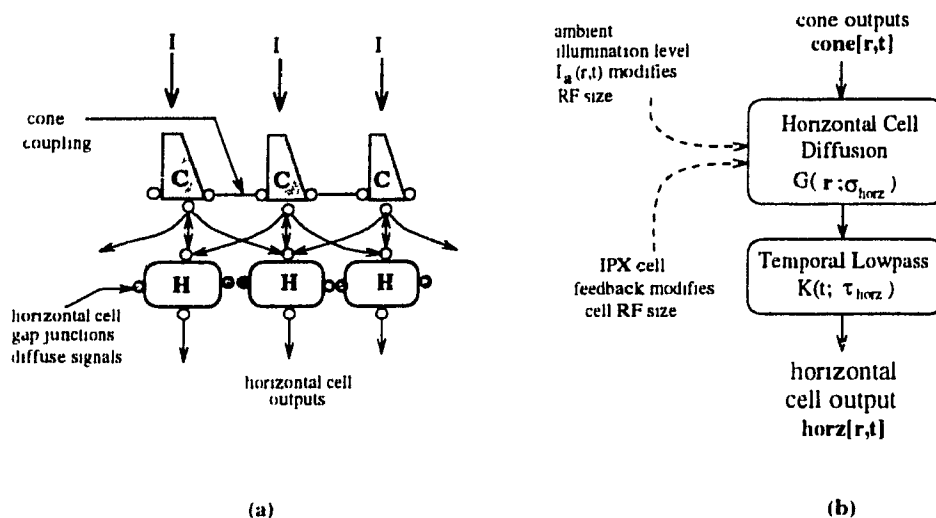
(a)   (b)

Figure 4.5: Horizontal Cell Output: Figure (a) shows schematically the connectivity of horizontal cells in the primate retina Each horizontal cell makes dendritic contacts with several cones In addition, the receptive field (RF) size of horizontal cells is greatly extended beyond its dendritic spread by the passive spread of current through gap junctions between neighbouring horizontal cells. The actual size of the RF is modulated by the conductivity of the gap junctions. Figure (b) shows a block diagram of the computations performed at the horizontal cell layer The summation of cone inputs within the horizontal cell is modeled by Gaussian weighted RF's and is implemented using diffusion. The size of the RF's is controlled locally by adapting the values of σ_{horz} to changing local illumination levels and to interplexiform cell (IPX) feedback. The temporal lowpass nature of the horizontal cell layer is modeled by passing the signals through a single exponential lowpass filter with time constant τ_{horz}.

difference-of-Gaussians model, a $\sigma_c:\sigma_s$ ratio of 1:2 results in receptive field surrounds which are approximately 5-6 times larger in diameter than the centre. This ratio is maintained as a base level in our model.

Biological evidence suggests that the RF size of horizontal cells is modulated by modifying the conductivity of gap junctions between horizontal cells [67]. Like the cones, the need for modulating horizontal cell receptive field sizes can be validated by signal processing arguments [62][81] and supported by psychophysical data showing improved visual acuity with rising illumination levels [65][75].

The conductivity of gap junctions between horizontal cells (and hence $\sigma_{horz}[\mathbf{r},t]$) may be modified in at least two ways. Dopamine released by interplexiform (IPX) cells (and perhaps amacrine cells) feeds back to the horizontal cell layer and modifies the conductivity of horizontal cell gap junctions[68]. In addition, there is a yet unknown mechanism triggered by the local background illumination level which alters the horizontal cell gap

junction conductivity without any change in dopamine levels released by IPX cells [1]. This electrophysiological evidence correlates well with psychophysical evidence which shows a rise in visual acuity with rising illumination levels [65][67].

Horizontal cell receptive fields are generated in our model by further diffusing the cone outputs. The number of iterations of diffusion n_{horz} is kept constant while the diffusivity $\epsilon_{horz}(\mathbf{r})$ is allowed to vary locally resulting in an equivalent Gaussian operator of width $\sigma_{horz}(\mathbf{r})$. Diffusion in both the cone and horizontal cell layers is equivalent to repeated convolution with Gaussians of width σ_{cone} and σ_{horz}. From equation (4.9), the overall effective horizontal cell Gaussian width σ_s is locally given by:

$$\sigma_{surround}^2 = \sigma_{cone}^2 + \sigma_{horz}^2 \qquad (4.18)$$

The widths of the centre and surround portions of the difference-of-Gaussians RF field formed at the bipolar and ganglion cell level are σ_{cone} and $\sigma_{surround}$ respectively. The ratio of these values is typically 1:2 in most models of primate ganglion cell RF's [21][37][47]. Using the equation (4.18), it can be seen that by choosing σ_{horz} to be $\sqrt{3}\sigma_{cone}$, a centre-surround sigma ratio (σ_{cone} to $\sigma_{surround}$) of 1:2 can be easily obtained. Electrophysiological evidence shows that horizontal cell RF sizes shrink in response to an increase in local illumination. The effect of illumination level on horizontal cell RF size is very similar to the effect it has on cone coupling. Thus, as equation (4.15) already accounts for the effect of ambient illumination I_a on cone coupling, the effect of the local illumination level modulating RF size is also carried over to the horizontal cells.

Horizontal cell RF size is also modulated by a second mechanism: dopamine release by interplexiform (IPX) cell feedback. No suitable model or sufficient quantitative data exists in the literature at this point to accurately model the effects of IPX feedback on horizontal cells. It is arbitrarily assumed here that the IPX signal multiplicatively alters the horizontal gap junction conductivity. The output of the interplexiform cell ($IPX[\mathbf{r},t]$) and its effect ($HC_{IPX}[\mathbf{r},t]$) on the horizontal cell coupling will be discussed later in section 4.9. The width of the Gaussian in the horizontal cell layer is thus specified by the following equation:

$$\sigma_{horz}[\mathbf{r},t] = (\sqrt{3}\sigma_{cone}[\mathbf{r},t])(HC_{IPX}[\mathbf{r},t]) \qquad (4.19)$$

In summary, the spatiotemporal lowpass filtering performed by the horizontal cell layer on cone outputs is modeled here by equation (4.17). The receptive field size of horizon-

tal cells is modulated locally to match the local ambient illumination level I_a, and the spatiotemporal contrast in the scene as represented by interplexiform cell feedback signals. The outputs of horizontal cells form the surround portion of both midget and diffuse bipolar cells. The next two sections describe the computations performed in the midget and diffuse bipolar cell layers.

4.7 Midget Bipolar Cell Output / P-cell Pathway

Figure 4.6 shows schematically the signal flow through a midget bipolar cell in the fovea. Midget bipolar cells receive centre input from a single cone in the fovea and surround input from one or more horizontal cells [49]. In the fovea, for both the *on* and the *off* pathways, there is a 1:1 ratio of the number of midget bipolar cells to cones. Furthermore, the outputs of these bipolar cells make 1:1 contacts with midget ganglion cells which project to the Parvocellular layers of the LGN and thereby forming the P-cell pathway. Because of the one-to-one connections from the midget bipolar to the midget/P-type ganglion cells, many of the properties of the P-cell pathway exhibit themselves at the bipolar cell level as well. The P-type ganglion cells appear to be little affected by amacrine cell outputs and thus may be assumed to simply convert the graded midget bipolar cell outputs into spike trains for transmission of information through the optic nerve [47][24].
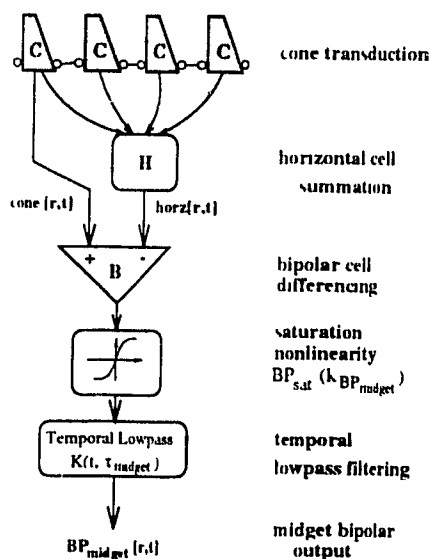

Figure 4.6: Midget Bipolar Schematic: The figure shows a schematic diagram of the information flow through a midget bipolar cell.

In modelling the bipolar cell response, several simplifications or assumptions are made. It is assumed that bipolar cells essentially perform a simple difference operation on the

signals from a single cone and a horizontal cell [17][21][28][30][49]. This operation is followed by a saturation nonlinearity and temporal lowpass filtering. In biological retinas, bipolar cells have two polarities, *on*-centre and *off*-centre cells, which signal positive and negative contrasts, respectively. For simplicity, only the *on*-centre cell is modeled here. In a computer model, there is no problem in representing positive and negative contrast signals within the same *neuron* and consequently, the implementation of *off*-centre cells is not necessary.

The differencing operation performed on the cone and horizontal cell signals gives rise to the spatially antagonistic centre-surround structure of bipolar cell receptive fields. Both cone and horizontal cells have Gaussian weighted receptive fields due to the coupling with neighbouring cones and horizontal cells respectively. This implies that the output of a given cone may be influenced by the outputs of several neighbouring cones. Thus, although the bipolar cell actually performs the difference operation on a single cone and horizontal cell output, the resulting RF of the bipolar cell may be modeled by a difference-of-Gaussians operator. The centre portion of the bipolar RF is driven by the cone input while the surround portion is attributable to the horizontal cell input. The size of the centre and surround portions of bipolar cell RF's is a function of the size of the RF's of the cones and horizontal cells. The ratio of the centre field diameter to surround diameter is usually in the range of 1:3 to 1:10 in most mammals [21][49]. In the present implementation, this ratio is approximately 1:5.

The temporal tuning of bipolar cells may also be largely attributed to the difference operation performed by the bipolar cell on the cone and horizontal cell signals. Horizontal cells have a much larger integration time constant than cones and thus, for temporal changes in the input signal, there is a small time-lag in the surround signal peak response as compared to the cone response at the bipolar cell level. The time constants chosen in the current implementation are based on values used by Richter which give a close fit to biological responses ($\tau_{cone} \approx 10ms$, $\tau_{horz} \approx 20ms$) [17].

In addition to the difference in time constants, there is some evidence that the horizontal cell signal may also be delayed ($\tau_{delay} \approx 3ms$) with respect to the cone input for some but not all bipolar cells at the bipolar cell terminal [47]. This results in an increased transient spike at the outputs of these bipolar cell. The two main classes of bipolar cells of interest to us are the midget and diffuse bipolar cells. Midget bipolar cells feed midget ganglion cells and form the the parvocellular (P-cell) pathway, and diffuse bipolars feed parasol ganglion cells which form the magnocellular (M-cell) pathway. Recall from Chapter 2 that the M-cell pathway is characterized by cells that respond vigorously to temporal transients in the visual signal. The P-cell pathway responds with greater sensitivity to high spatial frequencies but not to high temporal frequencies. It is thus likely that the horizontal cell signal delay exhibits itself only in diffuse bipolar cells. This may account for the increased

temporal responsivity of the diffuse bipolar / M-cell pathway as compared to the other retinal pathway. Thus, for simplification, it is assumed that this horizontal cell signal delay is significant only in diffuse bipolar cells and essentially zero for midget bipolar cells. The midget bipolar cell temporal response in the *computer retina* model is governed only by the difference in time constants between cone and horizontal cell responses.

Following the differencing operation is a saturation nonlinearity operation which defines the dynamic range of the midget bipolar cell. Retinal bipolar cells signal spatio-temporal *contrast* with a high gain and have a much narrower response range around a given background intensity compared to the cones. For low contrast signals, the midget bipolar cell output is quite linear; however, at contrast levels exceeding 1.7-2.0 orders of magnitude, the cell output exhibits saturation [71][72]. For simplicity, an arctangent function ($BP_{sat}(x)$) is used to model the bipolar cell saturation function in the *computer retina*. The choice of the saturation function is arbitrary; however, the arctangent function has some nice properties in that it behaves fairly linearly for small contrast signals, and is symmetric with respect to both positive and negative contrast signals. The symmetric nature of the saturation function is important in our model as it allows the bipolar cell to represent both positive and negative contrast equally well.

Bipolar cell outputs travel from the outer plexiform layer to amacrine and ganglion cells in the inner plexiform layer through the bipolar cell axons. Their long axons act as temporal lowpass filters of the bipolar cell signal, with a time constant on the same order of magnitude as that for horizontal cells [17][47]. Our familiar simple exponential lowpass temporal filter $K(t;\tau)$ (equation (4.3)) is used once again to model this characteristic with $\tau_{midget} = 15$ ms.

The computations at the midget bipolar cell level in the *computer retina* are implemented as in Fleet [24], Richter [47], and Curlander [17] (equation(4.20)) with the addition of a saturation function (equation(4.21)). As with most other models, the relative weightings given to the cone and horizontal cell inputs going into the bipolar cell are chosen to be equal ($k_{cb} = k_{hb} = 1$) in order to allow equal sensitivity for coding positive and negative contrasts.

$$BP_{midget}[\mathbf{r}, t] = BP_{sat}(k_{cb}cone[\mathbf{r}, t] - k_{hb}horz[\mathbf{r}, t]) * K(t; \tau_{midget}) \qquad (4.20)$$

$$BP_{sat}(x) = \frac{1}{\pi}tan^{-1}(\frac{x}{k_{BP_{midget}}}) \qquad (4.21)$$

where	$BP_{midget}[\mathbf{r}, t]$	= midget bipolar cell output
	$cone[\mathbf{r}, t]$	= cone cell output (equation (4.16))
	$horz[\mathbf{r}, t]$	= horizontal cell output (equation (4.17))
	$BP_{sat}(x)$	= symmetric bipolar saturation function
	$k_{BP_{midget}}$	= controls narrowness of response range (.027 $\approx$ 1.7 log units)
	$K(t; \tau_{midget})$	= lowpass temporal filter (equation (4.3))
	τ_{midget}	= time constant for midget bipolar ($\approx$ 15ms)
	k_{cb}, k_{hb}	= weighting given to cone and horizontal cell inputs (1.0)

In summary, the midget bipolar cell output ($BP_{midget}[\mathbf{r}, t]$) is computed by taking the difference of the cone and horizontal cell outputs ($cone[\mathbf{r}, t]$, $horz[\mathbf{r}, t]$) followed by a gain amplification ($k_{BP_{midget}}$) and saturation operation ($BP_{sat}(x)$), and finally by passing this signal through a temporal lowpass filter $K(t; \tau_{midget})$. The saturation function BP_{sat} used here is fairly linear for small signals but exhibits saturation for large positive and negative contrast signals. The value of $k_{BP_{midget}}$ is chosen so that a centre spot 50 times brighter than the surround results in a saturated bipolar cell output (90% of maximum output) [71]. Experimentally, it was found that a value of $k_{BP_{midget}}$ = .027 is appropriate in our model to give the midget bipolar cell a dynamic range of $\approx$ 1.7 log units. The outputs of midget bipolar cells go to midget ganglion (P-type) cells that form the parvocellular pathway.

4.8 Diffuse Bipolar Cell Output / M-cell Pathway

Diffuse bipolar cells provide signals which feed the Magnocellular (M-type) ganglion cell pathway. Just as the midget bipolar cells exhibit most of the properties of the P-type ganglion cell pathway, many of the spatiotemporal properties of M_Y-type ganglion cells begin at the diffuse bipolar cell layer. Figure 4.7 shows schematically the wiring of the diffuse bipolar / M-type ganglion cell pathway.

Recall from Chapter 2 that M_X cells make up the bulk (80%) of the M-cells, are linear in their summation of signals, and appear to receive relatively little amacrine cell input [57]. This situation is very much like that for midget bipolars and midget ganglion (P-type) cells whose outputs were assumed to be very similar. Thus, for simplicity, it is assumed in this model that diffuse bipolar cell outputs and M_X cell outputs are also similar. The remaining 20% of the M-type ganglion cells (M_Y cells) represent only 2% of the total ganglion cell population but receive the bulk of the amacrine cell input and have much more complex RF properties. However, because of the relatively small number of these outputs, the M_Y cell output and amacrine cell outputs are ignored in this model. For the remainder of this thesis, when we talk about M-cells, we will be referring only to the M_X cells unless explicitly stated otherwise.
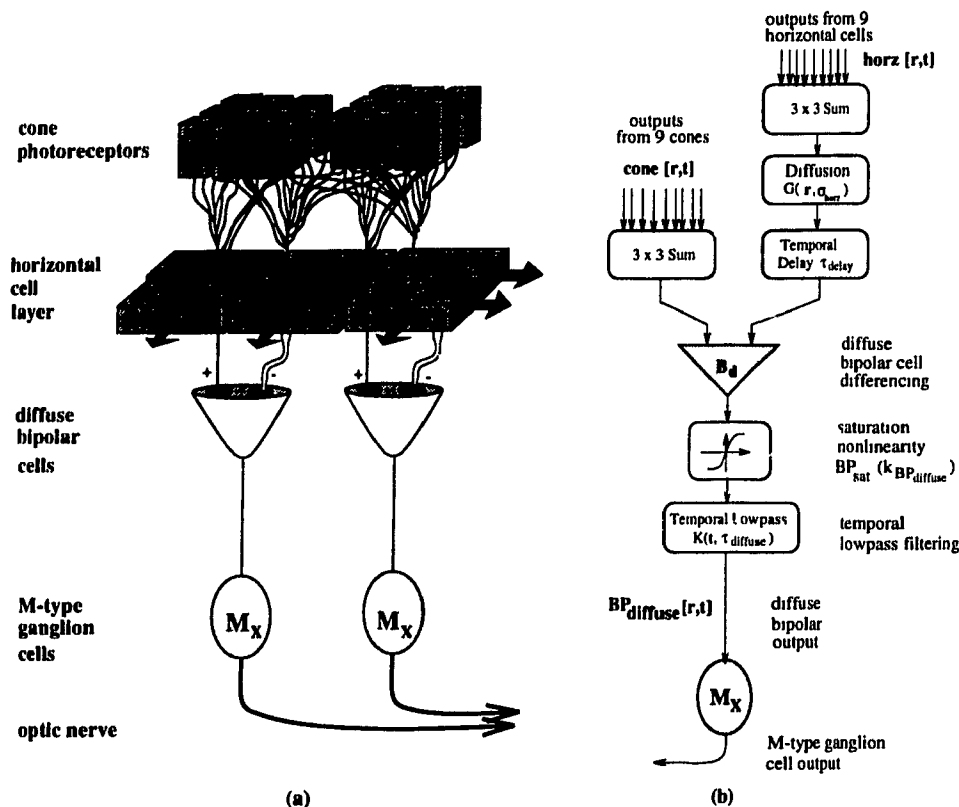
Figure 4.7: **Diffuse Bipolar Schematic:** Figure (a) shows schematically the connections in the diffuse bipolar cell / M-type ganglion cell pathway. Each diffuse bipolar cell receives centre input from 7-9 cones while horizontal cells provide surround input. Horizontal cells receive inputs from many cones from both direct connections with cones and passive conduction of signals through gap junctions in the horizontal cell layer. Diffuse bipolar cell outputs converge on M-type ganglion cells. There is approximately 1 M-type ganglion cell output for every 8-9 cones. Figure (b) shows in block form the computations performed at the diffuse bipolar cell layer.

The properties of the diffuse bipolar cell relevant to the current model are listed below:

- Each diffuse bipolar cell in the fovea receives centre input from at least 7-9 cones [49]. This number grows rapidly in the periphery as the ganglion cell density drops off faster with increasing eccentricity than does the cone density[4]. Thus, diffuse bipolar cells

---

[4]In the *computer retina* model, the convergence of an increasing number of cones into the ganglion cells is partially accounted for at the sampling stage by the log-polar mapping. The log-polar sampling models the dropoff of ganglion cell density and increasing RF size with increasing eccentricity found in the primate retina. Cone density drops off much more slowly than ganglion cell density and thus accounts for the convergence of increasing numbers of cones into ganglion cells. Rather than simply subsampling the input image in the periphery, the log-polar mapping function implements RF's which average an increasing number of pixel values with increasing eccentricity.

80

have receptive field centres about 3 times larger than the midget bipolar cells at all eccentricities. This matches the data on M-cells which show that they have receptive fields 3 times larger than P-cells [23][49][57]. The larger RF's of diffuse bipolars and M-cells leads to a poorer spatial resolution in the M-cell pathway compared to the high acuity P-cell pathway.

- According to Rodieck, there is a 1:1 ratio of the number of diffuse bipolar cells to cones, and thus there is a great deal of overlap between the centre portions of the diffuse bipolar cell receptive fields [49]. However, at the ganglion cell layer, the ratio of M-type ganglion cells to diffuse bipolars is only about 1:8. Thus, there is only one M-cell output for approximately every 8-9 cones.

- The surround input to these cells consists of input from several horizontal cells.[5] The total size of the surround RF is 2-3 times larger than for midget bipolars. This is accounted for by taking the average of 9 horizontal cells and then further diffusing this value to model the summation of signals over a large area.

- Cells in the diffuse bipolar / M-cell pathway are more responsive than P-cells to higher temporal frequencies in the visual signal. Furthermore, M-cells typically have faster axon conduction velocities [57]. The time constants in the cone and horizontal cell layers (τ_{cone}, τ_{horz}) are fixed. The larger latency of the horizontal cell layer compared to the cone layer leads to much of the temporal sensitivity of bipolar cells in general. Thus, to account for the higher diffuse bipolar cell temporal sensitivity, the temporal lowpass characteristic of diffuse bipolar cell axons is assumed to have much shorter time constants than midget bipolars ($\tau_{diffuse} = 5ms$ compared to $\tau_{midget} = 15ms$). This leads to a higher cutoff frequency for diffuse bipolar cell outputs when compared to midget bipolars.

- In addition to the difference in time constants of integration for the cone (τ_{cone}) and horizontal (τ_{horz}) cell outputs, the surround input is delayed compared to the centre by τ_{delay} ms [47] for bipolar cells. This delay appears to occur at the diffuse bipolar cell terminal and not at the horizontal cell output. The value used for τ_{delay} is chosen to be 3 ms or $\approx 0.2\,\tau_{horz}$ as suggested by Richter [47] and Fleet [24]. Fleet also shows that much of the temporal sensitivity of diffuse bipolar / M-cells may be accounted for by this small delay in the surround input.

- M-type ganglion cells react to contrast with a much higher gain than P-type ganglion cells and have a threshold to saturation range of only 1 log unit of contrast [57]. It is assumed here that this feature is exhibited at the diffuse bipolar cell level. The saturation characteristic is once again modeled using an arctan function (equation(4.25)) and the constant $k_{BP_{diffuse}}$ is chosen to be 0.015 to give a 1 log unit contrast dynamic range.

Fleet [24] shows that the centre-surround (CS) model may be used to model operators with a range of spatiotemporal sensitivities with only a change in some parameters. They show that the M-cell pathway, with its higher temporal frequency response but poor spatial

---

[5]The actual number of inputs from horizontal cells to diffuse bipolars is still unknown [7][21][49].

response, may be accommodated by CS-like operators using an adjustment of the centre and surround time constants and by introducing a time delay between centre and surround signals. The same approach is used here.

The basic computation of the outputs of diffuse bipolar cells is very similar to that for midget bipolar cells. It still involves a difference operation between the centre and surround signals, followed by a gain and saturation operation, and then temporal lowpass filtering. The main difference in the computation of diffuse bipolar cell outputs as opposed to midget bipolar outputs stems from their much larger receptive fields. To account for their larger receptive fields, the centre input for each diffuse bipolar cell is the sum of nine cone inputs in a 3x3 window centred around that bipolar cell. Likewise, the surround fields are computed by first summing horizontal cell outputs using 3x3 windows and then further diffusing to increase the surround receptive field size to be about 2-3 times larger than for midget bipolars. Furthermore, the surround input is delayed by $t_{delay} = 3$ms compared to the centre input. The diffuse bipolar output is computed by taking the difference of the centre and surround signals and passing this through a saturation function followed by a temporal lowpass filter.

The diffuse bipolar cell output is modelled here by the following equations:

$$BP_{diffuse}[\mathbf{r}, t] = BP_{sat}(k_{bc}centre[\mathbf{r}, t] - k_{bh}surround[\mathbf{r}, t]) * K(t; \tau_{diffuse}) \qquad (4.22)$$

$$centre[\mathbf{r}, t] = \sum_{3x3} cone[\mathbf{r}, t] \qquad (4.23)$$

$$surround[\mathbf{r}, t] = \sum_{3x3} horz[\mathbf{r}, t - \tau_{delay}] * G(\mathbf{r}; 3\sigma_{horz}[\mathbf{r}, t]) \qquad (4.24)$$

$$BP_{sat}(x) = \frac{1}{\pi} tan^{-1}\left(\frac{x}{k_{BP_{diffuse}}}\right) \qquad (4.25)$$

where

$BP_{diffuse}[\mathbf{r}, t]$	=	diffuse bipolar cell output
$centre[\mathbf{r}, t]$	=	centre signal is average of 9 cone inputs
$surround[\mathbf{r}, t]$	=	surround signal from delayed horizontal cell inputs
$cone[\mathbf{r}, t]$	=	cone cell output (equation (4.16))
$horz[\mathbf{r}, t]$	=	horizontal cell output (equation (4.17))
$BP_{sat}(x)$	=	symmetric bipolar saturation function
$k_{BP_{diffuse}}$	=	controls narrowness of dynamic range ($\approx .015 = 1$ log unit)
$K(t; \tau_{diffuse})$	=	lowpass temporal filter (equation (4.3))
$\tau_{diffuse}$	=	time constant for diffuse bipolar ($\approx 5ms$)
τ_{delay}	=	time delay between centre and surround (*approx* 3ms)
k_{cb}, k_{hb}	=	weighting given to cone and horizontal cell inputs ($= 1.0$)
$G(\mathbf{r}; \sigma)$	=	Gaussian operator of width σ (equation (4.2))
$\sigma_{horz}[\mathbf{r}, t]$	=	controls size of horizontal cell RF field

In summary, the diffuse bipolar / M-cell pathway is characterized by receptive fields that are about 3 times larger in diameter than those of the midget bipolar / P-cell pathway at all eccentricities. It is assumed in the present model that most of these properties exhibited at the M-type ganglion cell level are generated at the diffuse bipolar cell level. The larger RF's of M-cells lead to a poorer spatial resolution than in the P-cell pathway. M-cells are instead tuned to respond to higher temporal frequencies than P-cells and are thus better at signaling motion in the visual stimuli. The M-cells respond with a much larger gain to spatiotemporal contrast but have a much narrower dynamic range compared to P-cells (i.e. they saturate in response to high contrast input).

4.9   Interplexiform Cell Output

Anatomical studies show that interplexiform (IPX) cells in the primate retina receive input from bipolar cells and send their output into the outer plexiform layer to horizontal cells [21][49][68]. IPX cells have large overlapping receptive fields which, like all retinal cells, scale up with eccentricity. Figure 4.8 shows schematically the connectivity of interplexiform cells in the primate retina. Electrophysiological studies have implicated them in adaptation of horizontal cell receptive fields sizes [68]. The dopamine released by IPX cells under stimulation has been shown to reduce the conductivity of gap junctions in the horizontal cell layer and thus reduce the effective RF size of horizontal cells [68][78].

IPX cells primarily receive a spatio-temporal contrast signal from the outputs of several bipolar cells in their receptive fields. Foveal IPX dendritic fields are approximately 100-200μm in diameter (4-8 cone spacings) [49]. Their outputs feed back to horizontal cells where they modify the gap junction conductivity and multiplicatively alter the diffusivity. Umino's data show that flickering light leads to increased IPX output and up to a 30% reduction in the horizontal cell gap junction conductivity [68]. His results also show that
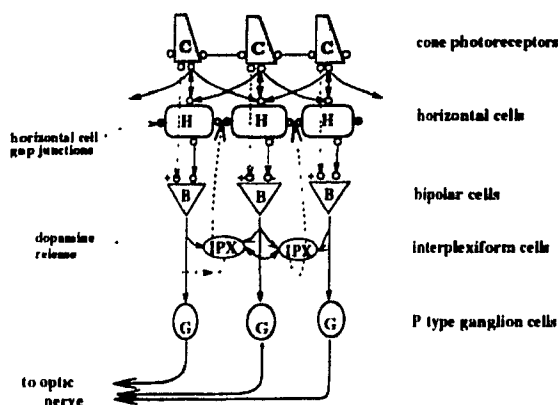
Figure 4.8: Interplexiform Cell Feedback: The figure shows schematically how interplexiform cells receive input from bipolar cells and have feedback paths to horizontal cells Stimulation of IPX cells releases dopamine which reduces the conductivity of gap junctions between horizontal cells. The reduced spread of signals in the horizontal cell layer effectively reduces the size of the horizontal cell receptive fields

changes in the background illumination level have no effect on the IPX cell outputs.

Although there are insufficient data in the published literature on which to base a quantitative model of the IPX output, it is possible to qualitatively model the effect of IPX cells on horizontal cells. It is assumed here that large outputs from bipolar cells result in increased release of dopamine by IPX cells. Since the magnitude of the bipolar cell response is large in regions of high spatial or temporal contrast, we propose that these sorts of stimuli should result in increased dopamine release by IPX cells, decreased horizontal cell coupling, and thus decreased horizontal cell RF size. To be consistent with Umino's data, IPX feedback is assumed to be able to alter the horizontal cell receptive field size by up to 30% [68]. This hypothesis is supported by Umino's data on increased IPX output in response to flickering light stimuli (high temporal contrast) [68]. Since the bipolar cell output is unaffected by global changes in illumination level (due to the "dc" subtraction mechanism), it is not surprising that IPX cell outputs are also unaffected for this condition.

The idea of using a measure of local signal contrast to control smoothing is one that is also prevalent in computer vision. Perona [44] uses a similar idea in a smoothing algorithm based on anisotropic diffusion in which the local diffusivity of a diffusive smoothing operation is drastically reduced in image regions having a high intensity gradient. Using such an algorithm smoothes noise in regions of uniform structure, while preserving the localization of edge information.

The effect of interplexiform (IPX) cell feedback on horizontal cells is modeled here in two parts:

$$IPX[\mathbf{r}, t] = k_{ipx}^{-1}(BP^2_{midget}[\mathbf{r}, t] + BP^2_{diffuse}[\mathbf{r}, t]) * G(\mathbf{r}; \sigma_{IPX})K(t; \tau_{IPX}) \qquad (4.26)$$

$$HC_{IPX}[\mathbf{r}, t] = 0.7 + \frac{0.5}{IPX[\mathbf{r}, t] + 1} \qquad (4.27)$$

Here $IPX[\mathbf{r}, t]$ represents the IPX cell output and is essentially a measure of the local spatiotemporal contrast (derived from a combination of the diffuse bipolar and midget bipolar cell outputs) over the receptive field of the IPX cell. The IPX receptive field is represented by a Gaussian of width $\sigma_{IPX} = 2.0$ $(G(\mathbf{r}; \sigma_{IPX}))$ which is convolved with midget bipolar cell outputs to give IPX receptive field diameters of between 4 and 8 cone spacings in the fovea. This value is chosen to be consistent with the anatomical data from Rodieck [49]. It is, however, quite possible that IPX receptive fields could be much larger than their dendritic field size. We assume that IPX cells have slightly longer temporal integration time constants than horizontal cells and thus a temporal lowpass filter ($K(t; \tau_{IPX})$) with time constant ($\tau_{IPX} = 30$ms), is used to model this. k_{ipx} is a constant that determines the rate with which an IPX cell output varies with the level of bipolar cell output. This was arbitrarily given a value of $k_{ipx}=0.25$ so that only bipolar cell outputs greater than 25% of their maximal value could reduce the horizontal cell coupling.

$HC_{IPX}[\mathbf{r}, t]$ accounts for the effect of interplexiform cell output on horizontal cell coupling. This function has a value that approaches 0.7 in regions of high spatiotemporal contrast and may be as high as 1.2 in regions of low spatiotemporal contrast. Recall that this function is assumed to multiplicatively alter the horizontal cell coupling as given by equation (4.19). The form of this function and its associated parameters were chosen arbitrarily with the main consideration being that interplexiform output preturbs the horizontal cell receptive fields by only as much as 30% from their nominal values thereby acting as a fine tuning adaptation mechanism only. This is shown in Figure 4.9 which plots the variation of horizontal cell coupling due to IPX cell feedback ($HC_{IPX}[\mathbf{r}, t]$) versus the level of bipolar cell signal output with $k_{ipx}=0.25$.

In summary, each interplexiform cell collects signals from several bipolar cells over its large receptive field. Since bipolar cells essentially code spatiotemporal contrast in the input signal, the IPX cell is responsive to both high spatial contrast (edge regions), and high temporal contrast (motion, flickering light). When stimulated, interplexiform cells release dopamine which feeds back to horizontal cells and reduces the conductivity of gap junctions in the horizontal cell layer. Thus, in regions of high spatiotemporal contrast, the horizontal cell receptive field size is diminished by IPX cell feedback.
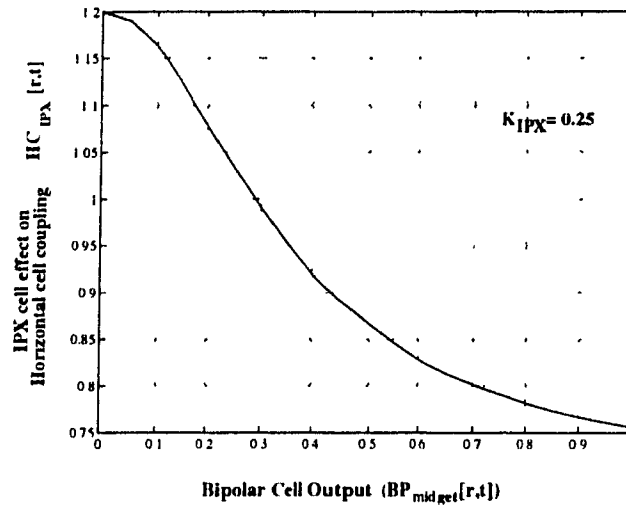
Figure 4.9: **IPX Cell Feedback Effect:** The figure shows the factor by which interplexiform cell feedback modifies the horizontal cell receptive field size with variation of the bipolar cell signal level (see eqns (4 26) and (4.27)) Bipolar cells are responsive to spatial and temporal contrast in the visual image. The interplexiform cell feedback is assumed to modify the horizontal cell receptive field size by a factor proportional to the IPX cell output Consequently, in regions of high spatio/temporal contrast, the horizontal cell receptive field size is diminished.

4.10 P-type Ganglion Cell Output

In the fovea, there is a one-to-one connection from midget bipolar cells to midget / P-type ganglion cells. The basic properties of P-type ganglion cells are, for the most part, a direct result of midget bipolar cell outputs. There are relatively few inputs from amacrine cells to these P-type ganglion cells and thus, for simplicity, the P-cell output here is assumed to be identical to the midget bipolar cell output as described in previous sections.

$$P_{cell}[\mathbf{r}, t] = BP_{midget}[\mathbf{r}, t] \tag{4.28}$$

Figure 4.10(a) plots the magnitude of the Fourier transform of the adaptive centre-surround operators as developed in this model at a bright illumination intensity. The figure shows the expected spatiotemporal tuning of P-type ganglion cells in our model. At bright illuminations, the model P-type ganglion cells have a peak response to spatial frequencies near 0.10 cycles/pixel (14 cycles/degree) and are able to resolve spatial frequencies as high as 0.40 cycles/pixel (60 cycles/degree). The peak model P-cell temporal frequency response is at 9 Hz. These values are comparable to the highest psychophysically discernible spatial frequencies of 50-60 cycles/degree and a peak temporal frequency response at 8-9 Hz for the

primate P-cell system [57][33].. Note that the spatial frequency sensitivity is much greater than that for temporal frequencies in the parvocellular pathway.

In summary, the P-type ganglion cell outputs represent the high spatial acuity pathway for the visual system. These cells have small receptive fields, and at high illuminations, are able to resolve features with sizes of the order of a single cone spacing. However, P-type ganglion cell outputs do not respond well to high spatial frequencies.

4.11 M-type Ganglion Cell Output

M-type ganglion cells receive their input primarily from diffuse bipolar cells and from some amacrine cells. The basic properties of 80% of the M-type ganglion cells are similar to the outputs of diffuse bipolar cells. These cells are much like cat X-cells and thus they behave similarly to P-cells in their linear summation of signals [57]. Amacrine cell input does not seem to have a major impact on the output of these cells. It is only the remaining 20% of the M-type ganglion cells (M_Y) that likely receive considerable input from amacrine cells. As M-type ganglion cells only represent 10% of the total ganglion cell population, M_Y cells account for only 2% of the total ganglion cell output. For this reason, the M_Y cell outputs are not modeled here.

It is further assumed here that the outputs of the M_X cells are sufficiently well represented by the diffuse bipolar cell outputs. The M-cell output is thus given by:

$$M_{cell}[\mathbf{r}, t] = BP_{diffuse}[\mathbf{r}, t] \qquad (4.29)$$

In summary, our model is constructed so that there is one M-cell output for every 9 cone inputs. A ratio of M-cell outputs to P-cell outputs of 1:9 is comparable to the 1:8 ratio found in primates. M-cells have receptive fields which are approximately 3 times as large as those for P-cells and have a much higher contrast gain. Figure 4.10(b) shows the response of the M_X type ganglion cell to spatial and temporal frequency modulation. The much larger receptive fields of the M-type ganglion cells compared to P-cells results in sensitivity with a lower peak spatial frequency response. The delay between the cone and horizontal cell signals at the diffuse bipolar cell level results in a much stronger sensitivity to temporal frequency modulation for M-type ganglion cells. Thus these cells are ideal for detecting motion at a coarse spatial resolution.

4.12 Model Summary

The retinal model developed in this chapter is a simple one which attempts to account for the adaptation of the retina to a wide range of illumination levels. The model is restricted to
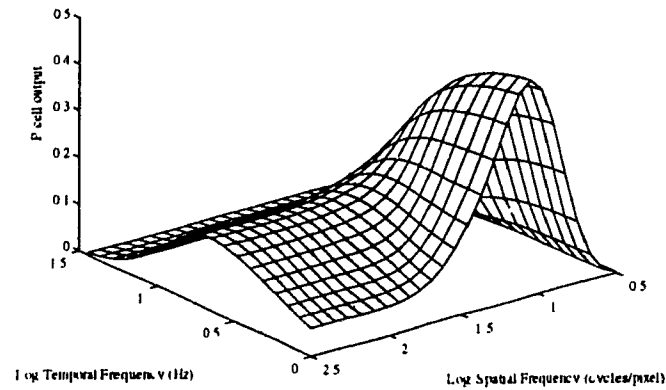
(a)
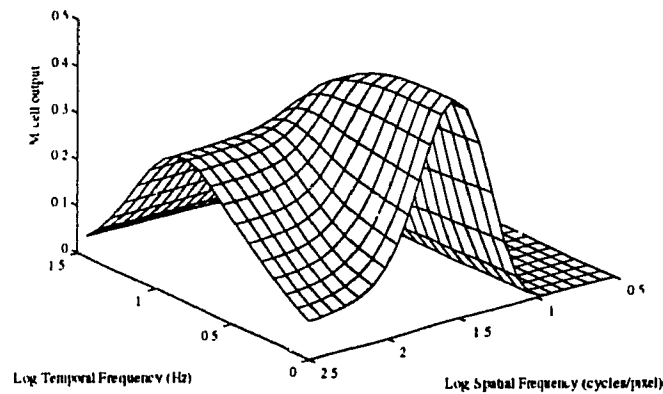
(b)

Figure 4.10: P-cell and M-cell Spatiotemporal Tuning: The figures show the frequency response of P-cells and M-cells in our model as a function of spatial and temporal frequency at one intensity level for small signal levels The P-cell responds to higher spatial frequencies than M-cells but has a poorer response to higher temporal frequencies.

the processing of achromatic information at photopic light levels. In this way, complications associated with modelling the rod system, rod-cone interactions, and color constancy are avoided.

A log-polar transformation is used to account for the data reduction due to nonuniform sampling, and the convergence of information, occurring within the retina. This mapping splits the incoming information into two separate streams: the fovea represented in the Cartesian domain, and the periphery represented in the log-polar domain. Since all computations are spatially localized, the data structures containing the fovea and periphery information may be processed separately and identically by the rest of the network. Features of the peripheral processing such as the increase of receptive field sizes with eccentricity are accounted for by the log-polar mapping and made transparent to the computations required in the model.

The model is an extension of the spatiotemporal centre-surround operators presented by Fleet [24] and Richter [47]. The extensions include modelling the nonlinear transduction and adaptation at the photoreceptor level, and adaptation of receptive fields of various cells with varying illumination levels. The model shows that the acuity changes found with changing illumination levels in the biological retina may be accounted for by the adaptation of cone and horizontal cell receptive field sizes. Furthermore, we suggest a possible mechanism by which interplexiform cell feedback modifies the horizontal cell coupling as a function of the local spatiotemporal contrast.

Figure 4.11 shows schematically the computations performed at each layer in our model. A hyperbolic nonlinearity at the receptor level converts image intensities to signals that are used by the rest of the retinal network. The sensitivity of the cones is controlled by a combination of both the local spatial ambient intensity I_S (modelling the effect of horizontal cell feedback), and a long term temporal ambient intensity I_T (modelling the effect of pigment bleaching). These adaptation mechanisms act to centre the 3 log unit response range of the cones around the combined ambient intensity signal I_a. Cones are coupled to neighbouring cones. The degree of coupling varies with illumination level and effectively controls the retinal visual acuity.

Cone outputs go to both horizontal cells and bipolar cells. Horizontal cells compute a spatiotemporal average of the cone signals over a large receptive field and also provide signals to bipolar cells. The cones and horizontal cells have different time constants leading to temporal transients at the bipolar cell level. There are two classes of bipolar cells and ganglion cells. Each midget bipolars cell receives a centre input from a single cone and a surround input from a horizontal cell. Each midget bipolar cell provides an output to one P-type ganglion cell. These cells comprise the high acuity visual pathway. Diffuse bipolar cells get centre input from nine cones and surround input from many horizontal cells. Both

the centre and surround portions of their receptive fields are three times larger than those of midget bipolars. A delay between the centre and surround signals enhances the diffuse bipolar cell response to high temporal frequencies in the input signal. Diffuse bipolar cells provide inputs to M-type ganglion cells. There is one M-type ganglion cell output for every nine cone inputs. This pathway has poorer spatial resolution, higher temporal sensitivity, and a larger contrast gain than the P-cell pathway. Bipolar cells also provide input to interplexiform cells which then feed back to horizontal cells. Increased spatiotemporal contrast causes IPX feedback to reduce the horizontal cell coupling.

In the next chapter, the behaviour of the model is examined in response to a variety of stimuli and compared to published data on biological retinas.
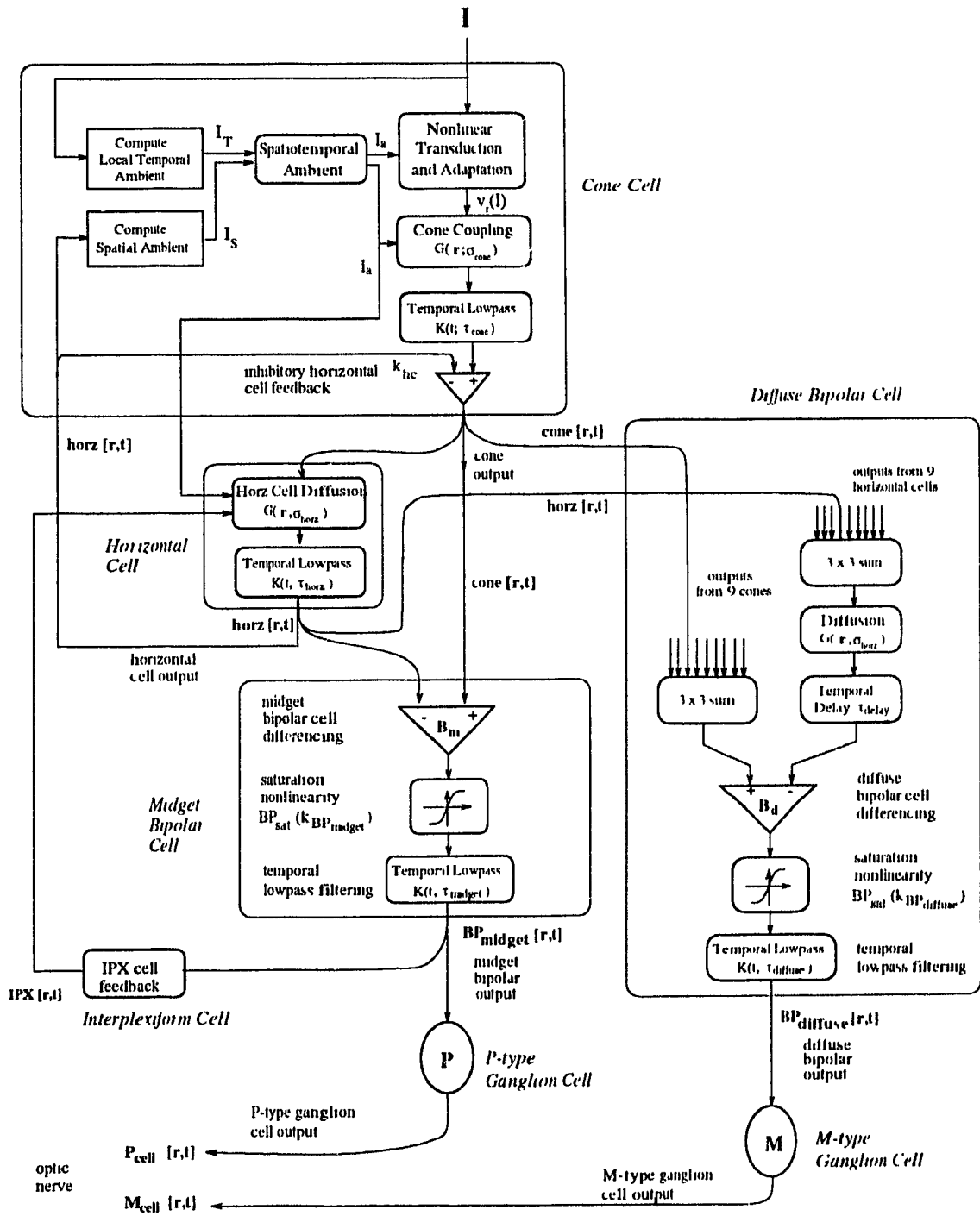
Figure 4.11: Retinal Model Schematic: The diagram shows the computations performed at each layer in our retinal model.

In this chapter, the response of the *computer retina* model to various simple visual stimuli is presented and compared to biological retinas. In addition, the response of the model to more complex images is also shown in order to demonstrate what the outputs in the retina might look. The aim is to show that the retinal model developed in this thesis, although quite simple, responds in a manner qualitatively similar to the primate retinal cone system. In particular, the model qualitatively accounts for the gain and sensitivity changes as well as visual acuity changes found in the retina with illumination levels varying over 7 orders of magnitude.

5.1   Methods

5.1.1   Model Implementation

The model of the retinal cone system as described in the previous chapter was implemented in C and executed on Sun4 Sparc machines.[1] The *computer retina* program takes in as input a sequence of images which are then processed by the model. Several sets of outputs are produced, one for each of the retinal neuron layers. The output data may be either displayed as images or analyzed using a mathematical package such as MATLAB.[2]

The *computer retina* program simulates both the temporal and spatial characteristics of retinal processing. The spatial domain is discretized into pixels with each pixel width assumed to represent the width and spacing of foveal cones in the human retina. The temporal domain is also discretized. The sequence of images read in as visual input is assumed to have a 3 ms interval between each successive frame. This value was chosen to simplify the implementation of a 3 ms delay (τ_{delay}) of the horizontal cell signal to the diffuse bipolar terminal required in the model [47]. For some experiments, thousands of image frames had to be processed by the *computer retina* because these experiments required the input image stimuli to be presented for several seconds of real-time. Typical execution times on a sequential SPARC-10 machine for 100 x 100 images (without using log-polar sampling) were about 5 seconds/frame.

The *computer retina* program allows flexibility in controlling the features of the model that are enabled or disabled. For example, the use of log-polar sampling can be enabled and disabled at will. For most of the experiments described in this chapter, log-polar (foveated)

---

[1]Sun4 Sparc is a registered trademark of Sun Microsystems, Inc.

[2]MATLAB is a registered trademark of The MathWorks, Inc.

sampling was disabled. With this feature disabled, there was no variation of receptive field (RF) sizes with eccentricity and the fovea encompassed the entire field of view. This simplified analysis and comparison of the model cell outputs to responses of biological retinal cells, most of which were measured in the fovea. Other *computer retina* program directives allow enabling/disabling of features such as the effects of horizontal feedback on cones, and adaptation of cone and horizontal cell receptive field sizes.

5.1.2 Input Stimuli

In order to test the adaptive aspects of the model, images with a large dynamic range of intensities (up to 7 orders of magnitude) are required. Commercial camera systems and frame grabbers are inadequate, as most only use 8 bits to represent the output intensity level. To represent 6-7 orders of intensity magnitude, at least 20 bits are required. Most image databases are also restricted to 8 bit intensity dynamic ranges and thus are not directly suitable.

To circumvent these problems, most of the images used in these experiments were synthetically generated. Two main types of experiments were conducted and the stimuli required for each type were generated in different ways.

To compare the outputs of this model with published data on biological retinas, some of the experiments commonly performed by electrophysiologists were replicated. Typically, these experiments measure the outputs of a few retinal cells in response to very simple stimuli such as flashed backgrounds, spots of light, step edges, and temporally modulated sine gratings. Such simple images, with dynamic ranges of up to 12 log units of intensity, were easily generated in software and used as input to the *computer retina*.

In addition to experiments with simple stimuli, the outputs produced by the model in response to more complex stimuli (more realistic images) are also shown. For these tests, some images were generated using a very simple ray tracing image generation package.[3] This package used 16 bits to quantize the image intensities allowing 4 orders of magnitude of image intensities to be represented in a single image. To further increase the input illumination dynamic range, the intensity values in synthetic images and images from image databases were exponentially scaled by various factors to crudely approximate the effects of increased illumination levels.

---

[3]The ray tracing package (*MakeImage*) used in the experiments was developed by Hiro Yamamoto of Canon, Inc.

5.1.3 Units

All intensity values in this thesis are expressed in photopic trolands (td) as this is the unit most commonly used in the biological literature. Photopic trolands are a measure of retinal illuminance and are defined as the product of luminance (cd/cm^2) and the pupil diameter in (mm). Time is expressed in seconds (s) or milliseconds (ms). Cell output values are normalized so that a maximal output is one. Spatial frequencies are represented in cycles/pixel or cycles/degree when compared with the primate data. Temporal frequencies are expressed in Hertz (Hz).

5.1.4 Model Evaluation

The results of four basic types of experiments are presented in this chapter. These are:

- Flashed background experiments

- Experiments with sinusoidal gratings

- Experiment with step edge stimuli

- Experiments with more complex real and synthetic images

The first two types replicate some of the typical experiments performed by electrophysiologists on biological retinas and thus allow comparison of the *computer retina* outputs to biological retinal cell responses. The last two types of experiments show the behaviour of the *computer retina* in response to more complex stimuli and illustrate the data reduction achieved by using log-polar sampling.

Wherever possible, comparisons of the *computer retina* outputs to those in biological retinas are made using published data on the primate retina. Although there have been a fair number of recordings of the outputs of primate cones and ganglion cells[4] [4][8][19] [46][55], the recording of most other retinal cells is extremely difficult to study in mammals because of their small size. What is available are recordings of these cells in other animals. Fortunately, for many visual properties, interspecies comparisons are possible when the underlying behaviour and structure of the retina are similar [15][57]. Many of the visual properties of interest here can be qualitatively compared with fish, cat, and monkey retinas. Therefore, comparisons of the model outputs are made with data from animals whose visual systems are believed to be similar to primates, when primate data was not available.

In making comparisons of the *computer retina* responses with biological retinal cells, the differences in the polarity of some retinal cell outputs as compared to the model responses

---

[4]Many of the ganglion cell characteristics are actually inferred from recordings of cells in the Lateral Geniculate Nucleus (LGN), where the bulk of the ganglion cell outputs terminate.

should be noted. In all biological vision systems the output potential of photoreceptors (rods and cones) and horizontal cells hyperpolarize (become more negative) in response to increased light stimulation. In contrast, our model cone and horizontal cell outputs are designed to become more positive to signal increased output levels. In biological retinas, bipolar cells are of two types: those that hyperpolarize in response to increased stimulation in their receptive field centres, and those that depolarize (become more positive). The bipolar cells outputs in the *computer retina* are positive when the receptive field centre is brighter than the surround and are negative when the surround is brighter than the centre.

5.2 Flashed Background Experiments

We conducted flashed background experiments similar to those conducted by Normann, Werblin, and Schnapf in order to show the temporal responses of our *computer retina* cells to full-field flash inputs [41][55][72]. In these experiments, a uniform background intensity (which fills the entire visual field) was presented to the retina interspersed with short intervals in which a background of a different intensity was "flashed" or substituted. The response of various cells are recorded for the entirety of the experiment. Four types of experiments were performed with flashed background stimuli. These were used to determine the following:

1. The cone "impulse" responses to short dim flashes

2. The effect of horizontal cell feedback on cone output

3. The temporal response of various cells to long full-field flashes

4. The intensity-response curves for various retinal cells

The following sections describe the results of the above tests.

5.2.1 Cone "Impulse" Response

Figure 5.1 (top) shows the superimposed responses of a model cone cell when the *computer retina* was subjected to short 30 ms "flashes" of increasing intensity and the responses of a monkey cone (bottom) in a similar test [55]. The monkey cone response is characterized by a peak due to the flash followed by an overshoot when returning to the resting potential. This overshoot is due to the effects of feedback from horizontal cells to the cone. The model response also exhibits this overshoot with the horizontal cell feedback enabled. The model cone output reaches a peak 30 ms after presentation of the "flash" while a monkey cone typically takes 50 ms. This discrepancy indicates that the cone time constant ($\tau_{cone} = 10$ ms) used in the model may be too small. However, the chosen cone and horizontal cell
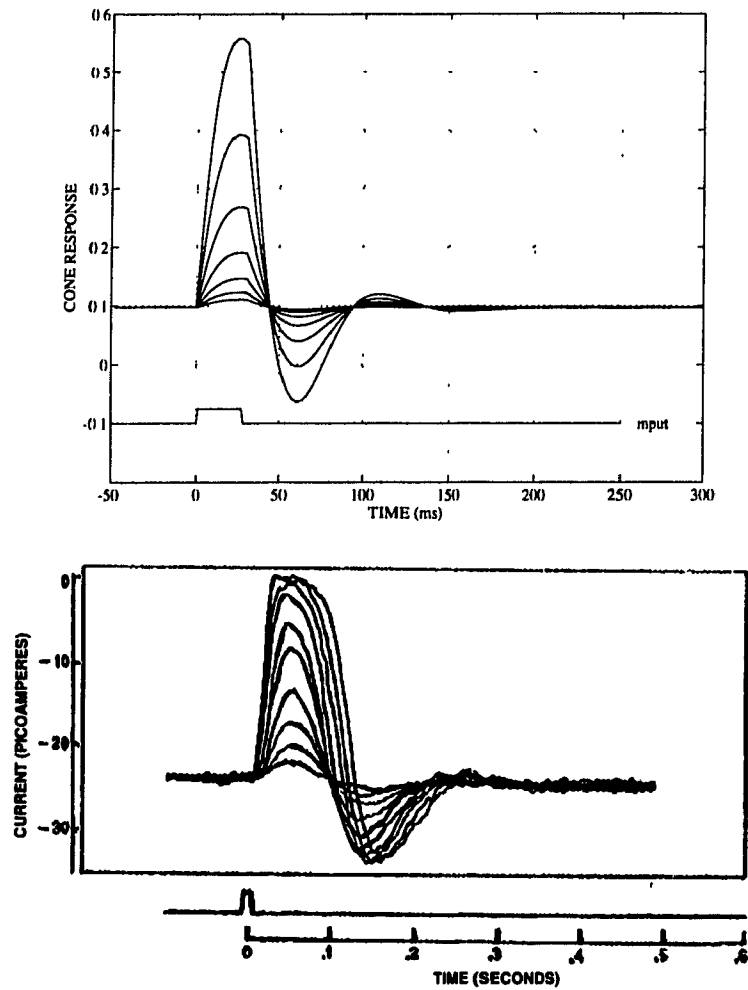
Figure 5.1: Cone Response to Short Full-Field Flashes: The top figure shows the model cone response to 30 ms full-field flashes at flash intensities of 10, 20, 40, 80, 160, 320, and 640 trolands added onto a background of 100 trolands. The bottom figure shows membrane current from a monkey cone as the flash intensities were progressively doubled (from Schnapf [55], ©1987 Scientific American).

time constants are consistent with the values used by Richter [47]. In all other aspects, the model's cone response appears to behave similarly to the monkey cone cell.

5.2.2 Effects of Horizontal Cell Feedback on Cone Output

To isolate the responses of cones alone, without the horizontal cell feedback, electrophysiologists often treat the retina with an aspartate solution. The presence of aspartate blocks the horizontal cell signal from influencing the cone output [21][41]. In the *computer retina* program, it is of course simple to turn off the horizontal cell feedback.
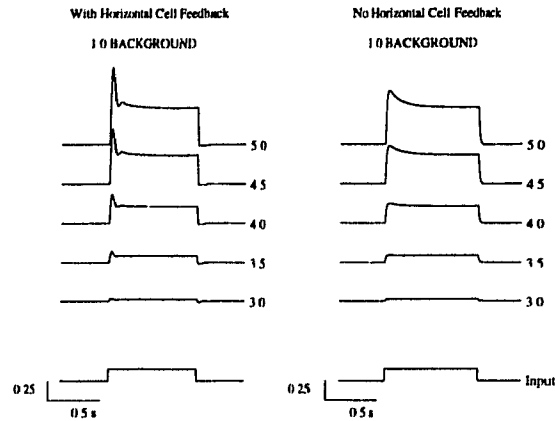
Figure 5.2(a) shows the model cone response to a flashed background test both with and without horizontal cell feedback. Data on the effects of horizontal cell feedback on primate cone responses are not available. However, for comparison, data for the *gecko* "cone-like" rod photoreceptors is shown in figure 5.2(b).

Although the temporal characteristics of the gecko rod are much slower than a primate cone and the input stimuli used are slightly different, the effects of horizontal cell feedback on the gecko photoreceptor responses are comparable to that observed in the model cone response. It can be seen that when horizontal cell feedback is present, the small delay in the feedback signal with respect to the cone serves to significantly increase the peak amplitude and sharpen the cone temporal response to a "flash". The initial cone peak response is quickly diminished by the effects of network feedback from the horizontal cells. This network adaptation mechanism acts to quickly return the cone potential to the near the middle of its response range, thereby preventing cone saturation.

5.2.3 Cell Responses to Full-Field Flashes

Shown next are the outputs of the model cone, horizontal, and bipolar cells in response to flashed background experiments performed at various ambient illumination levels. These outputs are compared to those recorded in fish retinas by Normann [41] and Werblin [72].

Figure 5.3 shows the model cone outputs (top) and the *Necturus* (a type of fish) cone recordings (bottom) when exposed to long (900 ms - 2 s) test flashes of various intensity at two different background intensities [41]. The *Necturus* cone recordings were made in an aspartate treated retina and thus were isolated from the effects of horizontal cell feedback [41]. To allow for a comparison, a separate experiment recorded the cone outputs in the absence of horizontal cell feedback. The model cone responses are similar to those recorded in the *Necturus*. The main difference is that the model cones have a much sharper decay from the initial peak response to a flash, and thus reach a stable plateau much faster (within 250 ms) than the *Necturus* cones (about 1 s). This decay to a stable plateau is a result of cone temporal adaptation mechanisms which adapt the cone sensitivity to the new ambient

(a)
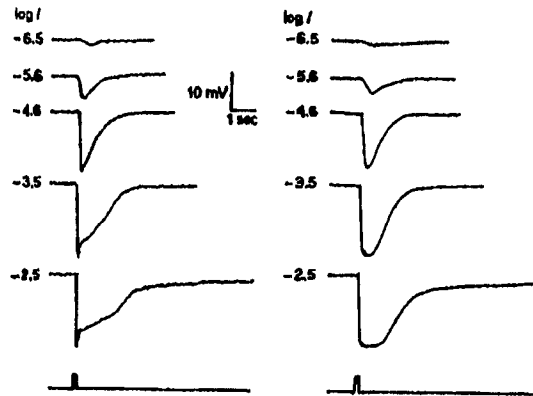
(b)

Figure 5.2: Effect of Horizontal Cell Feedback on Cone Response: (a) shows the normalized model cone responses to 900 ms flashes of varying intensity with horizontal cell feedback enabled (left) and disabled (right). The intensity of the flash is indicated beside each curve in log troland units. The background intensity was 1.0 log troland units. It can be seen that horizontal cell feedback causes the cone potential to very quickly return from a peak response to one nearer to the middle of its response range, thus "sharpening" the cone transient response. These responses may be compared with those obtained from recordings of *gecko* "cone-like" rod photoreceptors in (b) with horizontal feedback present (left) and absent (right) (from Dowling [21] with permission of Harvard University Press). The *gecko* rods hyperpolarize in response to increased illumination stimulation and thus their responses are inverted with respect to the model cone responses. Although the temporal characteristics of *gecko* photoreceptors are much slower than the primate cones and the input stimulus is different from that used in (a), the effect of the horizontal cell feedback in sharpening the photoreceptor transient response is comparable.

98

intensity. The observed difference is thus due to the much shorter time constant chosen for cone temporal adaptation in the *computer retina* (modeling pigment bleaching in the primate system) than exists in the *Necturus* retina.

Figures 5.4 and 5.5 show the data for horizontal and midget bipolar cells, respectively, for flashed background experiments as performed on the cones. In this case, horizontal cell feedback to the cones was enabled to allow comparison of model cell outputs against those of non-aspartate treated mudpuppy retinas [72]. The model cell outputs are comparable to those of the mudpuppy but have a much sharper transient responses due to the shorter time constants used in the model cells. Although primate horizontal and bipolar cell recordings are not available, Richter estimates that the time constant in mammals may be anywhere from 5-10 times shorter than in fish [47].

5.2.4 Intensity-Response Curves

Figure 5.6 shows the intensity-response curves for the model cone, horizontal, midget bipolar and diffuse bipolar cells. These curves were obtained by plotting the peak amplitudes of the cell output vs. the log intensity of the flashes as obtained from the flashed background experiments described in the previous section. A separate curve was obtained at each of the background intensities shown. The model cone and horizontal cell plots show that these cells have a dynamic range of about 2.5-3.0 log units centred around any given background intensity. Flashed intensities outside this range either elicit negligible cell response or a saturated response. Increasing the background intensity shifts the operating point of cone and horizontal cells and shifts their entire IR-curve to the right without a change in shape. Both the midget and diffuse bipolar cells also exhibit similar behaviour. The model midget bipolar cell has a dynamic range of approximately 1.5 log units while the diffuse bipolar cell has a very narrow 1.0 log unit response range around a given background intensity. For background intensities close to the "cone threshold" ($< 10^2$ td), most of the response range of bipolar cells is used to signal intensities brighter than the background (positive contrast). It is only at much brighter intensities that the model bipolar cells respond equally well to negative contrast as well as positive contrast. Figure 5.6 (bottom) shows the corresponding intensity-response curves obtained by Normann [41] and Werblin [72] in the *Necturus* (cone) and mudpuppy (horizontal and bipolar cell) retinas. Note that the slopes of the fish cone and horizontal cell curves are the negative of those for the corresponding *computer retina* cells because of the hyperpolarizing nature of these biological cells. The mudpuppy horizontal cells appear to have a dynamic range of slightly over 3.0 log units while the bipolar responds to only a 1.5 log unit range of intensities around the prevailing background intensity.

The flashed background experiments show that the outputs of the *computer retina* ap-
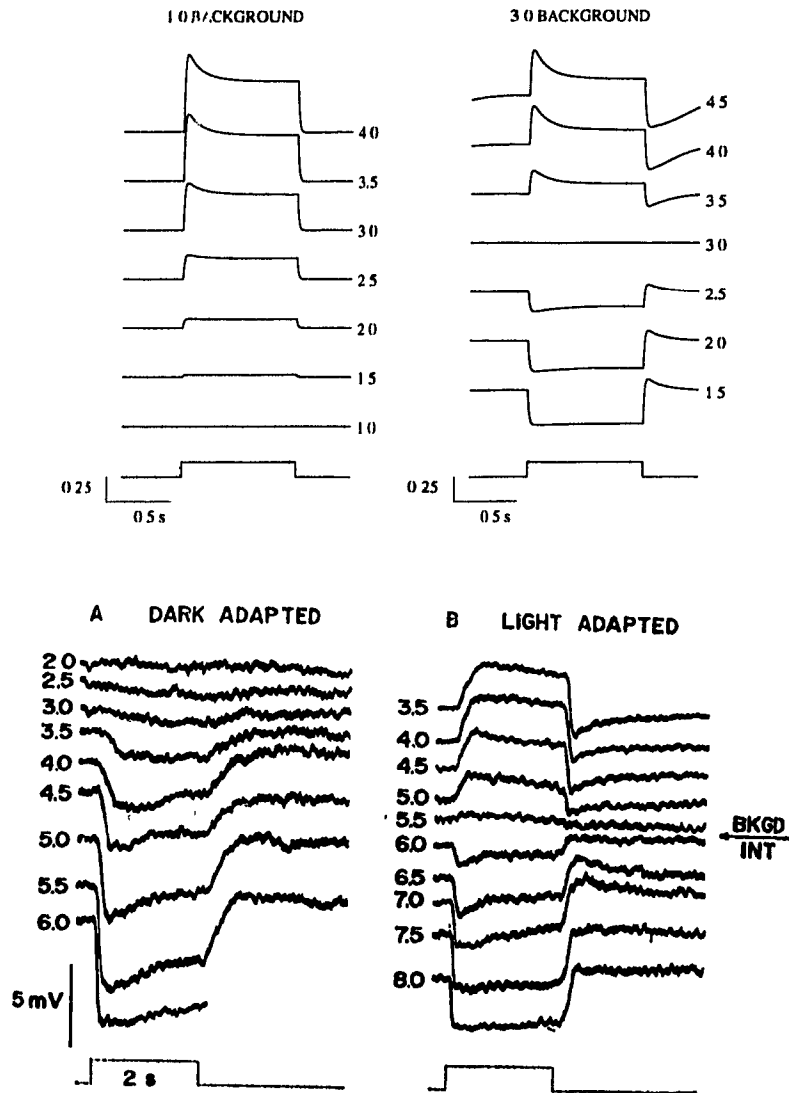
Figure 5.3: Cone Temporal Response to Full-Field Flashes: The top figure shows the temporal response of model cone cells when 900 ms test flashes were substituted for the background every 8 seconds at two different log background intensities (1.0 and 3.0 log td) indicated at the top of each set of curves. The intensity of the substituted flash is shown to the right of each trace in units of log trolands. The initial cone response to a "flash" slowly decays to a new resting potential as the cone adapts to the new illumination level. The model cone cell response curves are similar to cone responses obtained by Normann in the aspartate treated *Necturus* retina shown in the bottom figure [41] (with permission of the Rockefeller University Press). Note that the cone potential in the *Necturus* retina hyperpolarizes (becomes more negative) in response to brighter illumination levels and thus is opposite in polarity to the model cone responses. Increasing flash intensities are towards the bottom of the figure for the *Necturus* and the opposite of those for the model cone curves.
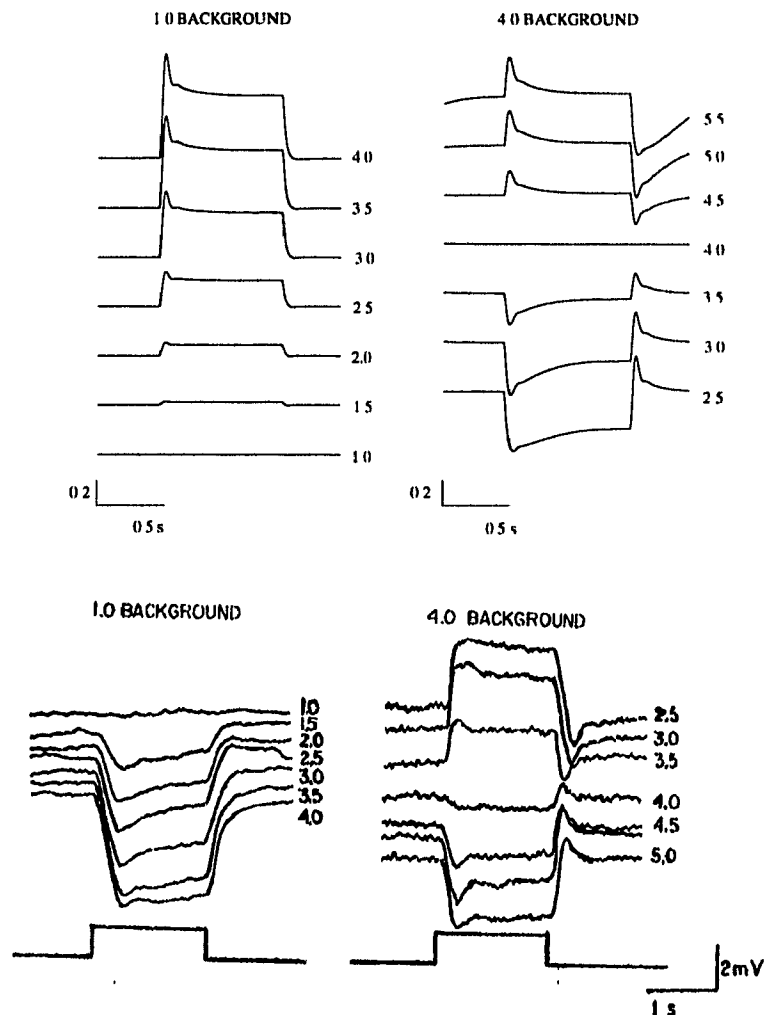
Figure 5.4: Horizontal Cell Response to Full-Field Flashes: The top figure shows the temporal response of model horizontal cells to 900 ms test flashes substituted for the background every 8 seconds at two separate background intensities (shown at the top in units of log trolands). The intensity of the substituted flash is indicated to the right of each curve in log trolands as in the cone experiment. The bottom figure shows horizontal cell recordings obtained by Werblin in the mudpuppy retina in a similar experiment [72] (with permission of the Rockefeller University Press). Note that mudpuppy horizontal cells hyperpolarize in response to increased stimulation while *computer retina* horizontal cell outputs increase in response to increased stimulation. As a result, the polarity of the model horizontal cell response is the opposite of that of a mudpuppy horizontal cell.
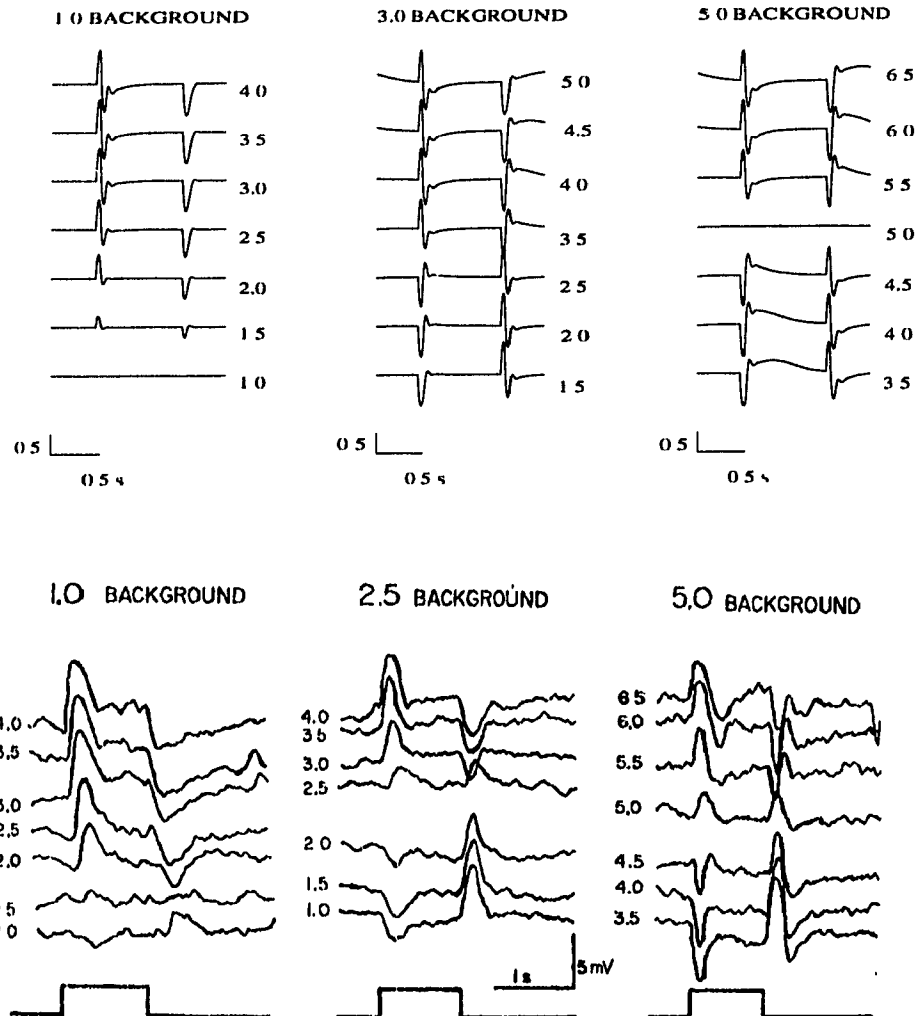
Figure 5.5: Midget Bipolar Cell Response to Full-Field Flashes: The top figure shows the time course of model midget bipolar cells to 900 ms test flashes substituted for the background every 8 seconds at three separate background intensities (indicated at the top in units of log trolands). The intensity of the substituted flash is shown to the right of each curve in log trolands. The bottom figure shows recordings from a depolarizing bipolar cell in the mudpuppy retina obtained by Werblin in a similar experiment [72] (with permission of the Rockefeller University Press).
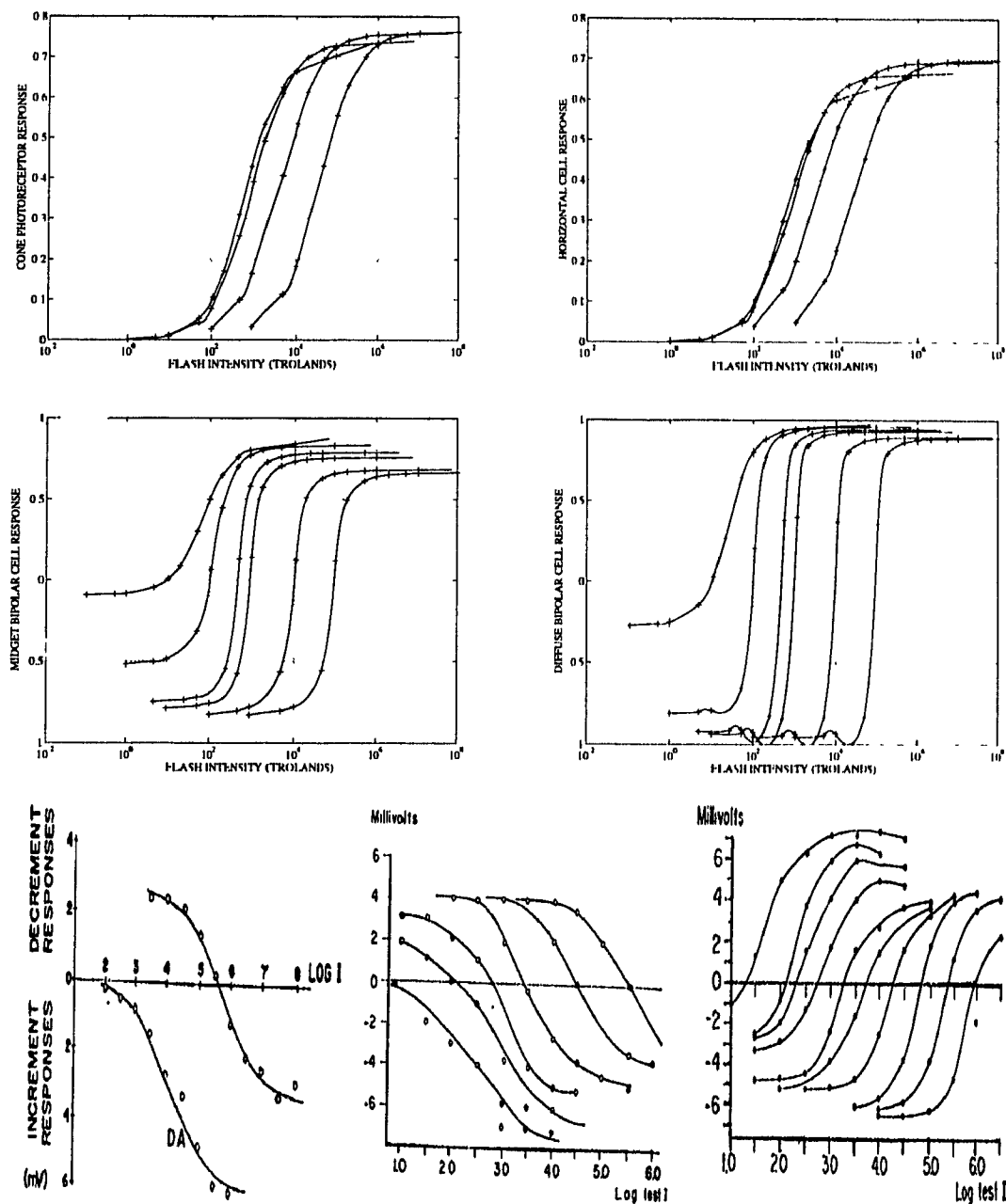
Figure 5.6: Intensity-Response Curves: The top four plots in the Figure show intensity-response curves for the model cone, horizontal, midget bipolar, and diffuse bipolar cells as obtained from flashed background experiments. The bottom plots show (from left to right), the corresponding data for similar experiments in the *Necturus* (cone) [41] and mudpuppy (horizontal and bipolar cell) [72] (with permission of the Rockefeller University Press). Note that the slopes of the fish cone and horizontal cell curves are the negative of those for the corresponding *computer retina* cells because of the hyperpolarizing nature of these biological retinal cells.

proximate to the first order the temporal nature of responses found in biological retinas. Where differences exist, most may be attributed to a difference in the time constants between fish retinas and those used in the model implementation which were based on estimates for a mammalian retina.

5.3 Sinusoidal Grating Stimulus Experiments

Sinusoidal grating stimuli are often used in visual psychophysics and electrophysiology since they allow researchers to characterize the response of the visual system over a wide spectrum of spatial and temporal frequencies. Typically, a sinusoidal grating stimulus consists of a pattern in which the intensity varies sinusoidally along one of the spatial coordinates. In addition, the stimulus may be modulated temporally so that the intensity also varies sinusoidally with time. Figure 5.3 shows a typical sinusoidal grating stimulus. The parameters that specify the sinusoidal grating pattern include its spatial frequency k (cycles/pixel), its temporal frequency of modulation ω (Hz), background intensity I_b and the contrast or depth of modulation c of the grating $(0 < c < 1.00)$.

Figure 5.7: Sinusoidal Grating Stimulus

In electrophysiological experiments on primates, the sinusoidal grating stimuli are presented while the outputs of cells in the parvocellular and magnocellular layers of the lateral geniculate nucleus (LGN) are recorded. The parvocellular and magnocellular layers are where the outputs of retinal P and M ganglion cells terminate, respectively. The LGN cells have very simple centre-surround receptive-field structures, just like the P and M retinal ganglion cells, and are thus believed to have properties, in most respects, similar to the ganglion cells which provide their input.

In these experiments, the recorded monkey P-cell and M-cell data may be expressed in any number of ways. The most common measures used are contrast sensitivity, gain and contrast gain. Contrast sensitivity for individual cells is typically defined as the reciprocal of the contrast required in the input stimulus to produce a criterion response (a minimum level of output that must be achieved in order to consider the input stimuli distinguishable from background noise) in the cell output. Gain and contrast gain are defined here to be consistent with Shapely [56] and Purpura [46]:

$$Gain = \frac{Mean\ cell\ response}{(Stimulus\ contrast)(Mean\ retinal\ illumination)} \qquad (5.1)$$

$$Contrast\ gain = \frac{(Mean\ cell\ response)}{(Stimulus\ contrast)} \qquad (5.2)$$

Only measurements of contrast gain or absolute gain are given for the *computer retina* ganglion cell responses. Determination of the contrast sensitivity was omitted as it requires a lengthy iterative procedure to determine the smallest input contrast required to elicit a criterion output response. Measuring it would have increased the execution time of the experiments by at least an order of magnitude. However, the measure of contrast gain is very similar to contrast sensitivity if one assumes a linear system and thus is sufficient for the qualitative comparisons made here.

Three types of experiments were conducted using sinusoidal grating stimuli to characterize the following features of the *computer retina*:

- Changes in spatial frequency sensitivity caused by illumination level,

- Changes in temporal frequency gain as a function of illumination level,

- Changes in contrast gain as a function of input contrast and temporal frequency.

The results from these experiments are presented next.

5.3.1 Spatial Frequency Sensitivity

In this experiment, the spatial frequency sensitivity of the model P-cells and M-cells was determined at several illumination levels. At each background illumination level, the peak responses of the P-cell and M-cell outputs were recorded as the spatial frequency of the grating was slowly varied over 3 orders of magnitude. The input stimulus was presented with a temporal modulation of 2 Hz while the grating contrast was kept fixed at $c = 0.20$ throughout the experiment. The ganglion cell output levels were divided by the contrast c to obtain a measure of contrast gain.

Figure 5.8 (top) shows the contrast gain of model P-cells and M-cells as a function of spatial frequency at several illumination levels. The spatial frequencies have all been converted from cycles/pixel to cycles/degree to aid comparison with *Macaque* monkey data from Derrington [19] shown at the bottom of Figure 5.8. The figure illustrates several aspects of the behaviour of the *computer retina* P-cells and M-cells which may be compared with known facts on the primate retina.

- The frequency response of primate P-cells and M-cells is spatially bandpass at photopic illumination levels [81][57].
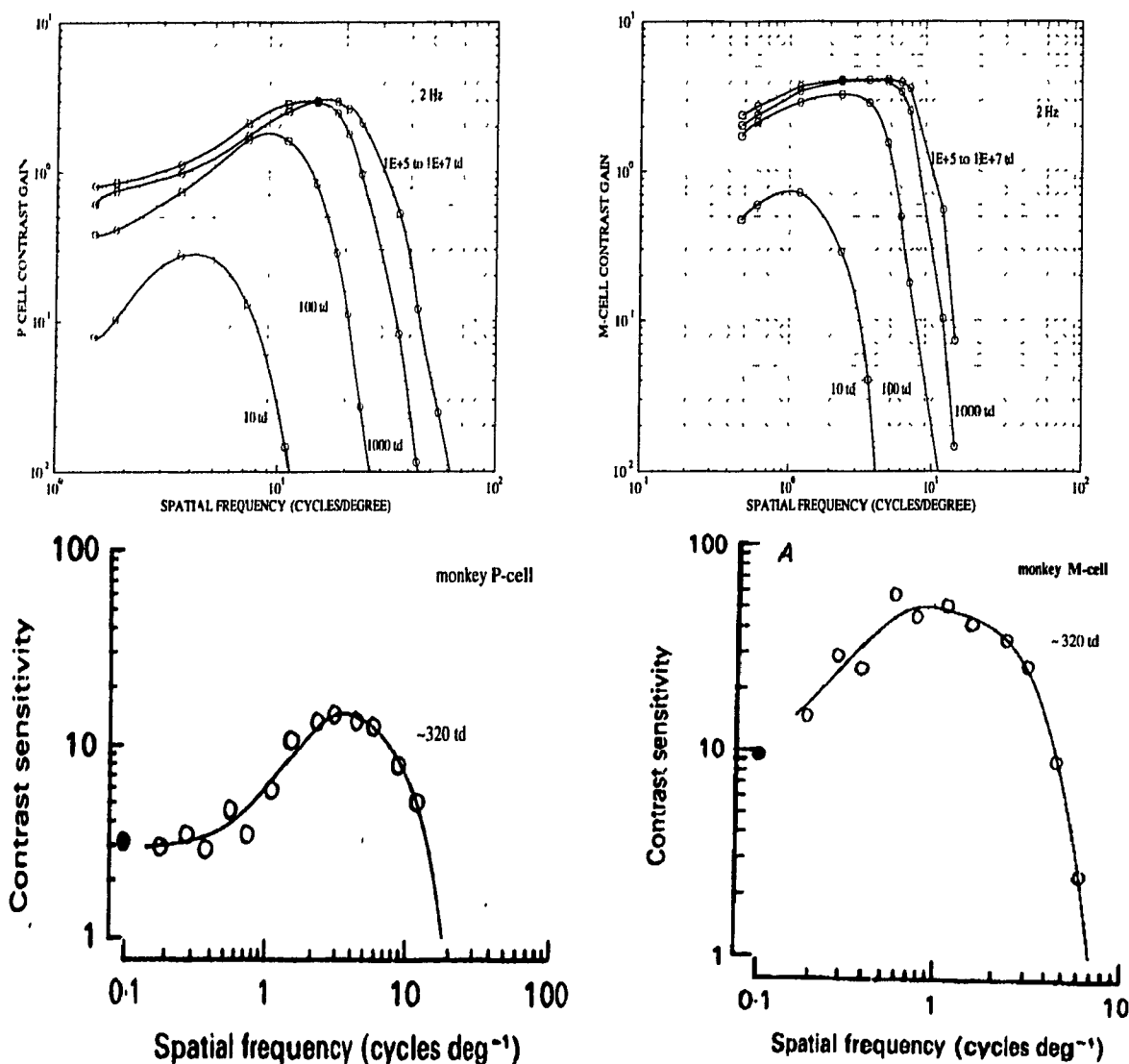
Figure 5.8: Ganglion Cell Spatial Frequency Tuning: The figures at the top show the contrast gain of the *computer retina* P-cells (top left) and M-cells (top right) as a function of the sinusoidal grating spatial frequency at several illumination levels $(10, 100, 1000, 10^5,$ and 10^7 trolands). The temporal frequency of modulation was maintained at 2 Hz and the grating contrast was fixed at $c = 0.20$ throughout the experiment. The spatial frequencies have been scaled from cycles/pixel to cycles/degree to allow comparison with primate data. Comparable data on the typical contrast sensitivity of individual *Macaque* monkey parvocellular (P) and magnocellular (M) LGN cells is shown in the bottom two figures (from Derrington [19] with permission of The Physiological Society ©1984). The grating stimuli used in the *Macaque* monkey experiment were modulated at a temporal frequency of 5.2 Hz at a background illumination of approximately 320 td.

- Increasing illumination levels are accompanied by increases in visual acuity and thus an ability to resolve higher sinusoidal grating frequencies [65][75].

- At low illumination levels, an increase in illumination level is accompanied by an increase in contrast sensitivity (contrast gain) [81].

- At still much higher illumination levels, the contrast sensitivity (contrast gain) as well as spatial acuity reach a plateau and become insensitive to any further increases in background illumination level [81].

- The M-cell system in the primate retina has a higher contrast gain than the P-cell system [57][4].

- P-cells are able to respond to much higher spatial frequencies (40-60 cycles/degree) than M-cells (10-20 cycles/degree) as a result of their much smaller receptive fields [33].

All of the above properties are qualitatively exhibited by our *computer retina*. As the illumination levels increase, the P-cell and M-cell contrast gain increases and the outputs reach a peak at much higher spatial frequencies of modulation. The M-cell outputs exhibit higher contrast gain (larger peak outputs) and are tuned to lower spatial frequencies than P-cells at all illumination levels. The model P-cells have a peak sensitivity to spatial frequencies of 12-15 cycles/degree and are able to signal frequencies up to 50-60 cycles/degree and is consistent with primate data. The model P-cells and M-cells also exhibit a slight spatial bandpass characteristic.

It should be noted that the shape of the spatial frequency response is dependent upon the temporal frequency of modulation as well. Figure 4.10, which shows the spatiotemporal tuning of P and M cells at one illumination level, illustrates this point. At very low temporal frequencies, both P and M cell responses exhibit a strong spatial bandpass characteristic. At moderate or high temporal frequencies of modulation, the spatial bandpass characteristic becomes much less pronounced and eventually becomes a lowpass characteristic. This effect is also observed in the primate and cat retinas [19][24].

5.3.2 Temporal Frequency Sensitivity

Figure 5.9 (top) shows the gain of the *computer retina* P and M ganglion cells as a function of temporal frequency when stimulated by sinusoidal gratings. For this experiment, the spatial frequency of the sinusoidal grating was held fixed at 3 cycles/degree (0.0208 cycles/pixel), and the grating contrast was set to $c=0.30$ throughout the experiment. The grating temporal frequency was varied slowly and held at each frequency for 4 seconds during which time the

mean P-cell and M-cell outputs were recorded and divided by the mean retinal illumination level and the contrast c to obtain the gain values. This experiment was repeated for several illumination levels to examine the effects of illumination level on the temporal frequency gain. The model response may be compared to data from recordings in the *Macaque* monkey LGN made by Purpura [46] shown in bottom of Figure 5.9.

The general temporal frequency properties of the *computer retina* P-cells and M-cells may be summarized as follows. Figure 5.9 shows that the M-cell system responds with a much larger gain to temporal stimulation and is thus able to respond better than the P-cell system at both low and high temporal frequencies. This is in agreement with generally cited properties of primate retinal P-cells and M-cells [33]. The gain of the *computer retina* M-cells is about 5-8 times larger than that for the P-cells and is comparable to the factor of 6-7 difference found in monkey cells. The peak P-cell temporal frequency is around 8-9 Hz and within the range of values (8-12) Hz found in primates [46]. In addition, the temporal frequency gain of both M-cells and P-cells is inversely proportional to the mean retinal illumination level at low temporal frequencies and thus is consistent with Weber's law. At higher temporal frequencies, the gain of the system depends increasingly on the temporal frequency and time constants of various cells in the retina and becomes relatively insensitive to the illumination level.

The *computer retina* model's temporal frequency gain compares reasonably well with the Macaque monkey data in most respects. The main difference is in the shift of the peak temporal frequency (the temporal frequency which gives a peak ganglion cell output) as a function of illumination level. In the monkey data, as the illumination levels rise, the peak temporal frequency also increases fractionally. This seems to indicate that in addition to modulation of receptive field sizes, the dynamic properties (time constants of various cells) of the retina also adapt to the illumination level. In our model, for the sake of maintaining simplicity, the time constants for all the cells are fixed with respect to illumination level and thus, the *computer retina* peak temporal frequency does not change with illumination level. The monkey data is accounted for by Purpura by adapting the time constants of several lowpass temporal filters (through which the input signal passes) as a function of the illumination level [46].

5.3.3 Contrast Gain

In order to measure the effect of input stimulus contrast on the contrast gain of P-cells and M-cells, an additional experiment was performed and the responses compared to data on a similar experiment performed on monkey retinal ganglion cells. In this experiment, the outputs of model P-cells and M-cells were recorded as a function of temporal frequency at
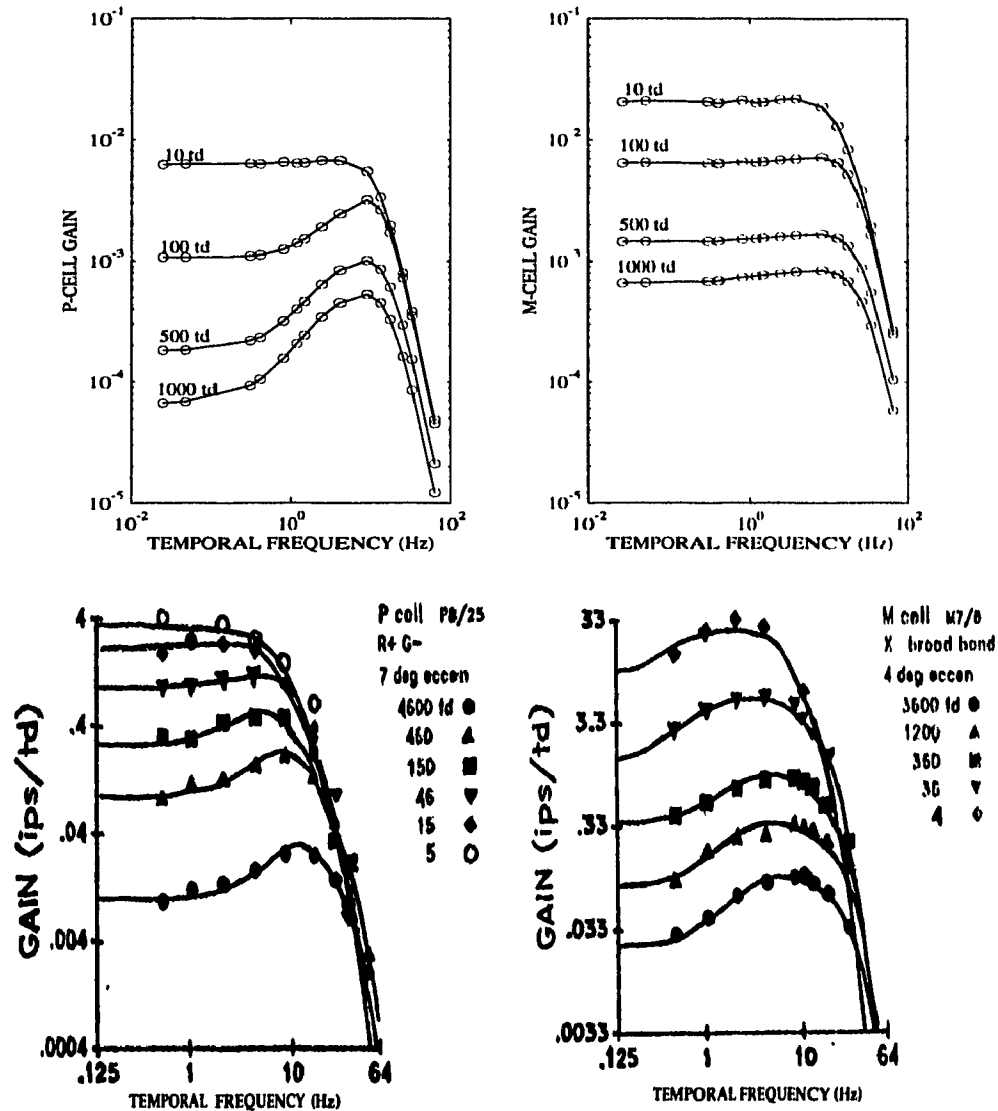
Figure 5.9: Ganglion Cell Temporal Frequency Gain: Response curves in the top two figures shows the gain of foveal model P-cells (top left) and M-cells (top right) as a function of sinusoidal grating temporal frequency at several background illumination levels (indicated on the curves). A grating of fixed contrast ($c = 0.20$) and spatial frequency 3 cycles/degree was used throughout the experiment. The gain was computed as the mean ganglion cell output level divided by the product of the stimulus contrast c and the background illumination intensity. The data may be compared with recordings of P-cells and M-cells made in the *Macaque* monkey LGN by Purpura [46] (reproduced with permission of Cambridge University Press ©1990). In Purpura's data, a grating of spatial frequency 3 cycles/degree and a grating contrast of 64% was used for the P-cell experiments while gratings of 1.6 cycles/degree and contrasts between 4% and 25% were used for the M-cell experiments.

several grating contrasts. The contrast gain was computed as defined in Equation 5.2. The parameters held fixed in this experiment were the retinal illumination level (1000 trolands) and the grating spatial frequency (0.009 cycles/pixel or 1.3 cycles/degree). Figure 5.10(top) shows the contrast gain of model M-cells and P-cells as a function of temporal frequency for several grating contrasts. Comparable data on retinal ganglion M-cells and P-cells in Macaque monkeys are reported by Benardete [4] and are shown at the bottom of Figure 5.10.

This experiment shows that the P-cell contrast gain is largely unaffected by the stimulus grating contrast while the M-cell contrast gain diminishes noticeably with increased contrast input at the cell's peak temporal frequency. Such behaviour is consistent with the notion that P-cells, which have a smaller contrast gain than M-cells, respond linearly with respect to contrast [33]. M-cells, however, are easily saturated by moderate to high contrasts in the input signal due to their high contrast gain and thus exhibit diminished contrast gain with increasing stimulus contrast. Again, the *computer retina* outputs are similar to the first order of approximation to the behaviour observed in monkey retinal ganglion cells.

5.4 Step Edge Responses

In order to illustrate the adaptation features of the model when confronted with changing illumination levels, the *computer retina's* behaviour in the neighbourhood of a spatial step edges was explored at several background illumination levels. The spatial step edge stimuli consisted of images in which the right half (of the image) was twice as bright in intensity as the left half at any given background intensity. The experiment was conducted so that a uniform intensity background was presented for 2 seconds in order to allow the retinal responses adapt to this intensity. This was followed by the presentation of the step edge stimuli for 0.5 s with the left half of the image intensity matching the adapting background intensity. The outputs of all cells along a line crossing perpendicular to the step edge (in the x-direction) were recorded. This procedure was repeated at several background intensities. The background intensities ranged from 100 trolands to 10^6 trolands in 1.0 log unit steps. The responses of the cone, horizontal, and midget bipolar, and interplexiform cells, as well as additional data from this experiment, are shown in Figure 5.4.

The plots (a)-(h) in Figure 5.4 illustrate several aspects about the model retina:

- Plot (a) shows the illumination intensity profile across the step edge at pixel position x=20. The right side of the image is twice as bright as the left half at each background intensity.

- Plot (b) shows the peak cone response approximately 40 ms after presentation of the step edge. For retinal illumination levels below 10^4 trolands (td), increasing background illumination levels result in a steady increase in the cone potential. However,
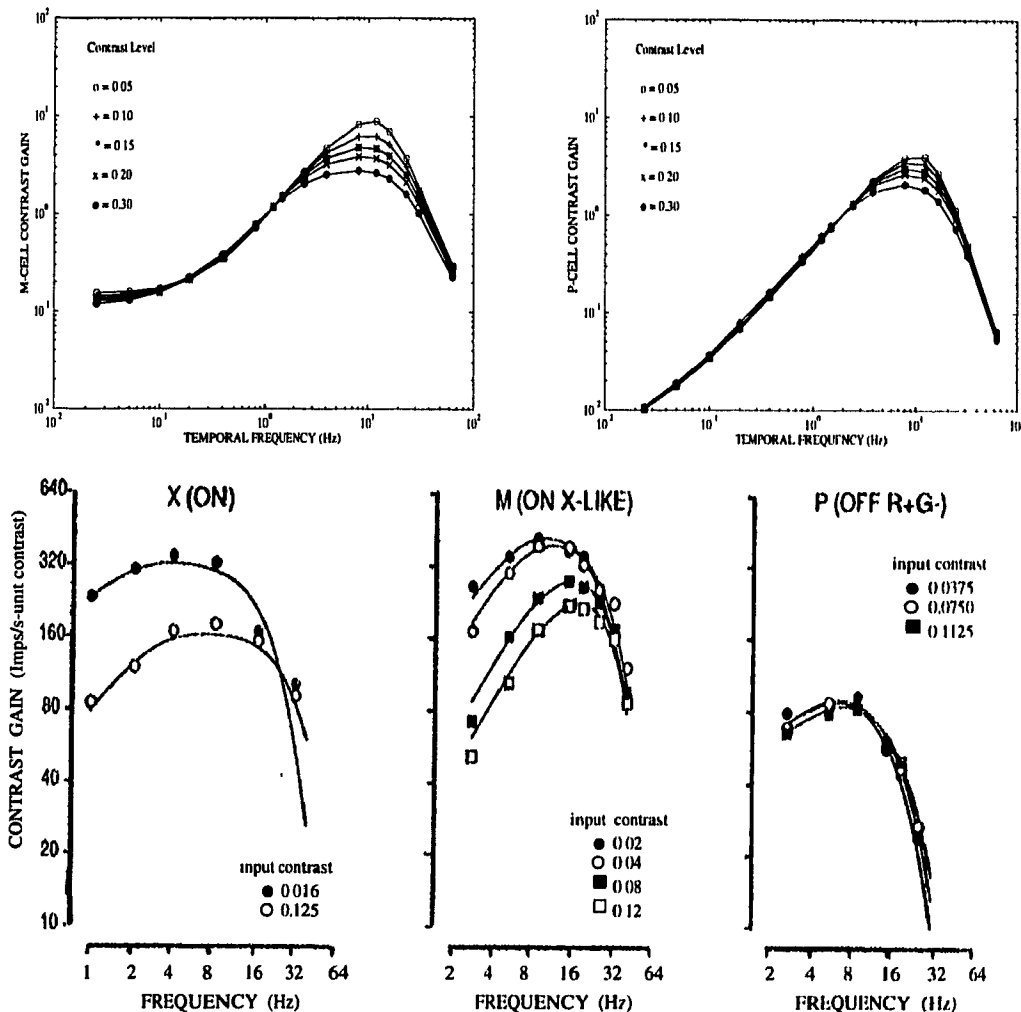
Figure 5.10: P-cell and M-cell Contrast Gain: The top two plots shows the contrast gain of model M-cells (left) and P-cells (right) as a function of temporal frequency at several grating contrasts. The tests were performed at a background illumination level of 10^3 td and a spatial frequency of 0.009 cycles/pixel (1.3 cycles/degree). The bottom figure (left to right) shows similar data for a cat X-cell, and a monkey (X-like) M-cell, and a monkey P-cell from Benardete [4] (with permission of Cambridge University Press ©1992). The M-cell is more sensitive to changes in contrast than the P-cell. Increased levels of contrast lead to diminished contrast gain in the M-cell system due to the nonlinear saturation function. This effect is much less pronounced in P-cells because of their smaller contrast gains.
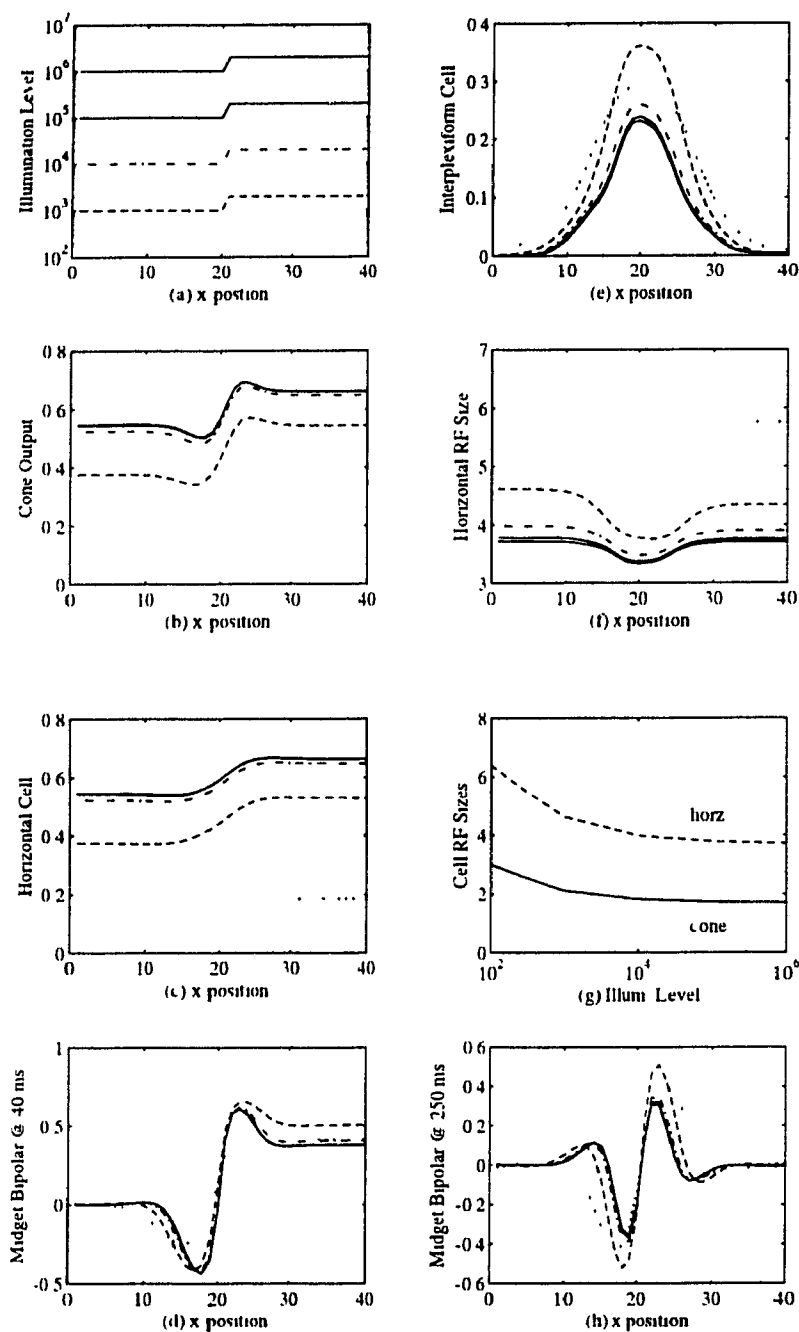
Figure 5.11: Step Edge Responses: The figures show the results of the spatial step edge experiment. Shown in the figure are (a) the step edge intensity profile, (b)-(d) the peak cone, horizontal and midget bipolar cell outputs, (e) the steady-state interplexiform cell outputs, (f) the Gaussian width of the Horizontal cell receptive field (RF) along the step edge profile, (g) variation of cone and horizontal cell RF's with illumination level and (h) the steady-state midget bipolar cell outputs. Explanations of these figures are found in the text.

for intensities above 10^4 td, mechanisms modelling the effects of pigment bleaching and horizontal cell feedback act to keep the cone potential near the middle of its operating range. The magnitude of the peak cone response to the step edge depends on the contrast of the step edge and very little on the illumination level.

- Plot (c) shows that the larger receptive fields of the horizontal cell layer result in a blurred version of the cone output.

- Plot (d) shows the peak midget bipolar cell output approximately 40 ms after presentation of the edge. Note that for decreasing illumination levels, the width of the step edge response becomes wider as cone coupling and horizontal cell coupling increases. In all other aspects, the bipolar cell response is insensitive to global changes in illumination level and instead responds to the contrast in the visual signal.

- Plot (e) shows the steady-state output of the interplexiform cell layer in the model. Interplexiform cells receive their input from bipolar cells and thus their outputs are large in regions where the bipolar cell outputs are large (like near the step edge).

- Plot (f) shows how the degree of horizontal cell coupling (expressed by the width of its Gaussian shaped receptive field) is reduced by increasing levels of illumination level. Dopamine released by interplexiform cells in the neighbourhood of the step edge further reduces the horizontal cell coupling in cells near the step edge.

- Plot (g) shows the cone and horizontal cell receptive field (RF) sizes (again expressed in the widths of the equivalent Gaussians describing their RF's) as function of background illumination level. At low illumination levels, cone and horizontal cell receptive fields expand in size in order to improve absolute contrast detection. At higher illumination levels, they shrink in order to improve acuity.

- Plot(h) shows the midget bipolar cell response 250 ms after presentation of the step edge. Note that, except in the vicinity of the edge, the bipolar cell response on the left side and right side of the image has now faded to zero. The figure also shows that the width of the step edge response gets narrower with increasing illumination levels and is as a result of the shrinking receptive field sizes.

The step-edge experiment has illustrated some of the adaptive properties of the retinal model more clearly. The remaining experiments, in the next section, show the response of the *computer retina* to real images from image databases and a ray tracing package.

5.5 Complex Images

The previous sections illustrated the response of the *computer retina* in response to very simple stimuli. We now show the model response to more complex images. The images used for this section are of two types. Some of the images were generated using a simple ray-tracing package which permitted intensity values to range over 4 orders of magnitude. Others were obtained from image databases and their intensities were exponentially scaled to expand the dynamic range of intensities in the input signal. Because of the considerable

storage and computational requirements to generate temporally varying images, the images used in these experiments were all temporally stationary.

In order to display the outputs of various layers of cells on the computer screen and to make figures for this thesis, the *computer retina* cell output ranges were scaled to fit intensity values from 0 to 255. For the bipolar and ganglion cells, which have outputs that may be positive or negative depending on the input contrast, the zero level of the outputs was set to a pixel intensity of 127, with the total output dynamic range covering intensities from 0 to 255.

5.5.1 Response to Large Dynamic Range Images

Figure 5.12 shows the steady-state outputs of the *computer retina* to an image containing 3 objects (a complex block, a sphere, and a cylinder) on a table surface. The intensities in this generated image varied over 3-4 orders of magnitude.

Even though the intensities in the input image range over 3-4 orders of magnitude, in any given local neighbourhood of the image, the cones adapt their sensitivity based on the local ambient intensity level. This adaptation mechanism tends to return the cone potential to near the middle of its range. As a result, the steady-state response of the cone layer to a stationary image is for the most part equal to the cone half-maximum response except in regions of sharp intensity gradient. The P-cell and M-cell steady-state responses are only sensitive to spatial edges in the image. All other features fade away in the steady-state response. This is similar to the "fixation blindness" observed in the primate retina where stabilized images on the retina fade away after a very short time [36]. Note that there is only one M-cell for every nine P-cells, and thus the outputs of the M-cell layer sample the image at a much coarser resolution than the P-cell layer.

Figure 5.13 shows the response of the *computer retina* to another sample image, this time taken from an image database. This image is of a rock climber on the face of a mountain. The image intensities in the original image (0-255) were exponentially scaled to cover approximately five orders of magnitude. In the original image, shown at the top left of Figure 5.13, it is difficult to see details on the relatively dark cliff surface. However, the *computer retina* locally adapts its sensitivity at the cone level (top right image) so that both the bright and dark regions of the scene can be seen. In particular, regions obscured by shadows in the original scene are more clearly visible in the P-cell and M-cell outputs.

5.5.2 Foveated Sampling and Data Reduction

For all previous experiments in this chapter, the changes in the processing of visual information associated with retinal eccentricity have been ignored. All comparisons made with
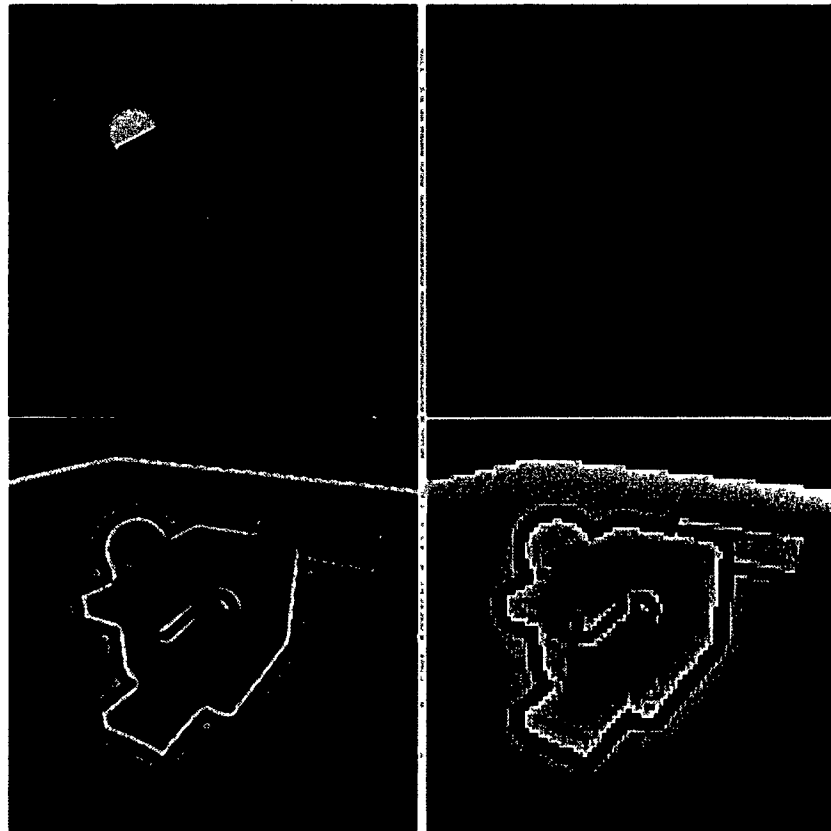
Figure 5.12: Steady-State Response to Blocks Image: The top left figure shows .he input image with the intensities normalized to fit into a greyscale of 0 to 255. The actual intensities in the input stimulus ranged from 1 to 5×10^4 trolands (4 log units dynamic range). The very dim cylinder and table are difficult to see in original image. The top right figure shows the steady-state cone response to the image after 350 ms. The cones locally adapt their sensitivity so that both bright regions and dim regions in the image are visible. The P-cell / midget bipolar and M-cell / diffuse bipolar cell outputs are shown in the bottom left and bottom right figures, respectively. All outputs are normalized to fit a greyscale of 0 to 255.

biological data were from data in the fovea where the ratio of cone cells to ganglion cells is one-to-one. For these experiments, the fovea was assumed to cover the entire image. This greatly simplified the comparison and analysis of the experimental data as the effects of nonuniform sampling and data reduction that occur in the periphery could be ignored.

However the *computer retina* is also able to crudely approximate the effects of increasing receptive field sizes and coarser resolution sampling occurring in the periphery. The *computer retina* program makes use of log-polar mappings which separate the image data into two regions: the fovea and the periphery[5]

In the fovea, there is a one-to-one mapping of the cone inputs to ganglion cell outputs.

---

[5]The computer program used to perform the log-polar mappings was developed by Marc Bolduc, McGill University, as part of his Master's thesis [6].
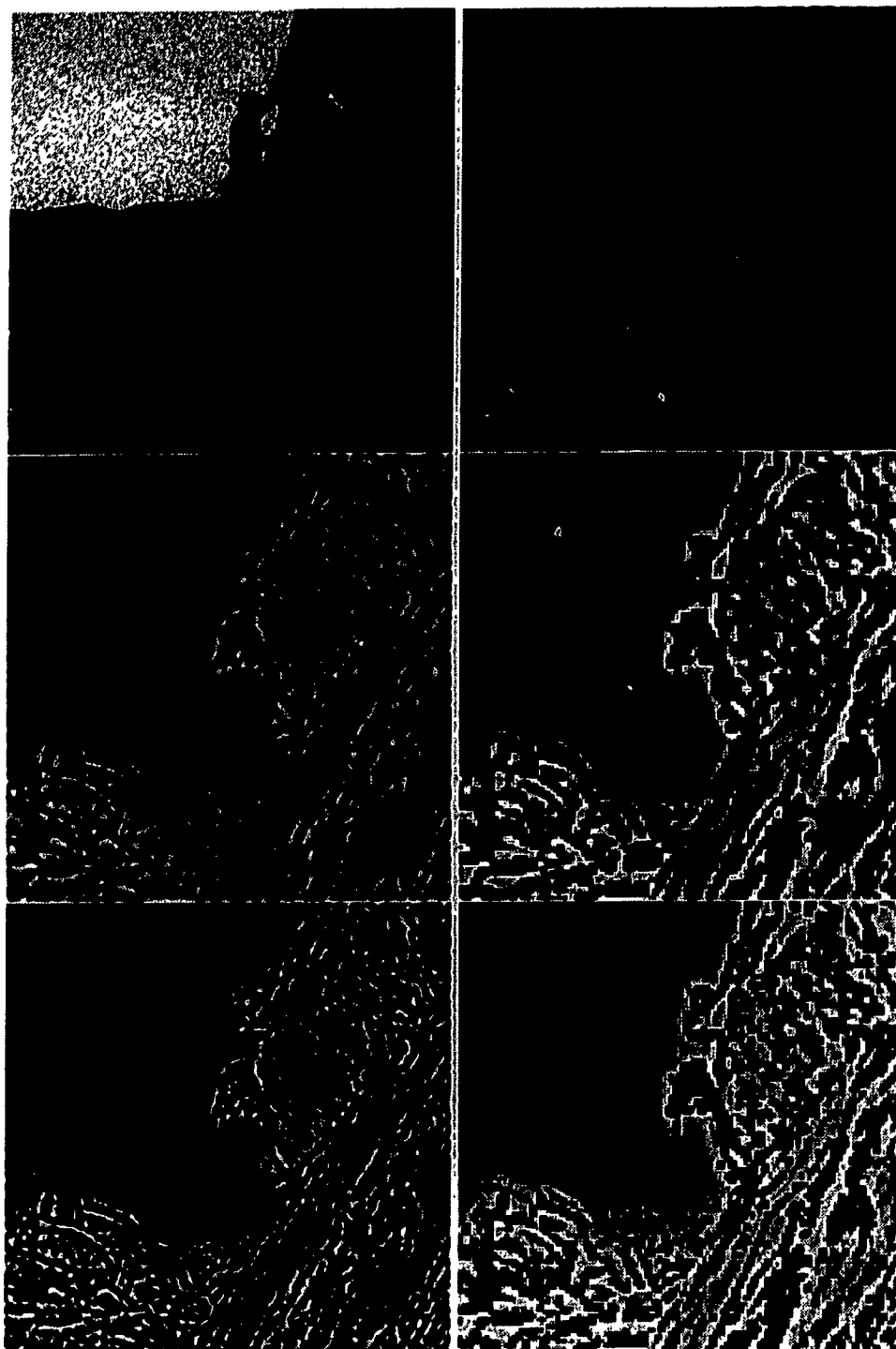
Figure 5.13: Rock Climber: The figures show the outputs of the *computer retina* to the "rock climber" image. The intensities in this image were scaled exponentially from 0-255 to cover approximately 5 log units before being processed by the *computer retina*. Shown from left to right, top to bottom, are the original image, followed by the cone, the peak P-cell and M-cell outputs, and the steady-state P-cell and M-cell outputs. Note that although it is difficult determine the absolute illumination level from the ganglion cell outputs, the local variations in contrast are quite visible in all parts of the image.

In the *computer retina* periphery, a log-polar sampling scheme, as described in Chapter 4, is used to model the nonuniform sampling occurring at the receptor level, as well as the convergence of information from the cones to the ganglion cell level.

The primate retina achieves tremendous data reduction through the use of a nonuniform sampling scheme that samples the image with increasingly coarser resolution with increasing retinal eccentricity. Further data reduction is realized by converging increasing numbers of cone inputs into ganglion cell outputs. The primate retina has just over a million ganglion cell outputs for about five million cone inputs and thus realizes a five fold reduction in the number of outputs to be processed at higher levels.

Figure 5.14 illustrates the data reduction realized by the *computer retina* when using a log-polar transformation on the periphery data. The input image size is 512x512 (262,144 pixels). The foveated *computer retina* generates separate outputs for the fovea and periphery for both P-cells and M-cells. The foveal data is represented in the original Cartesian domain while the peripheral information is represented in the log-polar domain. In the log-polar domain images, increasing log eccentricity is in the horizontal direction to the right, while the angular position in the retina is represented along the vertical axis. We arbitrarily selected the fovea diameter for the *computer retina* to be approximately 15% of the original image and required that the size of receptive fields on fovea and periphery boundaries match each other. The size of the outputs for each layer were as follows: P-cell fovea (79x79), M-cell fovea (26x26), P-cell periphery (121x305), M-cell periphery (40x102), for a total of 47902 pixels, including a 15% overlap region[6] between the fovea and periphery data structures. The *computer retina* thus achieves a 6 fold reduction in data required to be processed by subsequent stages of visual processing by the use of a log-polar mapping scheme.

In order to see the representation of the foveal and peripheral information in the original retinal domain, an inverse-mapping may be performed. Figure 5.15 shows the information in the fovea and the periphery data structures mapped back to the retinal domain.

5.6 Summary

The experiments in this chapter have illustrated the response of the *computer retina* for a variety of conditions. The experiments performed with sinusoidal grating stimuli and flashed background stimuli have shown, by direct comparison, that at least to a first order of approximation, the qualitative behaviour of the *computer retina* cells is similar to that of

---

[6]Near the fovea-periphery boundary the computation of the cell outputs requires information from both the fovea and the periphery. In order to decouple the computations in the fovea and the periphery, and thereby greatly reduce the computation complexity, the fovea and periphery data structures were extended by over 15% so that they overlapped each other. This allowed the computations in the fovea and the periphery to be performed independently of each other.
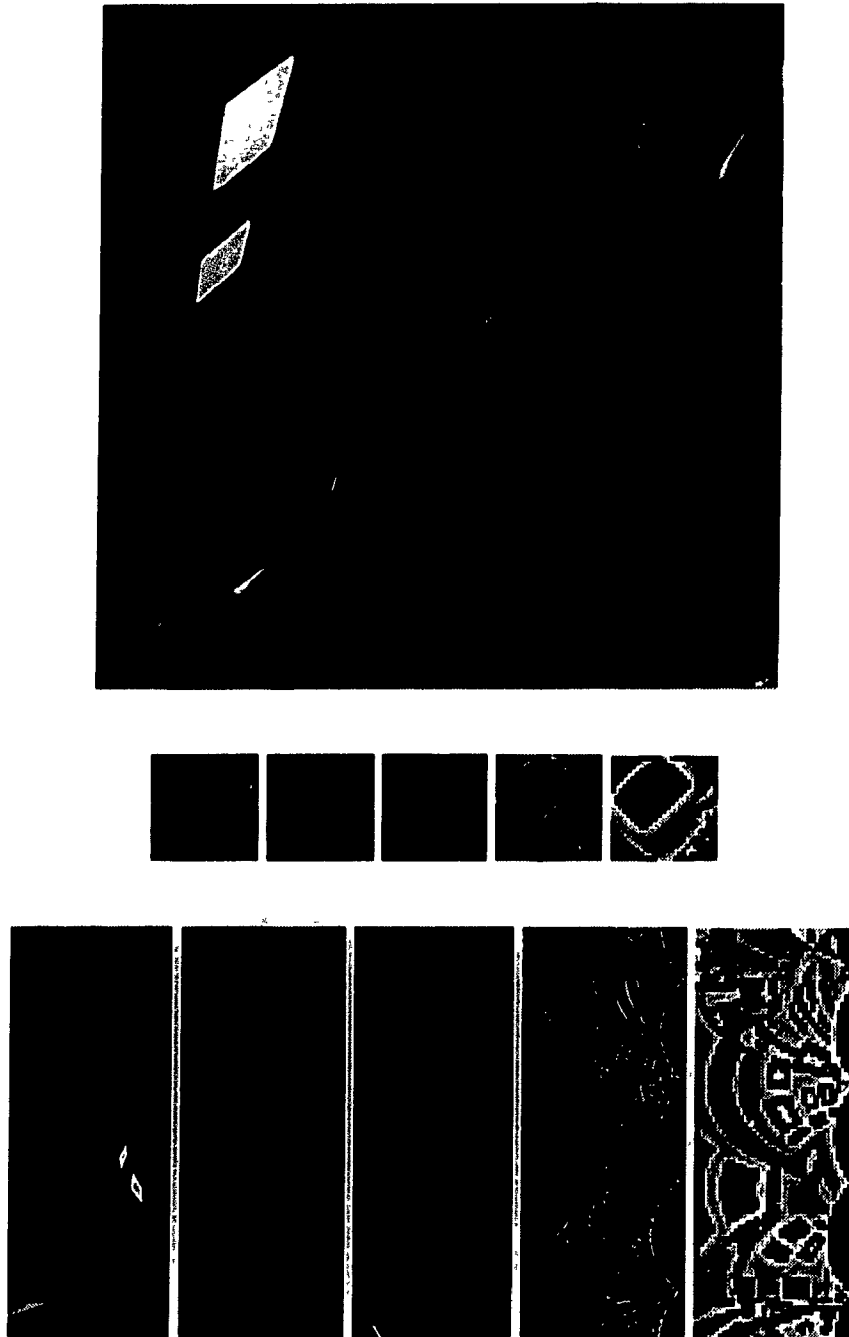
Figure 5.14: Foveated Retina Outputs: The top figure shows the original image as presented to the *computer retina*. The middle row of figures shows the foveal representations of the input image, and the cone, horizontal cell, midget bipolar / P-cell, diffuse bipolar / M-cell layer outputs (from left to right). The foveal portion of the image is quite small (about 79 pixels in diameter) and is located at the centre of the original image. The bottom row shows the log-polar domain periphery representations in the same order as for the fovea. Note that the actual number of M-cell outputs is only one-ninth of the those for P-cells but the M-cell output image has been expanded nine-fold for easier comparison here.

fish and primate retinas. Both the temporal and spatial frequency responses of the *computer retina* cells match the data from experiments on fish and primate retinas and thus validates our model [4][19][46][55][41][72]. The step edge experiment was presented to reveal the how the model responds to a spatial step edge over a large range of background intensity levels. This experiment also illustrated the manner in which horizontal cell and cone photoreceptor coupling varies with the illumination level and the local contrast in the scene. The final experiments, with more realistic images, illustrated that our retinal model accounts for not only the adaptational aspects of the retinal function but also mimics the data reduction found in the human retina.
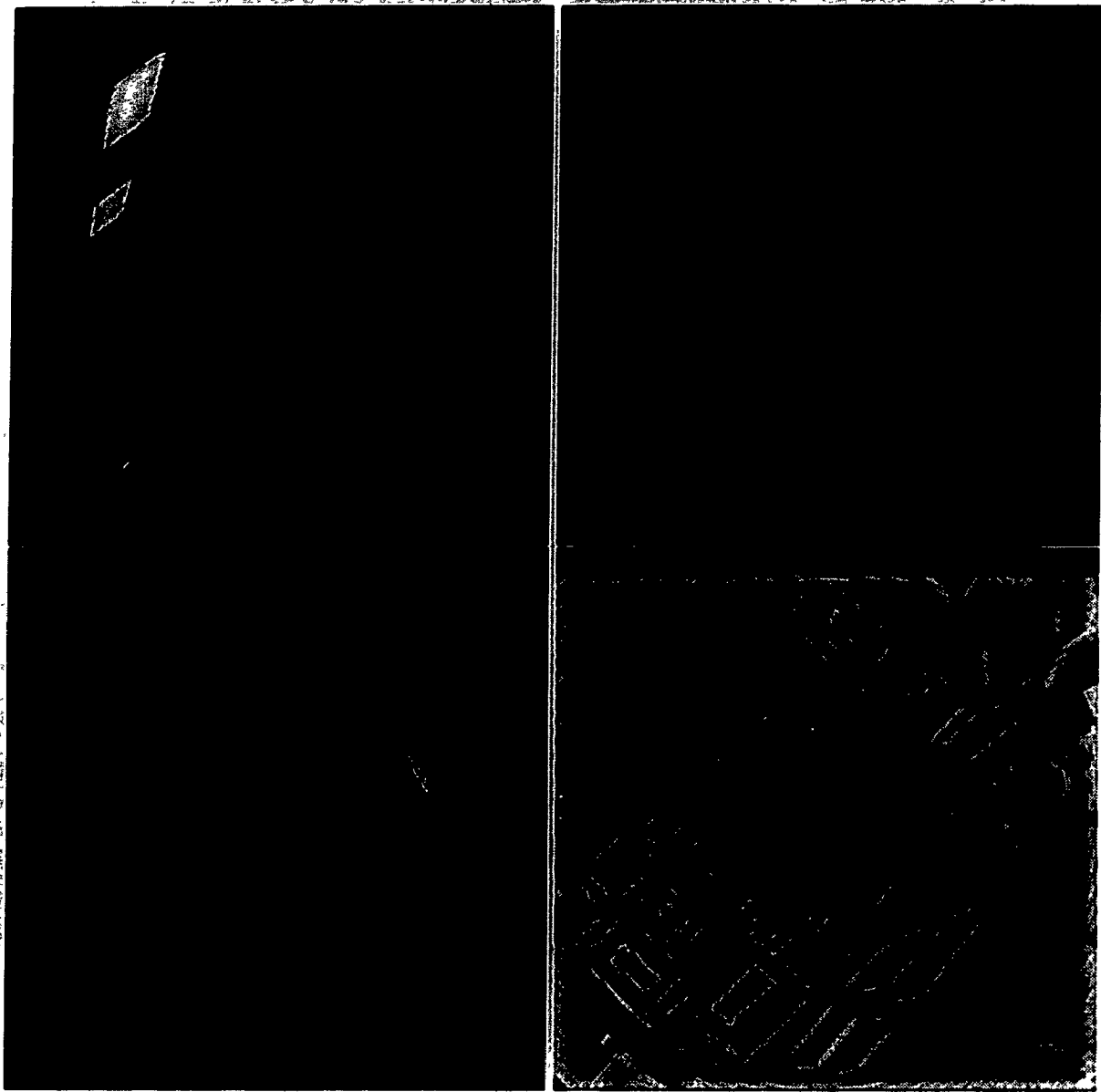
Figure 5.15: Foveated Data Mapped back to the Retinal Domain: The figure shows the data from the fovea and periphery data structures mapped back to the retinal domain using an inverse mapping. The inverse mapping is shown for the original image (top left), and outputs of the cone (top right), horizontal cell (bottom left), and midget bipolar / P-type ganglion cell layers (bottom right). The inverse mapping of the original image illustrates how log-polar mappings model the foveation in the retina. Although the foveal region is sampled at high resolution, features become blurrier with increasing eccentricity in the periphery. The P-cell outputs enhance spatial contrast in the original image. Note that certain regions in the image such as under the desk are enhanced and slightly easier to see in the P-cell output than in the original image.

The aim of this project was to develop a relatively simple model of information processing in the primate retina. It was required that the retinal model not only account for the data reduction strategies employed by the biological retina to meet the transmission bottleneck at the optic nerve, but also strategies used to deal with a large dynamic range of illumination intensities. It was further required that the model be relatively simple so that a potential silicon implementation may be considered in the future.

This thesis has presented an overview of primate retinal biology and reviewed existing models of different aspects of information processing and adaptation in the cone system. Based on this information, a simple model of the adaptation and achromatic information processing in the primate retina cone pathways was presented. The *computer retina* integrates different aspects of retinal processing such as local neighbourhood sensitivity control, enhancement of spatiotemporal contrast, and data reduction through nonuniform sampling into one coherent model. In addition, a model of the local adaptation of cell receptive field (RF) sizes with illumination level and spatiotemporal contrast was proposed and incorporated into the *computer retina*. Experiments similar to those performed by electrophysiologists on fish and primate retinas were conducted to validate the model. The responses of the *computer retina* were compared to those of biological retinas and shown to be qualitatively similar. In addition, the model response to synthetic and real images was presented to illustrate the effects of nonuniform sampling and adaptation. The experiments indicate that the *computer retina* model captures many of the essential properties of visual processing in the primate retina and thus may be used as a basis for a sensor design in silicon.

6.1 Summary of the Retinal Model Features

Figure 4.11 summarizes schematically the computations performed in the retinal model. The information processing strategies employed in the *computer retina* may be used as a starting point for the design of "smart" sensors more closely matched in performance to the human retina. These strategies may be summarized as follows:

- Nonuniform sampling at the photoreceptor level, modelled by the use of a log-polar mapping, significantly reduces the amount of data that needs to be processed at subsequent levels.

- The cone layer is responsible for converting the illumination intensity information into signals used by the rest of the retinal network. A measure of the local neighbourhood

spatiotemporal ambient intensity is used to locally set the sensitivity of each photoreceptor element and allows the *computer retina* to adapt to scenes containing a large dynamic range of retinal illumination intensities. This feature models the effects of pigment bleaching and horizontal cell feedback on the adaptation of cone sensitivity in biological retinas.

- Diffusion is used to model the coupling or spread of signals between cells in any given retinal layer and to generate Gaussian-weighted receptive fields. The diffusion operation requires information only from immediately neighbouring cells and thus is relatively simple to implement in silicon.

- The horizontal cell layer generates a spatial and temporal lowpass version of the visual signal. Horizontal cells have much larger receptive fields and integration time constants than cones.

- A difference operation between the *computer retina* cone and horizontal cell signals, each with different spatiotemporal characteristics, leads to the extraction and enhancement of spatiotemporal contrast in the visual signal at the bipolar and ganglion cell levels.

- Two output channels emerge at the bipolar and ganglion cell levels with visual information coded at different scales and with distinct spatiotemporal properties. The smaller receptive field sizes and greater number of midget bipolar and P-type ganglion cells make them sensitive to high spatial contrast. In comparison, diffuse bipolar and M-type ganglion cells have much larger receptive fields, are less numerous, and are better tuned to respond to temporal frequency modulation. The spatiotemporal properties of the *computer retina* P-cells and M-cells appear qualitatively similar to those of cells in Macaque monkey retinas.

- The diffusivity or coupling between cells in the cone and horizontal cell layers in the *computer retina* is changed as a function of the local neighbourhood illumination level. Altering the cell coupling in such a manner affects the size of receptive fields at the ganglion cell level and serves as an adaptation mechanism that attempts to maintain both high contrast sensitivity and high visual acuity. At low illumination levels, increased cone and horizontal cell coupling leads to larger receptive field sizes. This reduces the visual acuity but combats photon noise and improves the output signal-to-noise ratio (SNR) so that small contrasts in the visual signal can be detected. At higher illuminations, photon noise becomes insignificant compared to the intensity signal so that small contrasts may be detected even with reduced coupling and smaller receptive fields.

- Cells in the interplexiform (IPX) layer react vigorously in regions of high spatiotemporal contrast in the input image and reduce the RF size of horizontal cells. This adaptation mechanism reduces the relative size of the surround portion of bipolar and ganglion cell RF's in regions of high spatiotemporal contrast (spatial edges, flickering lights, etc.) which improves the localization of spatial and temporal edges.

6.2   Limitations of the Retinal Model

Although the *computer retina* behaves in a manner qualitatively similar to the primate retina in many respects, there are several limitations of the model. These may be summarized as follows:

- Only the cone system is modelled. The mode of operation in the biological retina switches smoothly from the rod regime at very dim illumination levels to the cone regime at brighter levels. The behaviour of the computer retina thus differs from the performance of the biological retina in the mesopic illumination range when both the cone and rod systems are in operation.

- Primate cone pathways carry chromatic as well as achromatic luminance information in the same channel. However, the *computer retina* model ignores the processing of colour information. The contrast sensitivity of primate P-cells to chromatically modulated gratings have been shown to be up to 8 times higher than for achromatic gratings and thus suggests a vital role for chromatic information in visual perception [11].

- Many simplifications were made in developing the model. The omission of certain features may have important consequences in the overall processing of visual information. M_Y-cells, which are relatively nonlinear and comprise approximately 2% of the ganglion cell population, are not incorporated into the model; only M_X and P cells are modelled. In addition, the effects of amacrine cells on the outputs of ganglion cells have been omitted. In order to reduce the number of outputs required in the *computer retina* at the bipolar and ganglion cell level by two, both the positive and negative contrast signals are carried in a single channel. By comparison, biological retinas split this information into separate *on*-centre and *off*-centre pathways at the bipolar cell level.

- The temporal properties of P-cells and M-cells in the computer retina differ from those of the respective primate ganglion cells in at least two ways. The first difference is in the peak temporal frequency sensitivity. The peak temporal frequency of the model

123

P-cells and M-cells differs only slightly from each other (10 Hz and 12 Hz respectively) whereas this difference is much larger in primates (8 Hz and 16 Hz respectively) [33].

- The contrast gain of primate ganglion cells drops off rapidly for temporal frequencies greater than the peak gain frequency so that P-cells and M-cells are unable to follow stimulus modulations more rapid than 30 Hz and 60-80 Hz respectively [33]. In comparison, the *computer retina* P-cell and M-cell contrast gain diminishes rather slowly, indicating a requirement for extra stages of temporal lowpass filtering or higher order lowpass filters in all stages of processing.

6.3 Suggestions for Future Research

This thesis has outlined a simple retinal model which incorporates many of the features observed in the primate retina. Although the many simplifications made in the model lead to some discrepancies between the behaviour of the *computer retina* and biological retina, the essential properties of adaptation to a wide range of illumination levels and data reduction have been incorporated. This model was developed with the hope that it may eventually be tested in silicon. Thus a logical next step may be to investigate the feasibility of a silicon implementation of the model.

Future research of possibly great benefit would be the extension of the model to incorporate features of the rod system for operation at very low illumination levels and the processing of chromatic information. In addition, many of the limitations of the model outlined above may be addressed at the expense of slight increases in model complexity and increased number of parameters. However, the benefit would be a more complete model of retinal information processing.

Other areas that require further exploration are the possible effects of the adaptation of the integration time constants and the relative weightings of the centre and surround portions of bipolar and ganglion cell receptive fields as a function of illumination intensity or spatiotemporal contrast.

The retinal model presented here is not a final product. Instead it is hoped that this will thesis serve as a foundation on which to base the design of "smart" sensors and that more comprehensive retinal models may be developed in the future.

References

[1] W.H. Baldridge and A.K. Ball. Background illumination reduces horizontal cell receptive-field size in both normal and 6-hydroxydopamine-lesioned goldfish retinas. *Visual Neuroscience*, 7:441-450, 1991.

[2] H.B. Barlow. Critical limiting factors in the design of the eye and the visual cortex: The Ferrier lecture. *Proceedings Royal Society of London B*, 212:1-34, 1981.

[3] D.A. Baylor and A.L. Hodgkin. Changes in time scale and sensitivity in turtle photoreceptors. *Journal of Physiology (London)*, 214:433-464, 1974.

[4] E.A. Benardete, E. Kaplan, and B.W. Knight. Contrast gain control in the primate retina: P cells are not X-like, some M cells are. *Visual Neuroscience*, 8:483-486, 1992.

[5] K.A. Boahen and A.G. Andreou. A contrast sensitive silicon retina with reciprocal synapses. In *Neural Information Processing Systems NIPS-91 Congress and Conference Proceedings*, Colorado, November 1991.

[6] M. Bolduc. *A Foveated Robot Eye, M.Eng Thesis*. McGill University, Montréal, In progress.

[7] B.B. Boycott and J.M. Hopkins. Cone bipolar cells and cone synapses in the primate retina. *Visual Neuroscience*, 7:49-60, 1991.

[8] R.M. Boynton and D.N. Whitten. Visual adaptation in monkey cones: Recordings of late receptor potentials. *Science*, 170:1423-1426, 1970.

[9] M.H. Brill, D.W. Bergeron, and W.W. Stoner. Retinal model with adaptive contrast sensitivity and resolution. *Applied Optics*, 26:4993-4998, 1987.

[10] P.R. Chang and B.F. Yeh. A retina-like image acquisition system with wide range light adaptation. *SPIE Visual Communications and Image Processing 91: Image Processing*, 1606:456-469, 1991.

[11] A. Chaparro, C.F. Stromeyer, E.P. Huang, R.E. Kronauer, and R.T. Eskew. Colour is what the eye sees best. *Nature*, 361:348-350, 1993.

[12] R.L. Chappell and K. Naka. Sensitivity transformation for vertebrate vision. *Visual Neuroscience*, 6:371-374, 1991.

[13] C.M. Cicerone, M.M. Hayhoe, and D.I.A. Macleod. The spread of adaptation in human foveal and parafoveal cone vision. *Vision Research*, 30:1603-1615, 1990.

[14] T.N. Cornsweet and J.I. Yellott. Intensity-dependent spatial summation. *Journal of the Optical Society America A*, 2:1769-1786, 1985.

[15] M.L.J. Crawford, R.A. Anderson, R. Blake, G.H. Jacobs, and C. Neumeyer. Interspecies comparisons in the understanding of human visual perception. In L.Spillman and J.S. Werner, editors, *Visual Perception: The Neurophysiological Foundations*, pages 23-52. Academic Press, New York, 1990.

[16] J.P. Crettez and J.C. Simon. A model for cell receptive fields in the visual striate cortex. *Computer Graphics and Image Processing*, 20:299–318, 1982.

[17] J.C. Curlander and V.Z. Marmarelis. Processing of visual information in the distal neurons of the vertebrate retina. *IEEE Transactions on Systems, Man, and Cybernetics*, SMC-13:934–943, 1983.

[18] S.M. Dawis. A model for light adaptation: Producing weber's law with bleaching-type kinetics. *Biological Cybernetics*, 30:187–193, 1978.

[19] A.M. Derrington and P. Lennie. Spatial and temporal contrast sensitivities of neurones in the lateral geniculate nucleus of Macaque. *Journal of Physiology*, 357:219–240, 1984.

[20] J.E. Dowling. Information processing by local circuits: The vertebrate retina as a model system. In F.O. Schmitt and F.G. Worden, editors, *Neurosciences - Fourth Study Program*, pages 163–181. MIT Press, Cambridge, MA, 1983.

[21] J.E. Dowling. *The Retina: An Approachable Part of the Brain*. Harvard University Press, Cambridge, MA, 1987.

[22] C. Enroth-Cugell and J.G. Robson. Functional characteristics and diversity of cat retinal ganglion cells. *Investigative Ophthalmology and Visual Science*, 25:250–267, 1984.

[23] D.C. Van Essen and C.H. Anderson. Information processing strategies and pathways in the primate retina and visual cortex. In S.F. Zornetzer, J.L. Davis, and C. Law, editors, *An Introduction to Neural and Electronic Networks*, pages 43–72. Academic Press, San Diego, California, 1990.

[24] D.J. Fleet, P.E. Hallett, and A.D. Jepson. Spatiotemporal inseparability in early visual processing. *Biological Cybernetics*, 52:153–164, 1985.

[25] R. Ginosar and Y.Y. Zeevi. Adaptive sensitivity/ intelligent scan imaging sensor chips. *SPIE Visual Communications and Image Processing*, SPIE 1001:717–723, 1988.

[26] M.M. Hayhoe and M.V. Smith. The role of spatial filtering in sensitivity regulation. *Vision Research*, 29:457–469, 1989.

[27] S. Hochstein and R.M. Shapely. Linear and nonlinear spatial subunits in Y cat retinal ganglion cells. *Journal of Physiology*, 262:265–284, 1976.

[28] D. Hubel. *Eye; Brain and Vision*. Scientific American Library and W.H. Freeman, NewYork, 1988.

[29] M.V. Klein and T.E. Furtak. *Optics*. John Wiley and Sons, New York, 1986.

[30] H. Kolb. Anatomical pathways for color vision in the human retina. *Visual Neuroscience*, 7:61–74, 1991.

[31] H. Kolb and E.V. Famiglietti. Rod and cone pathways in the inner plexiform layer of cat retina. *Science*, 186:47–49, 1974.

[32] R.E. Kronauer and Y.Y. Zeevi. Reorganization and diversification of signals in vision. *IEEE Transactions on Systems, Man, and Cybernetics*, SMC-15:91–101, 1985.

[33] P. Lennie, C. Trevarthen, D. Van Essen, and H. Wassle. Parallel processing of visual information. In L.Spillman and J.S. Werner, editors, *Visual Perception: The Neurophsiological Foundations*, pages 103-128. Academic Press, New York, NY, 1990.

[34] M.D. Levine. *Vision in Man and Machine*. McGraw-Hill, USA, 1985.

[35] Chao-Yi Li, Xing Pei, Yi-Xiong Zhow, and H.C.V. Mitzlaf. Role of the extensive area outside the X-cell receptive field in brightness information transmission. *Vision Research*, 31:1529-1540, 1991.

[36] M.A. Mahowald. Silicon retina with adaptive photoreceptors. In *SPIE/SPSE Symposium on Electronic Science and Technology: From Neurons to Chips*, pages 52-58, Orlando, Florida, April 1991.

[37] D. Marr. *Vision*. W.H. Freeman, San Francisco, CA, 1982.

[38] R.H. Masland. Amacrine cells. *Trends in Neuroscience*, 11:405-410, 1988.

[39] C. Mead and M.A. Mahowald. A silicon model of early visual processing. *Neural Networks*, 1:91-97, 1988.

[40] K. Naka. The cells horizontal cells talk to. *Vision Research*, 22:653-661, 1982.

[41] R.A. Normann and F.S. Werblin. Control of retinal sensitivity I: Light and dark adaptation of vertebrate rods and cones. *Journal of General Physiology*, 63:37-61, 1974.

[42] N.S. Peachey, K. Arakawa, K.R. Alexander, and A.L. Marchese. Rapid and slow changes in the human cone electroretinogram during light and dark adaptation. *Vision Research*, 32:2049-2053, 1992.

[43] D.R. Pepperberg. Rhodospin and visual adaptation: Analysis of photoreceptor thresholds in the isolated skate retina. *Vision Research*, 24:357-366, 1984.

[44] P. Perona and J. Malik. Scale-space and edge detection using anisotropic diffusion. *IEEE Transactions on Pattern Analysis and Machine Intelligence*, 12:629-639, 1990.

[45] M.H. Pirenne. *Vision and Eye*. Associated Book Publishers, London, 1967.

[46] K. Purpura, D. Tranchina, and E. Kaplan. Light adaptation in the primate retina: Analysis of changes in gain and dynamics of monkey retinal ganglion cells. *Visual Neuroscience*, 4:75-93, 1990.

[47] J. Richter and S. Ullman. A model for the temporal organization of X and Y-type receptive fields in the primate retina. *Biological Cybernetics*, 43:127-145, 1982.

[48] R.W. Rodieck. *The Vertebrate Retina*. W.H. Freeman, San Francisco, CA, 1973.

[49] R.W. Rodieck. The primate retina. In H.D. Steklis and J. Erwin, editors, *Comparative Primate Biology, vol. 4 Neurosciences*, pages 203-278. Alan R. Liss Inc., New York, NY, 1988.

[50] A.S. Rojer and E.L. Schwartz. Design considerations for a space-variant visual sensor with complex-logarithmic geometry. In *Proceedings of 10th International Conference on Pattern Recognition*, volume 2, pages 278-285, 1990.

[51] P. Saint-Marc, J-S. Chen, and G. Medioni. Adaptive smoothing: A general tool for early vision. *IEEE Transactions on Pattern Analysis and Machine Intelligence*, 13:514–529, 1991.

[52] H. Saito and Y. Fukada. Gain control mechanisms in X and Y-type retinal ganglion cells of the cat. *Vision Research*, 26:391–408, 1986.

[53] G. Sandini and et. al. A foveated retina-like sensor using ccd technology. In C. Mead and M. Ismail, editors, *Analog VLSI and Neural Network Implementations*, pages 1–23. DeKluwer Publ., Boston, 1989.

[54] P.H. Schiller. The on and off channels of the visual system. *Trends in Neuroscience*, 15:86–91, 1992.

[55] J.L. Schnapf and D.A. Baylor. How photoreceptor cells respond to light. *Scientific American*, 156:40–47, 1987.

[56] R. Shapely and C. Enroth-Cugell. Visual adaptation and retinal gain controls. In N.N. Osborne and G.J. Chader, editors, *Progress in Retinal Research*, pages 263–346. Pergamon Press, Oxford, 1984.

[57] R. Shapely and V.H. Perry. Cat and monkey retinal ganglion cells and their visual functional roles. *Trends in Neuroscience*, 9:229–235, 1986.

[58] J. Skrzypek. Lightness constancy: Connectionist architecture for controlling sensitivity. *IEEE Transactions on Systems, Man, and Cybernetics*, 20:957–967, 1990.

[59] J. Skrzypek and D. Gungner. Lightness constancy from luminance contrast. *International Journal of Pattern Recognition and Artificial Intelligence*, 6:1–36, 1992.

[60] J. Skrzypek and F.S. Werblin. Lateral interactions in absence of feedback to cones. *Journal of Neurophysiology*, 49:1007–1016, 1983.

[61] R.E. Soodak, R.M. Shapely, and E. Kaplan. Fine structure of receptive-field centers of X and Y cells of the cat. *Visual Neuroscience*, 6:621–628, 1991.

[62] M.V. Srinivasan and S.B. Laughlin. Predictive coding: a fresh view of inhibition in the retina. *Proceedings Royal Society of London*, 5:427–459, 1982.

[63] P. Sterling, M.A. Freed, and R.G. Smith. Architecture of rod and cone circuits to the on-beta ganglion cell. *The Journal of Neuroscience*, 8:623–642, 1988.

[64] K. Tanioka, K. Shidra, and T. Hirai. Wide-dynamic range HARP camera. *SPIE High-Resolution Sensors and Hybrid Systems*, 1656:1–12, 1992.

[65] J.P. Thomas. Spatial resolution and spatial interaction. In E.C. Cartertette and M.P. Friedman, editors, *Handbook of Perception*, volume 5, pages 233–264. Academic, New York, 1979.

[66] M. Tremblay and D. Poussart. Focal plane vlsi processing for multiresolution edge extraction. In *Proceedings SPIE Visual Information Processing and OE/Aerospace Sensing*, Orlando, Florida, 1992.

[67] Y. Tsukamoto, P. Masaarachia, S.J. Schein, and P. Sterling. Gap junctions between the pedicles of macaque foveal cones. *Vision Research*, 32:1809-1815, 1992.

[68] O. Umino, Y. Lee, and J.E. Dowling. Effects of light stimuli on the release of dopamine from interplexiform cells in the white perch retina. *Visual Neuroscience*, 7:451-458, 1991.

[69] J.D. Victor. The dynamics of the cat retinal x-cell centre. *Journal of Physiology*, 386:219-246, 1987.

[70] J. Walraven, C.E. Cugell, D.C. Hood, J.L. Schnapf, and D.I.A. MacLeod. Control of visual sensitivity. In L.Spillman and J.S. Werner, editors, *Visual Perception: The Neurophysiological Foundations*, pages 53-101. Academic Press, New York, 1990.

[71] F.S. Werblin. The control of sensitivity in the retina. *Scientific American*, 228:71-79, 1973.

[72] F.S. Werblin. Control of retinal sensitivity II: Lateral interactions at the outer plexiform layer. *Journal of General Physiology*, 63:62-87, 1974.

[73] F.S. Werblin. Integrative pathways in local circuits between slow-potential cells in the retina. In F.O. Schmitt and F.G. Worden, editors, *Neurosciences - Fourth Study Program*, pages 193-211. MIT Press, Cambridge, MA, 1983.

[74] F.S. Werblin and D.R. Copenhagen. Control of retinal sensitivity III: Lateral interactions at the inner plexiform layer. *Journal of General Physiology*, 63:88-110, 1974.

[75] G. Westheimer. Visual acuity and spatial modulation thresholds. In D. Jameson and L.M. Hurvich, editors, *Handbook of Sensory Physiology: Visual Psychophysics*, pages 171-187. Springer-Verlag, Berlin, 1972.

[76] S.W. Wilson. On the retino-coritcal mapping. *International Journal of Man-Machine Studies*, 18:361-389, 1983.

[77] T. Yagi, Y. Funahashi, and F. Ariki. Dynamic model of dual layer neural network for vertebrate retina. In *Proceedings of IJCNN-89*, pages 1787-1789, Washington DC, June 1989.

[78] M. Yamada, Y. Shigeemaatsu, Y. Umetani, and T. Saito. Dopamine decreases receptive field size of rod-driven horizontal cells in carp retina. *Vision Research*, 32:1801-1807, 1992.

[79] H. Yamamoto, Y. Yeshurun, and M.D. Levine. Evaluation of attentional mechanisms for active and foveated vision systems. *International Journal of Computer Vision*, 1992, submitted for publication.

[80] J. Yamazaki, K. Tanioka, and K. Shidara. Development of the super-HARP camera, a rival to the human eye, for the next generation of broadcasting. *SMPTE Journal*, 101:322-324, 1992.

[81] J.I. Yellott. Photon noise and constant-volume operators. *Journal of the Optical Society America A*, 4:2418-2446, 1987.

[82] Y.Y. Zeevi. Adaptive machine vision: What can be learned from biological systems. In *Proceedings SPIE Conference on Intelligent Robots and Computer Vision VIII: Algorithms and Techniques*, volume 1192, pages 560–568, Philadelphia, PA, November 6-10 1989.

[83] Y.Y. Zeevi and R. Ginosar. Neural computers in vision: Processing of high dimensional data. *NATO ASI Series, Neural Computers; Springer-Verlag, Berlin*, F41:169–178, 1988.

[84] Y.Y. Zeevi and S.S. Mangoubi. Noise suppression in photoreceptors and its relevance to incremental intensity thresholds. *Journal of the Optical Society America*, 68:1772–1776, 1978.

[85] S.W. Zucker and R.A. Hummel. Receptive fields and the representation of visual information. *Human Neurobiology*, 5:121–128, 1986.